THREE DIMENSIONAL MODELING OF AUTOTHERMAL REFORMING OF METHANE IN A Pt-Ni WASHCOATED MICRO-CHANNEL REACTOR

by

Bilge Kerem Aksakal

B.S., Chemical Engineering, Boğaziçi University, 2009

Submitted to the Institute for Graduate Studies
in Science and Engineering in partial fulfillment of
the requirements for the degree of
Master of Science

Graduate Program in Chemical Engineering

Boğaziçi University

2012

“beni bu güzel havalar mahvetti.”

ACKNOWLEDGEMENTS

Foremost, I wish to express my gratitudes to my advisors; Prof. Erhan Aksoylu, and Assoc. Prof. Hasan Bedir. Without their valuable contribution, I will never be able to accomplish my studies on catalysis and computational fluid dynamics. They become a inspiration for me in the academic circle, with their devotion to science.

I would like to thank to Ahmet Kerim Avcı specially. I benefit from his contributions to literature greatly on my thesis. I also want to thank to Ramazan Yıldırım and Mehmet Çamurdan, since their steady swimming in morning is an inspiration for me to train my body regularly.

With their work and contribution to literature CATREL team definitely deserves a special appreciation. Thanks to regular weekly meetings, I gained systematic working habit proper for academic career.

I owe too much to my friends; Onur Güngör, who always accompanies me in dinners, thought me lots of things in computational process. Without Ali Uzun, compiling period will be most boring probably. He was very humble table tennis partner for me. With his tireless working habit Yiğit Günay is an inspiration for me, unless we share same flat for eight years it is not possible for me to work like today I did. I will never end acknowledgements part without thanking Mustafa Karakaya, who becomes a patriarchal figure for all animals in Boğaziçi, who is the most humble and hard working person I ever seen.

I have very special thanks for my brother Can Aksakal. His existence is always a joy for me.

The financial support provided by Bogazici University through project BAP 5570 and TUBITAK through project 111M144 is greatly appreciated.

ABSTRACT

THREE DIMENSIONAL MODELING OF AUTOTHERMAL REFORMING OF METHANE IN A Pt-Ni WASHCOATED MICRO-CHANNEL REACTOR

Steady state behavior of hydrogen production from oxidative steam reforming of methane in a Pt-Ni bimetallic washcoated Al_2O_3 microchannel reactor was modeled and simulated three dimensionally by using CFD program. Internal channels of Al_2O_3 monolith reactor are covered with Pt and Ni in given metal loadings; in the simulations Pt and Ni clusters are considered randomly distributed according to ratio of 1/20 and 1/30. It is assumed that on Pt covered areas total oxidation of methane and on Ni covered areas steam reforming and water-gas shift reactions occur. Simulations are performed for cases with different steam to carbon and carbon to oxygen feeding ratios for 723-1023 K inlet temperature range by using FLUENT™. The system performance is evaluated on the basis of the obtained methane conversion, hydrogen yield and hydrogen to carbon monoxide selectivity ratio at the exit. An inlet temperature of 723 K was proven to be too low for efficient system performance. The results of the simulations reveal that methane conversion and hydrogen yield increases but H_2/CO selectivity ratio decreases with the increase in inlet temperature, for all feed compositions. Thus, an optimum "feed composition-inlet-temperature-catalyst composition" combination should be selected according to required hydrogen yield and H_2/CO selectivity at the exit of the OSR system. Sizing of microchannel reactor has been done to provide hydrogen for 5 kWe PEM fuel cell for each case.

ÖZET

METANIN MİKRO KANALLI Pt-Ni ile KAPLI REAKTÖRDE OTOTERMAL REFORMLAMASININ ÜÇ BOYUTLU SİMÜLASYONU

Kanal duvarları Pt ve Ni ile kaplanmış mikro kanallı reaktör içerisinde metan gazından oksidatif buhar reformlama ile hidrojen üretiminin üç boyutlu modellemesi ve simülasyonu HAD (hesaplamalı akışkan dinamiği) kullanılarak yapılmıştır. Simülasyonlarda mikro kanallı reaktörün kanallarının içi 1/20 ve 1/30 oranlarında, rastgele dağıtılmış, Pt ve Ni katalizörleriyle kaplanmıştır. Platin kaplı olduğu varsayılan alanda ısı veren yanma reaksiyonu, nikel kaplı alanda ısıya muhtaç buharlı reformlama reaksiyonu gerçekleştiği varsayılmıştır. 723-1023 K arasındaki giriş sıcaklıkları, farklı buhar / karbon ve karbon / oksijen oranları simüle edilerek en uygun reaktör giriş şartı incelenmiştir. Modellenen sistemin performansı; metanın dönüştürülmesi, hidrojen verimi ve hidrojenin karbon monoksite seçiciliği kullanılarak değerlendirilmiştir. Reaktör girişinin 723 K'e ısıtılması düşük metan dönüşümüne sebebiyet vermiş ve verimsiz olarak kaydedilmiştir, bununla beraber yüksek giriş sıcaklıkları hidrojenin karbon monoksite seçiciliğini düşürmüştür. Bu durumda oksidatif buhar reformlama reaktörünün çıkışında istenen H_2/CO oranı ve hidrojen verimini elde etmek için uygun bir "giriş kompozisyonu-giriş sıcaklığı-katalizör oranı" seçilmelidir. Buna göre 5 kWe'lık PEM tipi yakıt pilini besleyecek reaktörün boyutlandırılması yapılmıştır.

TABLE OF CONTENTS

LIST OF FIGURES

LIST OF TABLES

LIST OF SYMBOLS

A_c	Channel cross sectional area	m^2
A_s	catalyst surface area	m^2
C_j	Concentration of species j	$kmol/m^3$
$C_{v,\,i}$	Heat capacity of species i	kj/kg K
$C_{p,\,i}$	Heat capacity of species i	kj/kg K
$C_{p,\,mix}$	Heat capacity of mixture	kj/kg K
D_i	Diffusivity of species i into mixture	m^2/s
E_{cell}	Electric potential	V
H	Reactor channel height	mm
i	C_vT	kj/kg
I	Current density	I/cm^2
$\mathbf{J_i}$	Diffusion mass flux vector	kg/m^2 s
k_i	Thermal conductivity of species i	W/mK
k_{mix}	Thermal conductivity of mixture	W/mK
k_{wall}	Thermal conductivity of wall	W/mK
k_j	Reaction rate constant for reaction j	kmol/kgcat h
K_{jeq}	Equilibrium constant for reaction j	-
$K_{c,i}$	Adsorption constant of species i on Pt	1/bar
K_i	Adsorption constant of species i on Ni	1/bar
L	Reactor length	mm
$M_{w\,i}$	Molecular weight of species i	kg/kmol
$M_{w,mix}$	Molecular weight of mixture	kg/kmol
P	Power density	W/cm^2
p	Pressure	Pa
p_i	Partial pressure of species i	Pa
R	Gas constant	J/mol K
$rate_j$	Rate of reaction j	kmol/kgcat h
S_i	Source Term for Energy Equation	W/cm3
S_{Mx}	Source Term for Equation of Motion on x direction	$kg/m^2\ s^2$
S_{My}	Source Term for Equation of Motion on y direction	$kg/m^2\ s^2$

S_{Mz}	Source Term for Equation of Motion on z direction	$kg/m^2\ s^2$
T_{gas}	Temperature of gas	K
T_{inlet}	Temperature of feed	K
T_{wall}	Temperature of wall	K
u	Velocity magnitude in x-coordinate	m/s
u	Velocity unit vector	
u_{ave}	inlet average velocity	m/s
v	Velocity magnitude in y-coordinate	m/s
w	Velocity magnitude in z-coordinate	m/s
W	Reactor Channel Width	mm
x_i	Mol fraction of species i	-
z	length along z-coordinate	mm

$\Delta H_{rxn,j}$	Enthalpy of reaction j	kj/mol
$\Delta H_{rxn,j}^{0}$	Enthalpy of reaction j at reference temperature	kj/mol
$\Delta H_{f,i}^{0}$	Enthalpy of formation of species i	kj/mol
μ_i	Viscosity of species i	Pa s
μ_{mix}	Viscosity of mixture	Pa s
ρ_i	Density of species i	kg/m^3
ρ_{mix}	Density of mixture	kg/m^3
$\boldsymbol{\Phi}$	Dissipation source term	-

LIST OF ACRONYMS / ABBREVATIONS

AC	Alternating Current
AFC	Alkaline Fuel Cell
C/O	Carbon to Oxygen Ratio
CFD	Computational Fluid Dynamics
CHP	Combined Heat and Power
DC	Direct Current
DOE	United States Department of Energy
DR	Dry Reforming
FEM	Finite Elements Method
FVM	Finite Volume Method
HTS	High Temperature Water Gas Shift
LPG	Liquefied Petroleum Gas
LTS	Low Temperature Water Gas Shift
MCFC	Molten Carbonyte Fuel Cell
NSx	Navier Stokes Equation for Cartesian Coordinate x
NSy	Navier Stokes Equation for Cartesian Coordinate y
NSz	Navier Stokes Equation for Cartesian Coordinate z
PAFC	Phosphoric Acid Fuel Cell
PEMFC	Proton Exchange Membrane Fuel Cell
POX	Partial Oxidation
PrOX	Preferential Oxidation
S/C	Steam to Carbon Ratio
SIMPLE	Semi Implicit Method for Pressure-Linked Equations
SOFC	Solid Oxide Fuel Cell
SR	Steam Reforming
TOX	Total Oxidation
WGS	Water Gas Shift

1. INTRODUCTION

Fossil fuels have been used intensively to satisfy the energy demand of humanity since the dawn of industrial revolution. According to British Petroleum's world statistical report more than 90% of energy for heating, transportation and electricity production is based on the combustion of oil, gas and coal reserves of world. (British Petroleum, 2011). The world energy market forecasts indicate that increase in population and change of consumption habits in developing countries cause almost exponential increase in fossil fuel demand. Despite proven reserves over production ratios are diminishing, fossil fuels still have enough reserves to dominate the energy supply in the next century (British Petroleum, 2012). Due to recent technological advancements in engines and furnaces, and inventions like catalytic convertors, hazardous emissions like sulfur oxides, nitric oxides, carbon monoxide, dioxin and furan have been reduced greatly. On the other hand, climate change and global temperature rise, which has become severe especially during the last decade, impose the emission reduction for the main combustion product, carbon dioxide. In order to prevent man-made global warming, delegates of United Nations except US, accepted a protocol in Kyoto which plans to stop the increase the carbon dioxide concentration in atmosphere (United Nations, 1998). According to the protocol and the following agreements, renewable energy production, and developments in the fossil fuel conversion efficiency are subsidized. All these subsidies by governments, and research funds by both the governments and private sector for a sustainable energy future -within the context of Kyoto protocol and the current agreements reached in Durban, 2011- has a potential to make hydrogen a prominent energy carrier in the near future.

The modern electricity production/distribution networks, smart grids, are the essential part of the sustainable energy future and, as they have systems allowing bidirectional electricity flow, they support distributed electricity production by small units, like houses. In smart grids, each consumer is, at the same time, can be a producer. Increasing the share of renewable energy systems in electricity production, and their integration to the electricity distribution networks is another target of sustainable energy future. On the other hand, energy production in renewable systems, like wind turbines, photovoltaic cells etc.is intermittent as those units are flow-limited. Thus, there is a need of small scale systems which

can produce electricity continuously. One of the possible alternatives for small scale electricity production is the use of Proton Exchange Membrane Fuel Cells, PEMFC. PEMFC operates at ca. 90-95 ^{0}C and uses hydrogen as the feed. The only disadvantage in its use is that the hydrogen feed must have at most 50 ppm. CO as the PEMFC Pt-anode is prune to CO poisoning at the operation temperatures.

The main advantage of hydrogen as an energy carrier compare to electricity is the possibility of storing it. Although hydrogen production processes at industrial scale have been in use for a long time, there is no well established hydrogen distribution network; thus, small scale on site hydrogen production processes/units with high efficiency and low cost allowing decentralized hydrogen production are needed to be developed. The catalytic systems called Fuel Processors (FP), which include catalytic reforming, water-gas shift (WGS) and preferential oxidation (PROX) units in series, is a widely accepted way of small scale hydrogen production from various hydrocarbons. In an FP, hydrogen is produced in the reforming unit, the hydrogen concentration of the reformer effluent is increased while its CO level is decreased in the following WGS unit, and finally the CO level is decreased down below 50 ppm by the PROX unit. In most of the small scale fuel processors, oxidative steam reforming (OSR) is the preferred reaction in the reforming section due to the fact that in OSR, the energy needed by the endothermic steam reforming (SR) reactions is supplied by simultaneous exothermic total oxidation (TOX) eliminating the need for an external heating unit. By the use of FP-PEMFC integrated systems, continuous electricity production from a hydrocarbon having a well established distribution network, like natural gas, is possible for small scale stationary applications.

Novel catalysts for the FP reactions have been developed in particle form by our group; those catalysts are Pt-Ni/Al_2O_3 system OSR, Au-Re system for WGS and Pt-Sn/AC system for PrOX reactions. As the micro reactors have better temperature control, compactness and mostly eliminate pressure gradient inside the reactor, analyzing the performance of Pt-Ni OSR catalyst in a micro-channeled reactor model is a prerequisite for design and development of micro-channeled OSR reactor. In the current study methane OSR reaction is simulated three dimensionally in nine wall-coated channels representing a micro reactor. The walls of the reactor channels are made of Al_2O_3 and coated with nickel and platinum, which are randomly dispersed with pre-determined Pt:Ni ratios on each channel.

Under the light of previous experimental findings, steam to carbon and oxygen to carbon ratio in the feed stream, platinum and nickel ratio on the reactor wall and the inlet temperature of the feed stream are considered as parameters in simulations (Gökaliler, Göçmen, & Aksoylu, 2008). Steam to carbon ratio is kept higher than certain a level in order to guarantee the conditions preventing coke deposition on the reactor walls.

In this work; literature survey on fuel cells and different reactions occurring in the fuel processors: steam reforming, total oxidation, water-gas shift followed by mentioning of other computational studies been done on Chapter 2. Chapter 3 includes the mathematical and computer model of this research. Results of simulations are in Chapter 4 with relevant discussions. Finally, conclusions and recommendations for future work are in Chapter 5.

2. LITERATURE SURVEY

2.1. Fuel Cells

Fuel cells convert chemical energy into electrical energy and heat. Steady flow of fuel has to be supplied to fuel cells and unlike thermal engines, electrical energy is directly produced without any significant emissions as the result of the reactions that take place in fuel cells. Fuel cells have no mechanically moving parts and they are not limited by Carnot efficiency like conventional combustion or steam engines. They are thermodynamically more efficient, mechanically more stable and quieter comparing to thermal engines (Hoogers, 2003).

Fuel cell consists three main parts like batteries; anode, cathode and electrolyte. For proton exchange membrane fuel cells in particular electron is taken from the hydrogen molecule by the specific chemical reaction at anode layer:

$$2H_2 \rightarrow 4H^+ + 4e^- \tag{2.1}$$

Electrons are transmitted with a conductive material to produce current and hydrogen ions are transmitted by the electrolyte. Nafion® membrane is selected as electrolyte. At the cathode side electrons that has been conducted by a cable, and hydrogen ions which have been transmitted via the acidic electrolyte react with oxygen molecule which is found in air.

$$O_2 + 4H^+ + 4e^- \rightarrow 2H_2O \tag{2.2}$$

Overall reaction can be shown simply:

$$O_2 + 2H_2 \rightarrow 2H_2O \tag{2.3}$$

For the reactions above anode and cathode layer of the fuel cells have to be coated with special catalysts. Platinum is used as the catalyst in PEM fuel cells.

Each fuel cell type has a unique voltage current graph, which states operating voltage, current and efficiency of fuel cell. A typical voltage current graph for a proton exchange membrane fuel cell is given in Figure 2.1.

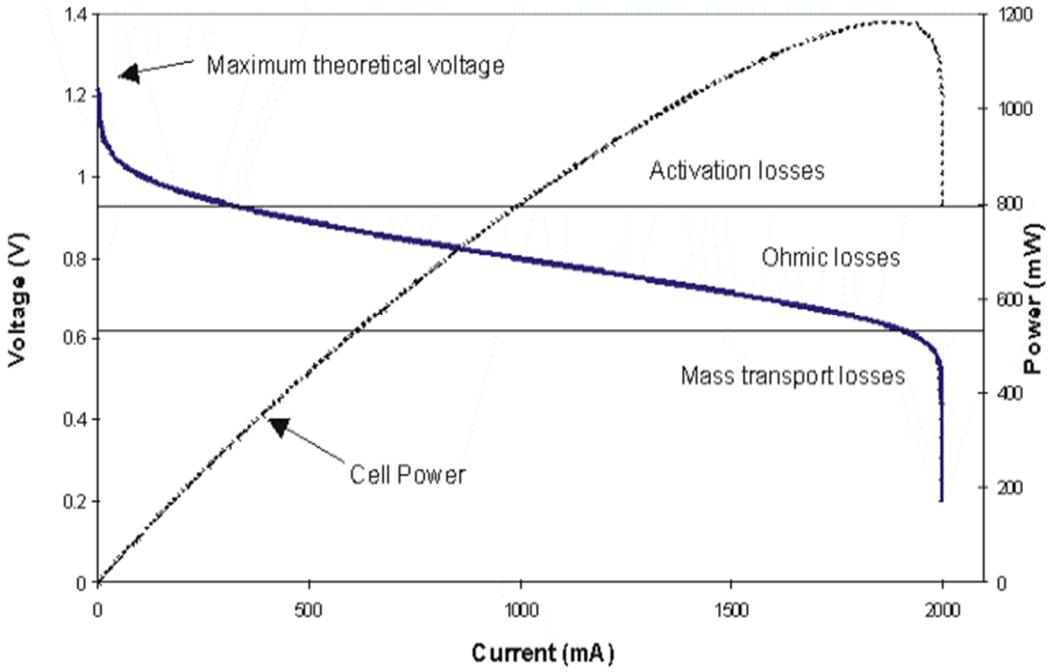

Figure 2.1. Voltage-current graph for PEM fuel cells (EPA, 2004).

1.23 V is theoretical limit for one PEM fuel cell unit, which uses H_2 as a fuel; but commercial fuel efficiencies are far from theoretical values. Activation losses are mainly due to slow anode reaction and research on catalyst is still in progress to reduce the voltage loss. Ionic resistance of electrolyte, anode and cathode causes ohmic losses, which are linear to current. At high currents, mass transport of reactants cause main boundary for efficiency. Differences between losses are more obvious in colder working environments.

As seen from Figure 2.1, average fuel cell has an operating voltage range of 0.4 to 0.8 V. And efficiency range of 40 to 50%. Since fuel cells create low direct current voltage, a stack of serially connected cells are needed. Connecting the edges of each anode to the other cell's cathode layer can cause higher ohmic loss. Usually, 'bipolar plates' are to be used in order to eliminate the extra efficiency loss. One side of bipolar plate is anode for one cell, while the other side is cathode for a different cell (Larmine & Dicks, 2003).

Chemical energy is converted to fluctuating direct current electrical energy and some heat in fuel cells. That requires cooling, voltage regulation and, if it is fed to the grid, AC/DC inverter is needed.

Since reactions on electrodes are exothermic all fuel cells except small portable ones need cooling. Heat exchangers are usually used to take off the heat. Heat can be utilized by radiators in combined heat and power (CHP) systems. For larger high temperature fuel cell systems, steam can be produced by from heat exchangers, which will enhance the process efficiency.

According to United States Department of Energy 60 % efficiency can be achieved with PEM fuel cells in transportation. Since PEM type fuel cells are used for both transportation and distributed energy production for various small scale applications like houses, more literature survey is going to be conducted on proton exchange membrane FC, rather than other types of fuel cells (EPA, 2004).

Solid polymers are used as electrolyte material for PEM fuel cells. They work at low temperatures, which make it easier to startup and shutdown. They are natural selection vehicular and small scale applications.

To fasten up the anode reaction, electrode is coated with platinum catalyst which is the main parameter affecting cost of fuel cell. In years, platinum density has been down to 0.15 mg per cm^2 from 28 mg per cm^2. This development will increase the possibility of commercialization of PEM FC in coming years (Sinha, 2010).

Solid polymer used as the electrolyte has to be insulating material and also should transfer hydrogen ions from anode to cathode. Nafion® material that has been created by the DuPont Company has superior properties for its chemical resistance, mechanical strength, softly acidic content and ability to absorb large quantity of water. They can be thinned to 50 µm films. For the travel of hydrogen ions they need to be hydrated, causing water management problems. Typical membrane has conductivity around 0.1 S per cm which is linear to water concentration in the membrane.

Water management is a serious problem for PEM fuel cells. It has to be high in order to ease the hydrogen ion conduction, but high concentrations can cause blocking of pores on anode. The optimum amount of water in electrolyte has to be sustained. High temperature air flow around 60 ^{0}C or higher current densities causes drying of electrolyte (Ren & Gottesfeld, 2001). In order to overcome the problem, air feed can be humidified. For cells that will operate at higher temperatures, reactant feed should have water vapor content (Büchi & Srinivasan, 1999).

Fuel cells are usually operated at atmospheric pressure, but fuel cells with capacity larger than 10 kW can be operated at higher pressures. The aim is simply to increase the energy density of the fuel cell. Pressure increase shifts the voltage current graphic up, leading increase in the efficiency, but fuel cell casing become thicker and additional compressor will increase the costs and maintenance.

Researches show that, carbon monoxide poisons the catalyst on the anode electrode. In order to protect expensive platinum, fuel gas has to be purified via certain reactions like preferential CO oxidation as CO content higher than 10 ppm causes serious decline in the fuel cell efficiency. Carbon dioxide has no negative effect on the catalyst or the electrolyte of the PEM (Mishra, Yang, & Pitchumani, 2005).

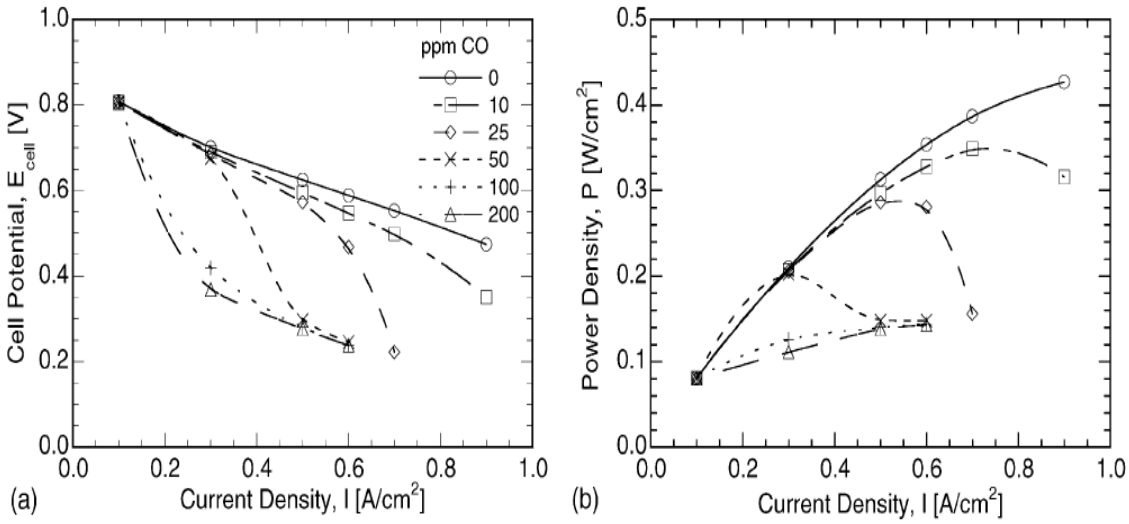

Figure 2.2. Effect of CO concentration on voltage and power (Mishra *et al.*, 2005).

2.2. Hydrogen Obtaining

2.2.1. Hydrogen Production Methods

Despite hydrogen is the most abundant molecule in universe, there is no direct source of hydrogen in Earth. It cannot be mined, drilled or harvested. It has to be produced from other products or separated as a byproduct of other processes. Therefore hydrogen is considered as an energy carrier rather than energy source.

Several methods and processes are used in the market for hydrogen production. 50% of the hydrogen is extracted from the dehydrogenation processes in refineries. As shown in Equation 2.4 40% of the hydrogen is produced by the steam reforming reaction and the rest is obtained by different methods.

$$C_nH_{2n+2} \rightarrow C_nH_{2n} + H_2 \tag{2.4}$$

Hydrogen can be produced in electrolyzers by applying direct current. Produced hydrogen can be used by fuel cells or stored for future demand. For places which are not connected to grid solar and wind energy plants produce energy with daily fluctuations, but demand for energy is also necessary in night while solar plant is not operable. Wind regime is fluctuating daily and seasonally therefore theoretical production is not exactly equal to the real production values. In order to compensate the difference between production and demand, excess energy has to be stored as electrical energy in batteries or as hydrogen to feed fuel cells whenever demand is greater than supply. Each has different cycle efficiencies, drawbacks and advantages. Batteries are expensive and constant maintenance is needed for them. Batteries are not able to store energy for long time due to self-discharge properties, and also wide usage of metallic batteries can cause significant rise in lead prices. Hydrogen storage on the other hand is expensive and risky due to low energy per volume ratio of fuel. Compression or liquefying is reducing the efficiency and increase the overall cost of the system. Energy density and costs for hydrogen storage in the year of 2006 is given in Figure 2.3 (Chalk & Miller, 2006).

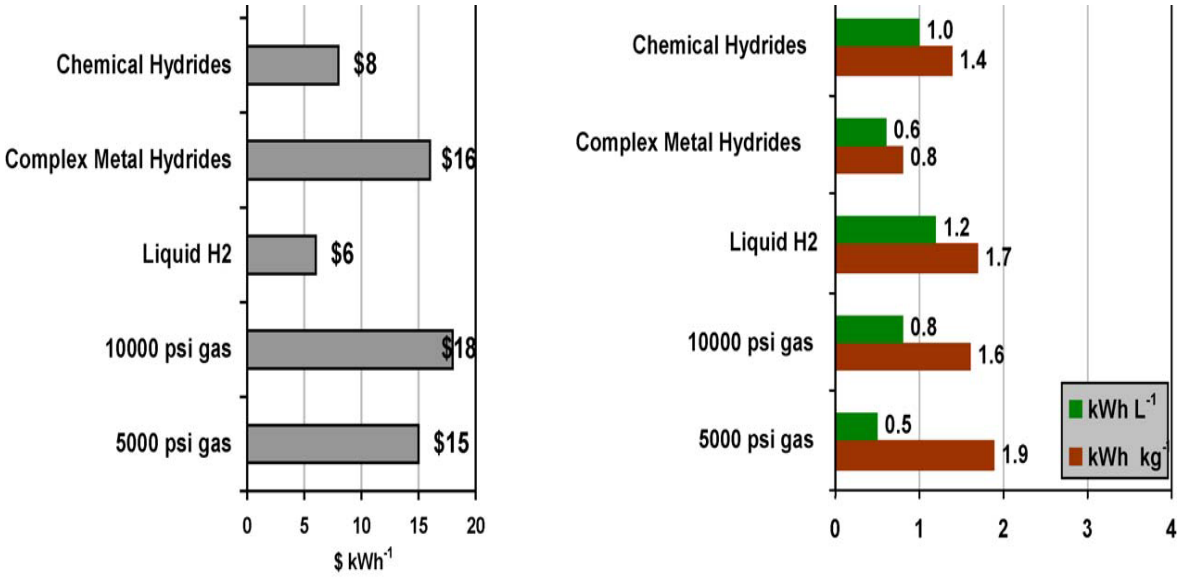

Figure 2.3. Cost and Energy density of H_2 storage.

Despite hydrogen storage is an important research topic; it is still not cost efficient to store hydrogen safely for small scale stationary or on-board applications. Therefore research currently focuses on the production of hydrogen in the area of its use for stationary and on-board for mobile applications.

2.2.2. Hydrogen Production

2.2.2.1. Hydrogen Production from LPG and Gasoline. Since hydrogen storage has some serious flaws, distributed hydrogen production is of great interest among researchers. Safe storage of fossil fuels is a well developed process; therefore hydrogen production from fossil fuels using steam reforming or partial oxidation on-board or off-grid processes is possible.

For on-board applications; LPG (reactions in Equation 2.5 and 2.6) which consists of half propane half butane, and gasoline, which is modeled mainly as octane, consists of hydrocarbons from pentane to octane (reaction in Equation 2.7) is used as the feed for steam reforming. Steam reforming reactions for hydrocarbons is widely studied and successfully summarized in literature (Rostrup-Nielsen J. R., 2002) (Rostrup-Nielsen J. R., 2000).

$$C_3H_8 + 3H_2O \rightarrow 3CO + 7H_2 \qquad \Delta H_{rxn}{}^0 = 498.1\ \text{kj/mol} \qquad (2.5)$$

$$C_4H_{10} + 4H_2O \rightarrow 4CO + 9H_2 \qquad \Delta H_{rxn}{}^0 = 651.7\ \text{kj/mol} \qquad (2.6)$$

$$C_8H_{18} + 8H_2O \rightarrow 8CO + 17H_2 \qquad \Delta H_{rxn}{}^0 = 1259.6\ \text{kj/mol} \qquad (2.7)$$

Water gas shift reaction (WGS) always accompanies steam reforming reaction. Water gas shift reaction is enhanced with gold catalyst, but without gold this reaction also proceeds especially at low temperatures. For temperatures higher than 400 ^{0}C reverse WGS reaction is dominant.

$$CO + H_2O \rightarrow CO_2 + H_2 \qquad \Delta H_{rxn}{}^0 = -40.6\ \text{kj/mol} \qquad (2.8)$$

Since steam reforming reactions are endothermic, additional heat has to be supplied. For larger processes these reactions are held in furnaces but this is not practical for small scale applications therefore exothermic combustion or total oxidation reaction (TOX) accompanies steam reforming for the supply of necessary energy.

Hydrogen, carbon dioxide and carbon monoxide mixture can react to produce methane and steam in a reaction known as methanation. This reaction in Equation 2.9 has pronounced activity especially at low temperatures. This reaction decreases hydrogen yield but can be preferable as it decreases the concentration of carbon monoxide at the same time (Rostrup-Nielsen, Pedersen, & Sehested, 2007).

$$CO + 3H_2 \rightarrow CH_4 + H_2O \qquad \Delta H_{rxn}{}^0 = -206.2\ \text{kj/mol} \qquad (2.9)$$

Some of fuel can be burned to feed the endothermic steam reforming reactions with widely known combustion or total oxidation (TOX) reactions. Total oxidation reaction for propane, butane and gasoline is given in Equations 2.10, 2.11 and 2.12.

$$C_3H_8 + 5O_2 \rightarrow 3CO_2 + 4H_2O \qquad \Delta H_{rxn}{}^0 = -2045.2\ kj/mol \qquad (2.10)$$

$$C_4H_{10} + \frac{13}{2}O_2 \rightarrow 4CO_2 + 5H_2O \qquad \Delta H_{rxn}{}^0 = -2658.9\ kj/mol \qquad (2.11)$$

$$C_8H_{18} + \frac{25}{2}O_2 \rightarrow 8CO_2 + 9H_2O \qquad \Delta H_{rxn}{}^0 = -5119.6\ kj/mol \qquad (2.12)$$

These reactions reduce the fuel conversion efficiencies but eliminate the need for external heat supply to reactor, which is necessary for endothermic steam reforming reaction. High surface area ceria is used under SOFC operating conditions (Laosiripojana & Assabumrungrat, 2006). These reactions are active on both of the metallic surfaces; platinum has known properties for increasing the combustion and steam reforming rate but for catalyzing steam reforming reaction nickel is natural choice, due to its low cost. Performance of bimetallic Pt/Ni catalyst in oxidative steam reforming for pure propane and LPG hydrocarbon feeds for different S/C and C/O ratio was studied at Boğaziçi University (Çağlayan, Avcı, Önsan, & Aksoylu, 2005) (Gökaliler, Çağlayan, Önsan, & Aksoylu, 2008). According to the results of these studies, higher steam concentration increases the selectivity and hydrogen production activity over on 0.2 wt%Pt–15 wt% Ni/δ-Al_2O_3. For higher the butane content in LPG, deactivation of catalyst due to coke formation is observed. Optimum amount of Ni:Pt ratio is around 50, and gold addition to catalyst to enhance water gas shift reaction has negative effect (Gökaliler, Göçmen, & Aksoylu, 2008).

Steam reforming reaction of n-butane on Ni/δ-Al_2O_3 catalyst and oxidative steam reforming reaction of n-butane on Pt-Ni/ δ-Al_2O_3 bimetallic catalyst is researched and effectiveness of the catalysts is compared. Additionally power law type reaction kinetics has been determined (Avci A. K., Trimm, Aksoylu, & Önsan, 2004).

Oxidative steam reforming for gasoline was also conducted on 0.3 wt% Rh /3 wt% MgO/20 wt%CeO_2–ZrO_2 supported on cordierite monolith in a temperature range of 650-800 ^{0}C (Qi, Wang, Ni, & Wu, 2007).

Partial oxidation reactions for propane, butane and gasoline are given below. These reactions are slightly exothermic and creating hydrogen rather than steam. Correct balanc-

ing of catalyst and hydrogen can supply the heat needed from steam reforming reaction from partial oxidation reaction, and will result autothermal reforming of the hydrocarbon.

$$C_3H_8 + \frac{3}{2}O_2 \rightarrow 3CO + 4H_2 \qquad \Delta H_{rxn}{}^0 = -227.9\ kj/mol \qquad (2.13)$$

$$C_4H_{10} + 2O_2 \rightarrow 4CO + 5H_2 \qquad \Delta H_{rxn}{}^0 = -316.2\ kj/mol \qquad (2.14)$$

$$C_8H_{18} + 4O_2 \rightarrow 8CO + 9H_2 \qquad \Delta H_{rxn}{}^0 = -676.4\ kj/mol \qquad (2.15)$$

Partial oxidation and oxidative steam reforming of propane is compared by the researchers in Norwegian University of Science and Technology for 0.01 wt. % Rh/Al_2O_3 catalyst. Optimal temperature for reaction was found as 700 ^{0}C and additional steam has showed negative effect on catalyst durability (Silberova, Venvik, Walmsley, & Holmen, 2005).

2.2.2.2. Hydrogen Production from Natural Gas. Liquid fuel should be supplied to fuel processors for portable application, but for small scale applications like in houses natural gas is easier to be used as the fuel. Therefore simulations for combined heat and electricity production for small scale applications was done for methane fuel processors.

Turkey has well established natural gas distribution network. Nearly all regions have access to natural gas. According to natural gas infrastructure company in Turkey, natural gas consists of 82 to 98% methane. Ethane concentration is between 0.2 to 7%, and propane concentration has a range of 0 to 4%. Cumulative oxygen, nitrogen and carbon dioxide concentrations are between 0 to 4 %. Compositions differ for the source of natural gas supply (BOTAŞ, 2009).

2.3. Reactions in Natural Gas Steam Reforming

Reactions that produce hydrogen from methane, purify hydrogen from carbon monoxide and cause coke deposition on catalyst are listed in Table 2.3. Further literature survey has been conducted on these reactions. (Kolb, 2008).

Table 2.1. Significant reactions in steam reforming of methane.

Reaction name	Equation	ΔH_{rxn}(kj/mol)	
Steam Reforming	$CH_4 + H_2O \leftrightharpoons CO + 3H_2$	206.2	(2.16)
Side SR	$CH_4 + 2H_2O \leftrightharpoons CO_2 + 4H_2$	165.1	(2.17)
Partial oxidation	$CH_4 + 0.5O_2 \longrightarrow CO + 2H_2$	-35.8	(2.18)
Combustion	$CH_4 + 2O_2 \longrightarrow CO_2 + 2H_2O$	-802.9	(2.19)
Dry reforming	$CH_4 + CO_2 \leftrightharpoons 2CO + 2H_2$	247.4	(2.20)
Water gas shift	$CO + H_2O \leftrightharpoons CO_2 + H_2$	-40.4	(2.21)
Preferential oxidation	$CO + 0.5O_2 \longrightarrow CO_2$	-283.0	(2.22)
Side Preferential oxidation	$H_2 + 0.5O_2 \longrightarrow H_2O$	-242.1	(2.23)
Thermal cracking	$CH_4 \longrightarrow C + 2H_2$	75.0	(2.24)
CO hydrogenation	$CO + H_2 \longrightarrow H_2O + C$	-131.0	(2.25)
Boudouart reaction	$2CO \leftrightharpoons CO_2 + C$	-172.0	(2.26)
Gasification	$C + H_2O \leftrightharpoons CO + H_2$	131.4	(2.27)
Combustion of coke	$C + O_2 \longrightarrow CO_2$	-393.8	(2.28)

2.3.1. Steam Reforming of Methane

Steam reforming of methane to produce carbon monoxide and hydrogen mixture in packed bed tubular reactors is a much known process. Heat has to be supplied externally; therefore tubes are placed in furnaces. (Rostrup-Nielsen J. R., 1984) (Rostrup-Nielsen & Alstrup, 1999) Unfortunately this application is very vulnerable as there is a formation of hot spots in the reactor, which diminishes the catalyst deactivation by sintering seriously.

(Bengaard *et al*., 2002). Activity of various catalysts for steam reforming is sequenced by Rostrup-Nielsen and Hansen first (1993), and then the sequence is corrected on other researches (Karakaya, Keskin, & Avci, 2012). The activity sequence of metals for steam to carbon ratio is in range of 0.5 to 3 and temperatures between 600 to 800 ^{0}C are given as.

$$Ru, Rh < Ir < Pd, Ni, Pt < Re < Co$$

Steam reforming, in other words CO producing steam reforming, and side reaction of steam reforming, ie. CO_2 producing steam reforming and water gas shift reactions cannot be separated (Xu & Froment, 1989). All of the three reactions have thermodynamic limits; elevated temperature shifts the conversion of methane but increasing pressure shifts the reactions reversely. Effect of temperature and pressure is given in Figure 2.4 (Kolb, 2008).

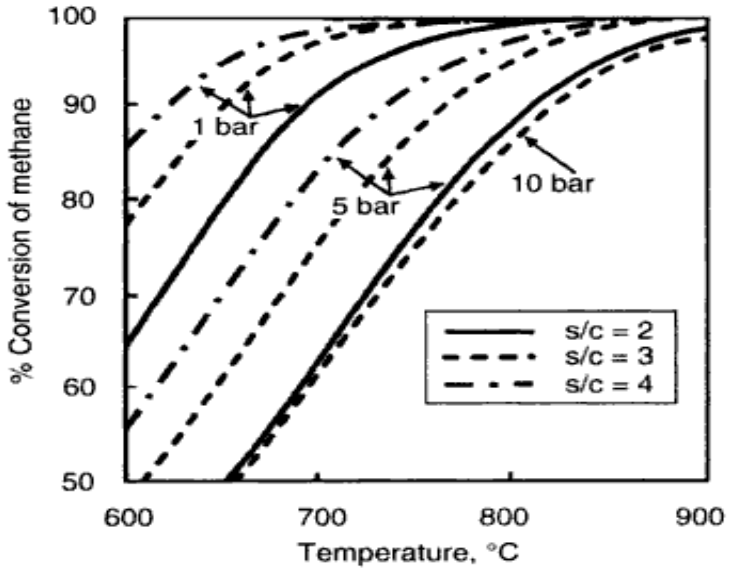

Figure 2.4. Effect of temperature and pressure on equilibrium conversion of methane.

Since Ni is the most abundant and cheapest compared to precious elements, despite its moderate activity, it is the most cost efficient metal to be used in catalyst for steam reforming applications. High temperature applications cause sintering of the nickel active sites, also strong oxidization accompanies to sintering due to high steam content. Therefore studies aim to decrease the operating temperature of the reactor.

Kinetics of steam reforming reaction based on Langmuir-Hinshelwood type rate law has been studied by Xu and Froment (1989). Steam reforming, CO_2 producing steam reforming and water gas shift reaction on Ni/δ-Al_2O_3 catalyst are given below.

$$rate_{SR} = \frac{k_{SR}\left(P_{CH4}P_{H2O} - {P_{H2}}^3 P_{CO} \Big/ K_{2,eq}\right)}{{P_{H2}}^{2.5} * (DEN)^2} \tag{2.29}$$

$$rate_{sideSR} = \frac{k_{sideSR}\left(P_{CH4}{P_{H2O}}^2 - {P_{H2}}^4 P_{CO} \Big/ K_{3,eq}\right)}{{P_{H2}}^{3.5} * (DEN)^2} \tag{2.30}$$

$$rate_{WGS} = \frac{k_{WGS}\left(P_{CO}P_{H2O} - P_{H2}P_{CO2} \Big/ K_{4,eq}\right)}{{P_{H2}}^{3.5} * (DEN)^2} \tag{2.31}$$

$$DEN = 1 + K_{CO}P_{CO} + K_{H2}P_{H2} + K_{CH4}P_{CH4} + \frac{K_{H2O}P_{H2O}}{P_{H2}} \tag{2.32}$$

2.3.2. Oxidative Steam Reforming

In order to overcome the heat supplying problem to steam reformer reactor, feed is mixed with oxygen or air, and simultaneous combustion reaction is catalyzed, to provide the heat necessary for hydrogen production (Avci, Önsan, & Trimm, 2001). Reaction temperature is limited with 1100 K, which is the threshold for sintering of nickel particles.

Two exothermic oxidation reactions are available for methane; one of them is well known combustion reaction as in Equation 2.20 and the other one is partial oxidation reaction (POX) which is shown in Equation 2.19. H_2 can be produced by POX (Hickman & Schmidt, 1993). It needs high temperatures, and but as the product of POX has high CO concentration for PEMFC applications, only SR and TOX is considered as the OSR reactions in the simulations.

Platinum is used to catalyze TOX. Light off temperature for methane on platinum is around 600-650 K, and larger hydrocarbon molecules like ethane or propane is easier to activate. Decreasing the hydrocarbon content in the flow increases the light off temperature. Catalytic oxidation of methane fastens with the increase in the concentration of hydrocarbon source when oxygen is enough and slowly loses speed with the decrease in oxygen amount. Langmuir-Hinshelwood type reaction rate law for methane TOX has been given by Ma, Trimm, & Jiang (1996).

$$rate_{TOX} = \frac{k_{TOX}(K^c_{CH4}P^c_{CH4})\sqrt{K^c_{O2}P^c_{O2}}}{\left(1 + K^c_{CH4}P^c_{CH4} + \sqrt{K^c_{O2}P^c_{O2}}\right)^2} \tag{2.33}$$

In order to conduct total oxidation with steam reforming at lower temperatures, small amounts of platinum ranging between 0.1 to 0.3 wt. % is to be added to the catalyst (Avci, Trimm, & Önsan, 2001). It has been shown that sequential impregnation of Pt and Ni gives better performance rather than co-impregnation, and Ni particles are more resistant to oxidation while there is Pt present in the catalyst (Li *et al.*, 2007).

One dimensional simulation for bimetallic catalyst, which includes oxidation and SR, has been conducted in M.S. thesis of Mustafa Karakaya (2006). Simulations based on the kinetic expression given in the works of Xu and Froment (1989), and Numaguchi and Kukichi (1988) has been compared. For steady state simulations kinetics from Xu and Froment and for transient simulations kinetics from Numaguchi and Kukichi has been used.

As a result of TOX and CO_2 producing SR, CO_2 concentration increases along the reactor. Therefore, dry reforming reaction in Equation 2.21 may be a significant side reaction besides water gas shift and oxidation. DR reaction has slow kinetics especially with low carbon dioxide concentrations.

2.3.3. Water Gas Shift Reaction

Even when very high amount of steam is used in SR, carbon monoxide concentration cannot be decreased down below the safe limit for PEM fuel cells. Therefore addition-

al water gas shift reactor has to be installed at the exit of steam reformer. Steam reformer outlet temperatures should be reduced by heat exchangers, because WGS is thermodynamically controlled reaction and it shifts backward at higher temperatures. WGS reactors are also widely used processes for ammonia synthesis. The reaction itself is also a source for hydrogen production in addition to carbon monoxide removal.

There are two suitable temperature ranges for WGS reaction; high temperature shift (HTS) is operable around 350-400 ^{0}C, and low temperature shift (LTS) takes place around 180-250 ^{0}C. In industrial applications, the use of Fe_3O_4/Cr_2O_3 and $Cu/ZnO/Al_2O_3$ is standard for HTS and LTS, respectively. Because of slow kinetics, long preconditioning time and sensitivity to air for these catalysts, research has been conducted for design and development of more stable catalysts under transient conditions. Au-Re on ceria bimetallic catalyst is proved to be superior (Çağlayan & Aksoylu, 2011). Water gas shift reaction reduces the carbon monoxide concentration to 1-3 %.

2.3.4. Preferential Oxidation of Carbon Monoxide

Despite the water gas shift reaction eliminate most of carbon monoxide in the stream, hydrogen rich gas still has high CO concentration which is not acceptable for PEM fuel cell anode. Therefore additional reaction has to be applied in order to reduce the CO content to desired 50 ppm value. Preferential oxidation of CO (PrOX), through which the concentration of CO at the exit stream of WGS reactor of a fuel processor, 1-2%, is selectively decreased down below 50 ppm. There the catalyst must be designed such as not to oxidize valuable H_2 (Kolb, 2008).

Platinum based catalysts are used for preferential oxidation in a temperature range of 50-200 ^{0}C. Excess air has to be supplied in order to achieve O/CO ratio necessary to decrease the CO level of the stream down below 50 ppm at temperatures ca. 110 ^{0}C keeping H_2 oxidation activity as low as possible.

Stream gas which has to be purified from CO is most likely containing CO_2. Research on activated carbon supported Pt-Sn and Pt-Ce systems shows that introduction of carbon dioxide increases the CO conversion while reaching practically 100% CO conversion (Şimşek, Özkara, Aksoylu, & Önsan, 2007).

2.3.5. Methanation

Alternative to PrOX, reverse steam reforming reaction, known as methanation can be applied to reduce CO content in the stream. This reaction has obvious drawback as there is a loss of three molecules of hydrogen for one molecule of CO. If carbon dioxide concentration is high, CO_2 producing steam reforming is also favored and thus the situation worsens due to loss of four molecules of hydrogen per molecule of CO_2.

It has been seen that nickel and ruthenium catalysts are particularly active for methanation reaction. Temperatures should be kept close to 250 ^{0}C. According to literature, most of the CO is converted to methane with nickel on alumina catalyst doped with calcium oxide. Obviously not as efficient as PrOX in reducing CO but is used in order to reduce costs and increase safety of the process as well by preventing additional air inlet. IN papers analyzing methanation as an alternative to decrease CO content of the fuel processor product, it is claimed that as carbon monoxide content is relatively low after WGS, loss of additional hydrogen is acceptable (Men *et al.*, 2007).

2.3.6. Coke Deposition

Reactions in Equations numbered between 2.25 and 2.29 involve solid graphite particles. Especially high temperatures accompanied by low steam and/or low oxygen content in the feed with larger hydrocarbon input quickens the activity loss of the catalysts due to coke deposition. Critical temperature for coke formation through thermal cracking of methane is around 600 ^{0}C under conditions without excess steam (Trimm, 1999).

In order to prevent coke deposition on nickel while increasing hydrogen production, steam to carbon and carbon to oxygen ratio has to be carefully controlled. According to Chan *et al.*, (2000) the minimum O/C ratio should be 0.67 and minimum S/C ratio must be 0.88 for preventing coke formation. Heavier hydrocarbons have greater coke formation tendency (Chan & Wang, 2000).

2.4. Reactor Configuration and Simulations

Oxidative steam reforming simulations have been made for one dimensional platinum and nickel bimetallic catalyst on alumina previously. (Karakaya, 2006) For tubular single channel reactor, two dimensional analysis for which five mm of Ni covered region is followed by one mm of Pt has been simulated by Kurdoğlu (2009). In this study, the simulations were conducted with steam to carbon ratios between 1.5 to 2.5, and carbon to oxygen ratios between 1.9 to 2.3. According to results, temperature of the stream inside the channel was not close to isothermal, and optimal inlet temperature has been determined as 850 K.

Micro channel reactors, for which different channels are coated with different mono metallic catalysts, are commonly used in the literature for simulation works. There precious metals to catalyze oxidation reaction are used in one channel and nickel catalyst for steam reforming reaction in the other. By this way, heat needed for steam reforming is supplied by oxidation proceeds in the neighboring channel. Thermal conductivity of wall material and channel wall thickness are primary control parameters. Due to the fact that thick channel or low thermal conductivity of wall may cause low heat transfer and opposite may result in hot spots for reactor. Three dimensional studies have been conducted by Avci *et al.*, The channel geometry used in that study is given in Figure 2.5 (Avci, Karakaya, & Trimm, 2010).

In another study, a two dimensional simulation was conducted for a micro channel system for which oxidation channel is coated with platinum and reforming channel is coated with rhodium (Zhai, Ding, Cheng, Jin, & Cheng, 2010). There, optimum wall thickness was found as 0.5 mm in simulations conducted utilizing FLUENT.

A similar three dimensional geometry, with square channels and additional micro baffles, was used for isooctane fuel feed. Simulations were conducted with COMSOL™, and 0.4 mm is found as optimal thickness while baffles were found increasing hydrogen yield of the reactor (Karakaya & Avci, 2011).

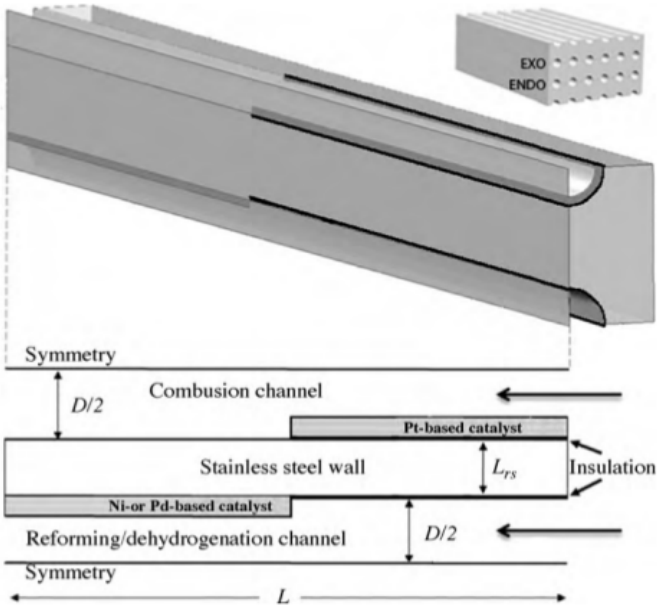

Figure 2.5. Geometry and boundary conditions of microchannel reactor that has been simulated (Avci, Karakaya, & Trimm, 2010).

3. MATHEMATICAL AND COMPUTER MODELING

3.1. Geometry

In the current study, oxidative steam reforming of methane is studied on nine channels, which satisfy the symmetry conditions to represent a wall coated microreactor. The inner walls of the each channel are modeled as coated with bimetallic Pt-Ni catalytic system with a predetermined Ni:Pt ratio. The inlet feed having experimentally designed gas composition is assumed homogenous, and in order to achieve fully developed flow, 12 mm at the entrance of reactor and the last five mm at the exit of the reactor is used as mixing regions and kept catalyst free.

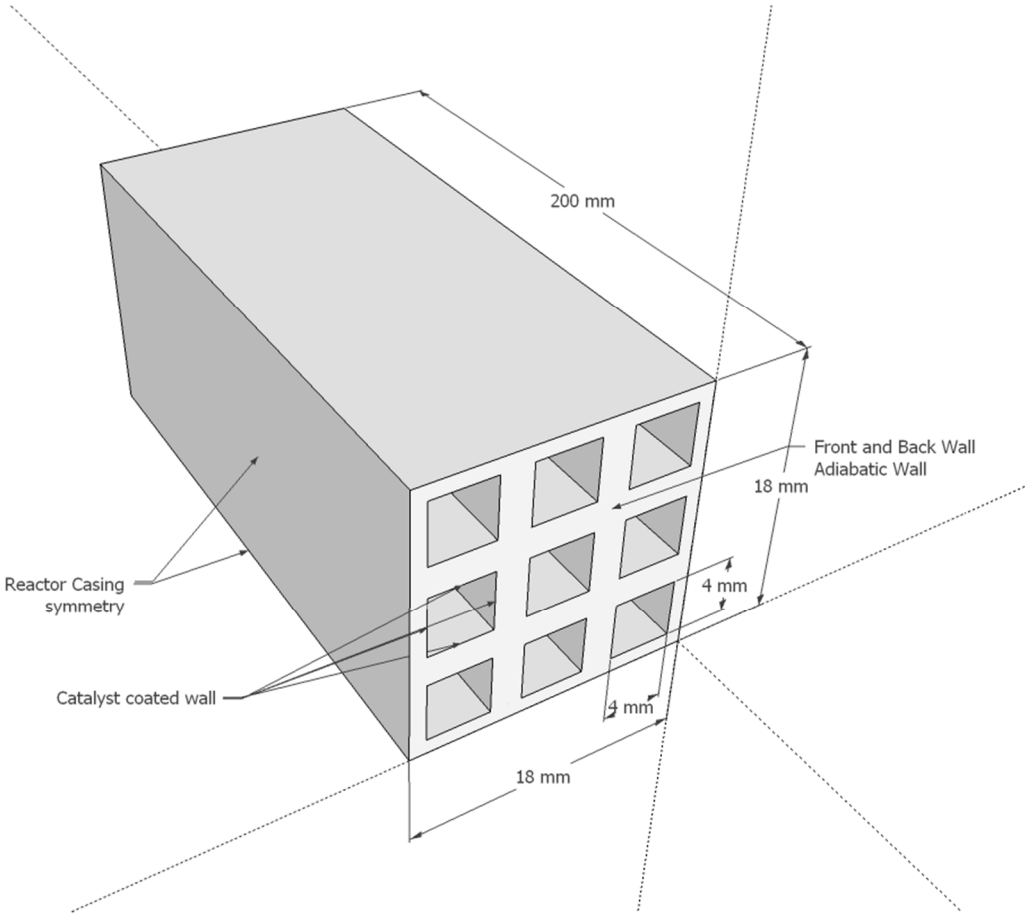

Figure 3.1. Reactor geometry and types of wall boundary conditions.

3.2. Catalyst Dispersion

Pt-Ni bimetallic catalyst system with two different Ni:Pt ratio surface molar ratio, 20 and 30 are modelled on the inner walls of the nine channels. There, Pt and Ni metal sites are randomly distributed through the use of “rand” function of Excel, which generates random numbers by uniform distribution method (Figures 3.1 and 3.2). Pt and Ni clusters are shown by yellow and red areas while blue areas represent catalyst free zones.

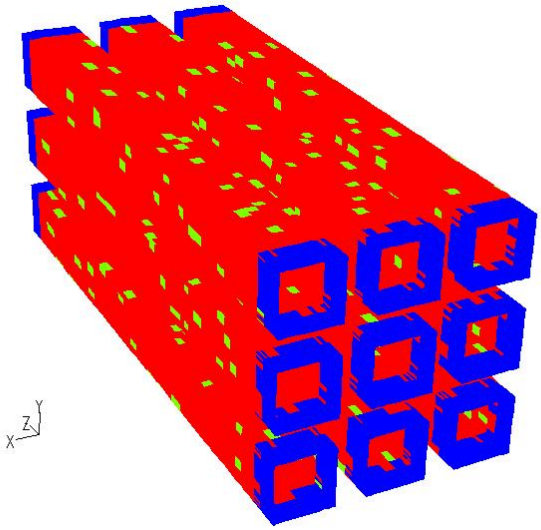

Figure 3.2. Catalysts after randomly dispersed in Pt:Ni ratio of 1:20.

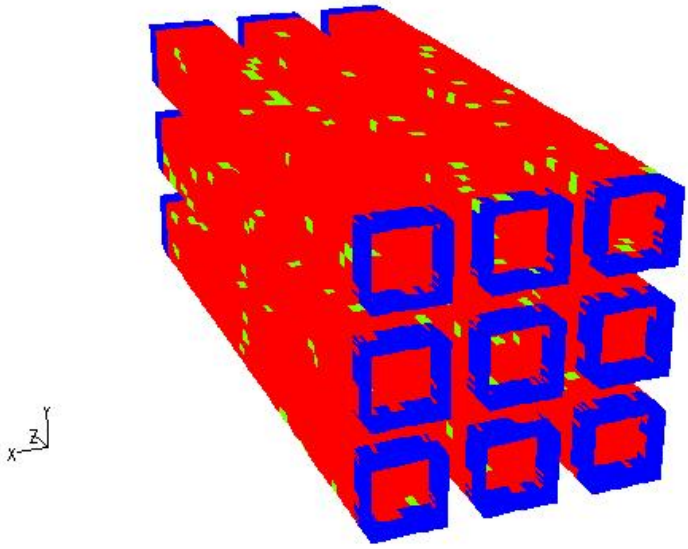

Figure 3.3. Catalysts after randomly dispersed in Pt:Ni ratio of 1:30.

3.3. Assumptions

The assumptions of the current work are listed below:

(i) Nickel and platinum do not interact and/or form alloy with each other.
(ii) Flow is uniformly distributed between the channels.
(iii) Possible steam reforming reaction on platinum and total oxidation reaction on nickel sites are neglected.
(iv) Only combustion (Equation 2.19) on Pt sites and, steam reforming (Equation 2.16), CO_2-producing steam reforming (Equation 2.17) and water gas shift (Equation 2.21) reactions on Ni sites are taken into account.
(v) Material properties are changing linear with temperature.
(vi) Possible coke deposition, especially for low S/C and high C/O_2 cases, on the metallic surface is neglected.
(vii) Catalyst deactivation due to sintering, poisoning or oxidation is neglected.
(viii) Ideal gas model is applied to fluid mixture.
(ix) Laminar flow condition is assumed. As (Re is between 40-100)
(x) Flow is assumed incompressible, and pressure loss is considered insignificant.
(xi) Steady state conditions are achieved.
(xii) Diffusion through Al_2O_3 is neglected.

3.4. Transport Equations

3.4.1. Equations

In order to model the flow with reaction, equations of motion, continuity, energy and species are simultaneously solved for Cartesian coordinates (Versteeg & Malalasekera, 1995). '$\boldsymbol{\Phi}$' is dissipation source term that caused mainly from the heat released due to friction. S_i is source term that comes from the heat released or absorbed by the reactions. 'S_{Mx}', 'S_{My}', 'S_{Mz}' are source terms for Navier Stokes equation, which resembles body forces namely gravity.

$$(\nabla \cdot \rho \boldsymbol{u}) + \frac{\partial \rho}{\partial t} = 0 \tag{3.1}$$

$$\frac{\partial(\rho u)}{\partial t} + (\nabla \cdot \rho u \boldsymbol{u}) = -\frac{\partial p}{\partial x} + \left(\nabla \cdot \mu(\nabla u)\right) + S_{Mx} \tag{3.2}$$

$$\frac{\partial(\rho v)}{\partial t} + (\nabla \cdot \rho v \boldsymbol{u}) = -\frac{\partial p}{\partial y} + \left(\nabla \cdot \mu(\nabla v)\right) + S_{My} \tag{3.3}$$

$$\frac{\partial(\rho w)}{\partial t} + (\nabla \cdot \rho w \boldsymbol{u}) = -\frac{\partial p}{\partial z} + \left(\nabla \cdot \mu(\nabla w)\right) + S_{Mz} \tag{3.4}$$

$$\frac{\partial(\rho i)}{\partial t} + (\nabla \cdot \rho i \boldsymbol{u}) = -p(\nabla \cdot \boldsymbol{u}) + \left(\nabla \cdot k(\nabla T)\right) + \Phi + S_i \tag{3.5}$$

$$\Phi = \mu\left\{2\left[\left(\frac{\partial u}{\partial x}\right)^2 + \left(\frac{\partial v}{\partial y}\right)^2 + \left(\frac{\partial w}{\partial z}\right)^2\right] + \left(\frac{\partial u}{\partial y} + \frac{\partial w}{\partial x}\right)^2 + \left(\frac{\partial u}{\partial z} + \frac{\partial w}{\partial x}\right)^2 + \left(\frac{\partial v}{\partial z} + \frac{\partial w}{\partial y}\right)^2 - \frac{2}{3}(\nabla \cdot \boldsymbol{u})^2\right\} \tag{3.6}$$

$$\frac{\partial(C_j)}{\partial t} + \left(\nabla \cdot C_j \boldsymbol{u}\right) = -p\left(\nabla \cdot \boldsymbol{J_j}\right) + R_j \tag{3.7}$$

3.4.2. Boundary Conditions

In the simulations: temperature, mass fractions of species, and flow rate (or velocity normal to the boundary) are needed to be supplied. These values are tabulated in Table 4.1 and 4.2. Driving force for flow is the pressure gradient.

3.5. Solution of Partial Differential Equations

Partial differential equations are discretized which involves the substitution of approximation for sources to obtain a set of algebraic equations. Semi-implicit method for pressure linked equations algorithm (SIMPLE) is used for pressure-velocity coupling. The algorithm given in Figure 3.4, utilizes the equations below.

Discretized momentum equations:

$$a_{i,J}u^*_{i,J} = \sum a_{nb}\, u^*_{nb} + \left(p^*_{I-1,J} - p^*_{I,J}\right)A_{i,J} + b_{i,J} \tag{3.8}$$

$$a_{I,j}u^*_{I,j} = \sum a_{nb}\, v^*_{nb} + \left(p^*_{I,J-1} - p^*_{I,J}\right)A_{I,j} + b_{I,j} \tag{3.9}$$

$$p = p^* + p' \tag{3.10}$$

$$u = u^* + u' \tag{3.11}$$

$$v = v^* + v' \tag{3.12}$$

Pressure correction equation:

$$a_{I,J}p'_{I,J} = a_{I-1,J}p'_{I-1,J} + a_{I+1,J}p'_{I+1,J} + a_{I,J-1}p'_{I,J-1} + a_{I,J+1}p'_{I,J+1} + b'_{I,j} \tag{3.13}$$

Pressure and velocities are corrected, through equations below:

$$p_{I,J} = p^*_{I,J} + \alpha_p p'_{I,J} \tag{3.14}$$

$$u_{i,J} = u^*_{i,J} + d_{i,J}(p'_{I-1,J} - p'_{I,J}) \tag{3.15}$$

$$v_{I,j} = v^*_{I,j} + d_{I,j}(p'_{I,J-1} - p'_{I,J}) \tag{3.16}$$

All the discretized transport equations are solved to obtain new source term

$$a_{I,J}\phi_{I,J} = a_{I-1,J}\phi_{I-1,J} + a_{I+1,J}\phi_{I+1,J} + a_{I,J-1}\phi_{I,J-1} + a_{I,J+1}\phi_{I,J+1} + b\phi_{I,J} \tag{3.17}$$

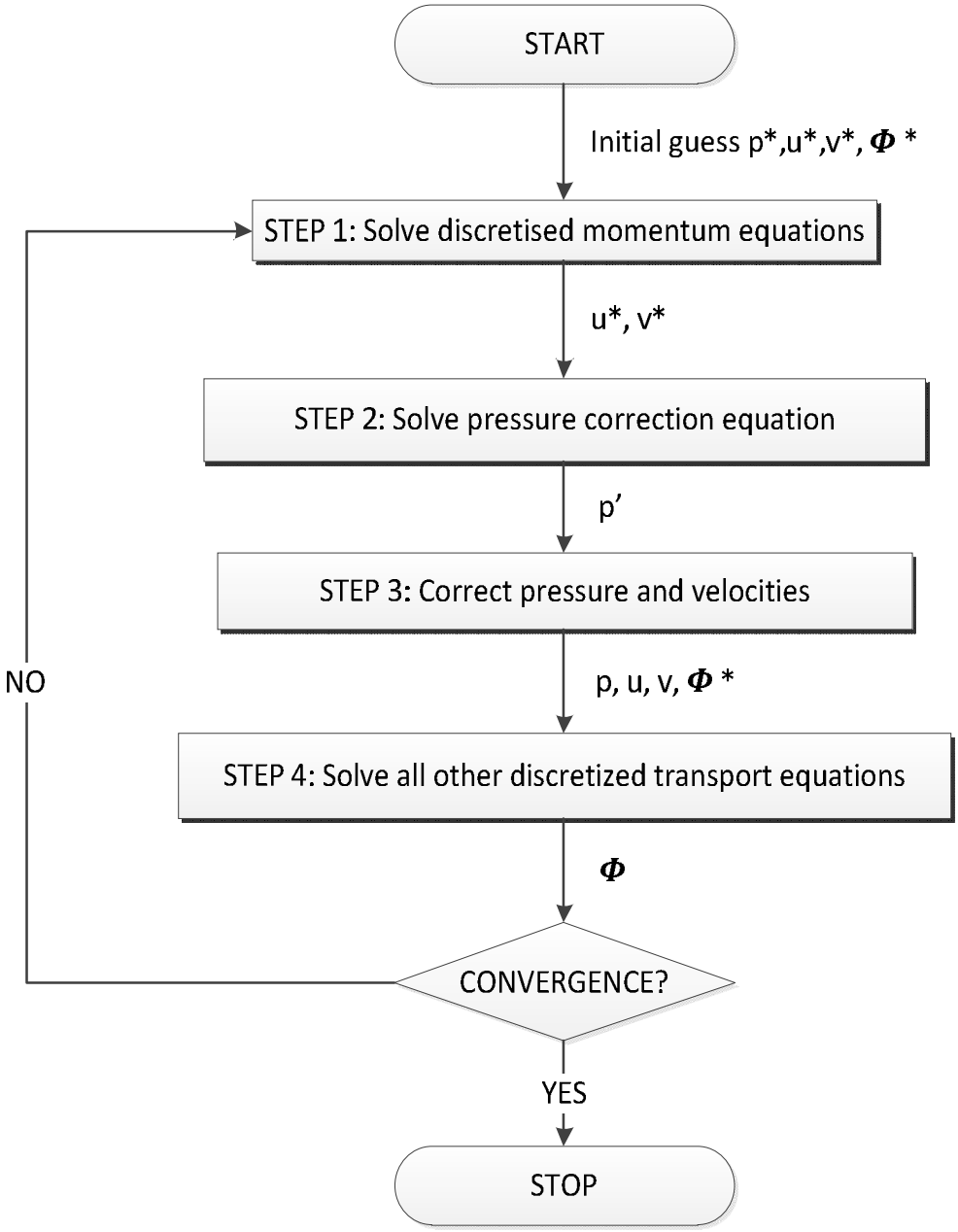

Figure 3.4. Algorithm of SIMPLE velocity-pressure coupling method.

FLUENT™ 6.3.26 for Linux edition is used in simulations. Implicit formulation with absolute velocity formulation is selected. Green-Gauss cell based gradient option is checked on. Stiff chemistry solver adjusted to iterate once per chemistry update. Surface reactions are input via user defined functions, for the wall surface like Pt and Ni dispersion map.

Linear discretization for partial differential equations is made with second order upwind method except pressure parameter, which uses standard discretization technique. “Under relaxation parameter” for pressure, momentum and energy are 0.3, 0.7 and 0.995,

respectively. Fractions of species and velocities for each coordinate have no relaxation. Convergence criteria for continuity and momentum equations are 10^{-3}, while species and energy equations have convergence value of 10^{-6}.

3.6. Grid Structure

The grid structure has been generated through the use of GAMBIT™ 2.3.16. Cooper type of grid pavement selected for meshing the volume. Boundary layer is taken as 0.1 mm thick and widens with multiple of 1.3. Generated grid structure is shown in Figure 3.2. Each channel is four millimeter in both width and height and has a length of 200 mm. Overall dimensions of the model are 18 x 18 x 200 mm.

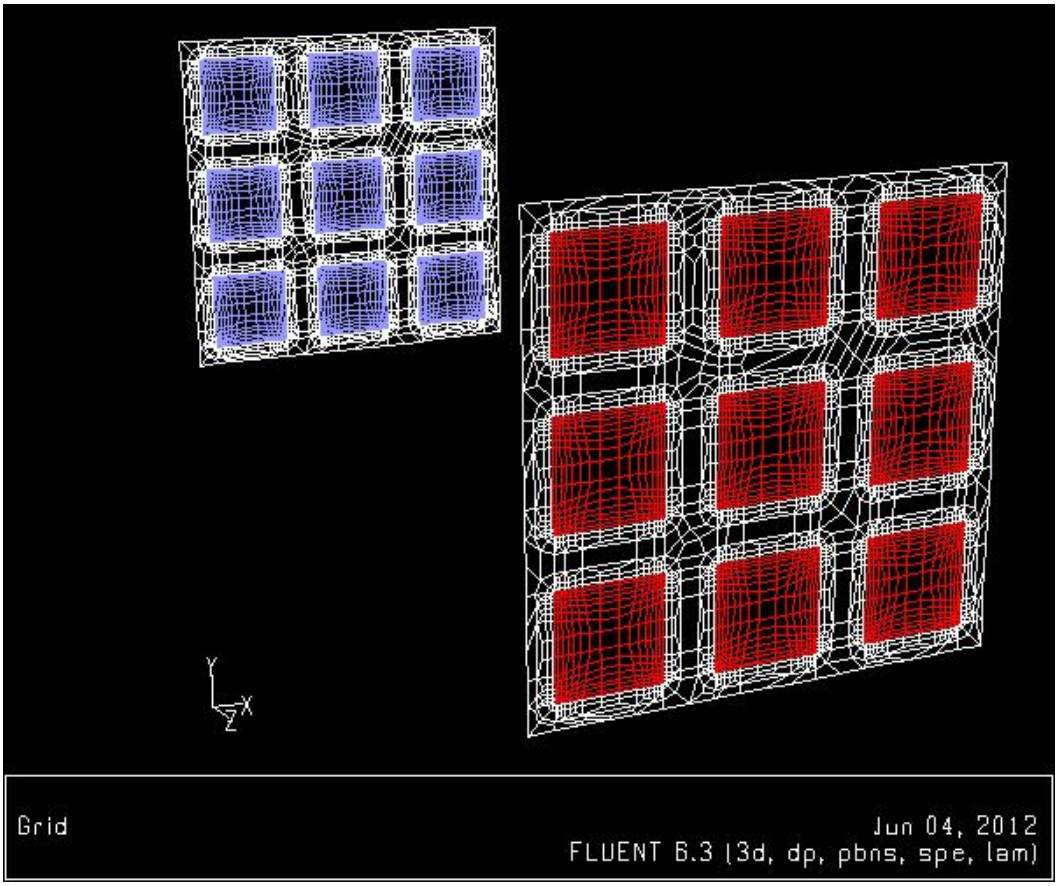

Figure 3.5. Meshed geometry of front and backside of reactor, red and blue color signifies fluid inlet and outlet respectively while white is reactor front and back wall.

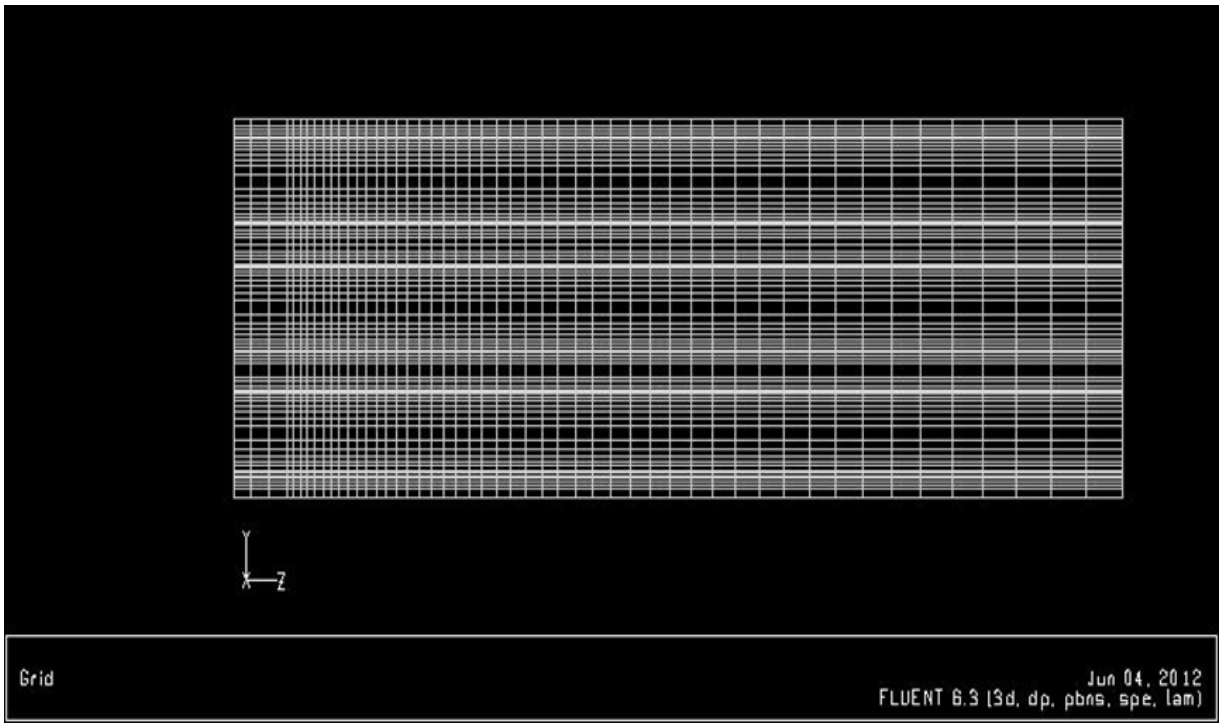

Figure 3.6. Meshed geometry along z direction.

In the model 211350 cells, 667077 faces, two cell zones and eight face zones are meshed. Grid refinement has been done and it has bee assured that solution is grid independent.

3.7. Reaction Kinetics

3.7.1. Total Oxidation

Total oxidation reaction (TOX) is given below.

$$CH_4 + 2O_2 \longrightarrow CO_2 + 2H_2O \qquad \Delta H_{rxn}{}^0 = -802.9 \qquad (2.19)$$

Langmuir Hinshelwood type kinetics for methane oxidation reaction on Pt/Al_2O_3 has been taken from the works of Ma, Trimm, & Jiang (1996). Total platinum metal surface area is 0.35 m^2/g. R is gas constant and is equal to 8.314 J/mol K. Kinetic equation for methane TOX, temperature dependence of reaction rate constant and adsorption coefficients of methane and oxygen is given in Table 3.1.

Table 3.1. Kinetic parameters of total oxidation reaction.

$rate_{TOX} = \frac{k_{TOX}(P^c_{CH4})\sqrt{P^c_{O2}}}{\left(1 + K^c_{CH4}P^c_{CH4} + K^c_{O2}\sqrt{P^c_{O2}}\right)^2}$	$\left(\frac{mol}{gcat\ h}\right)$	(3.18)
$k_{TOX} = (5.852 \times 10^{17})exp\left(\frac{-204000}{RT}\right)$	$\left(\frac{1}{bar}\right)^{1.5}$	(3.19)
$K^c_{CH4} = (4.020 \times 10^{5})exp\left(\frac{-103500}{RT}\right)$	$\left(\frac{1}{bar}\right)$	(3.20)
$K^c_{O2} = (5.080 \times 10^{4})exp\left(\frac{-66200}{RT}\right)$	$\left(\frac{1}{bar}\right)$	(3.21)

3.7.2. Steam Reforming and Side Reactions

Steam reforming reactions with significant side reactions are modeled from the Langmuir Hinshelwood type kinetics acquired from the works of Xu and Froment. (1989) Total nickel metal surface area is 9.3 m^2/g.

SR: $CH_4 + H_2O \leftrightharpoons CO + 3H_2$ $\Delta H_{rxn}{}^0 = 206.2$ (2.16)

Side SR: $CH_4 + 2H_2O \leftrightharpoons CO_2 + 4H_2$ $\Delta H_{rxn}{}^0 = 165.1$ (2.17)

WGS: $CO + H_2O \leftrightharpoons CO_2 + H_2$ $\Delta H_{rxn}{}^0 = -40.4$ (2.21)

Rate equations of CO and CO_2 producing SR and WGS reactions, and temperature dependence of rate constants and adsorption coefficients of carbon monoxide, carbon dioxide, methane, and steam have been tabulated in Table 3.2.

Table 3.2. Kinetic parameters of steam reforming and side reactions.

Equation of kinetic parameter	Unit of left hand side	Equation number
$rate_{SR} = \frac{k_{SR}\left(P_{CH4}P_{H2O} - {P_{H2}}^3 P_{CO} / K_{2,eq}\right)}{{P_{H2}}^{2.5} \times (DEN)^2}$	$\left(\frac{mol}{gcat\ h}\right)$	(3.22)
$rate_{sideSR} = \frac{k_{sideSR}\left(P_{CH4}{P_{H2O}}^2 - {P_{H2}}^4 P_{CO} / K_{3,eq}\right)}{{P_{H2}}^{3.5} \times (DEN)^2}$	$\left(\frac{mol}{gcat\ h}\right)$	(3.23)
$rate_{WGS} = \frac{k_{WGS}\left(P_{CO}P_{H2O} - P_{H2}P_{CO2} / K_{4,eq}\right)}{{P_{H2}}^{3.5} \times (DEN)^2}$	$\left(\frac{mol}{gcat\ h}\right)$	(3.24)
$k_{SR} = (4.225 \times 10^{15}) exp\left(\frac{-240100}{RT}\right)$	$\left(\frac{1}{bar}\right)$	(3.25)
$k_{SRside} = (1.020 \times 10^{15}) exp\left(\frac{-243900}{RT}\right)$	$\left(\frac{1}{bar}\right)$	(3.26)
$k_{WGS} = (1.955 \times 10^{6}) exp\left(\frac{-67130}{RT}\right)$	$\left(\frac{1}{bar}\right)$	(3.27)
$K_{2,eq} = (5.750 \times 10^{12}) exp\left(\frac{-11476}{RT}\right)$	bar^2	(3.28)
$K_{3,eq} = (7.240 \times 10^{10}) exp\left(\frac{-21646}{RT}\right)$	bar^2	(3.29)
$K_{4,eq} = (1.260 \times 10^{-2}) exp\left(\frac{4639}{RT}\right)$	-	(3.30)
$DEN = 1 + K_{CH_4}P_{CH_4} + K_{H_2}P_{H_2} + K_{CO}P_{CO} + \frac{K_{H_2O}P_{H_2O}}{P_{H_2}}$	-	(3.31)
$K_{CH_4} = (6.650 \times 10^{-4}) exp\left(\frac{38280}{RT}\right)$	$\left(\frac{1}{bar}\right)$	(3.32)
$K_{H_2} = (6.120 \times 10^{-9}) exp\left(\frac{82900}{RT}\right)$	$\left(\frac{1}{bar}\right)$	(3.33)
$K_{CO} = (8.230 \times 10^{-5}) exp\left(\frac{70650}{RT}\right)$	$\left(\frac{1}{bar}\right)$	(3.34)
$K_{H_2O} = (1.770 \times 10^{5}) exp\left(\frac{-11476}{RT}\right)$	-	(3.35)

3.8. Properties of Materials and Mixture

Table 3.3. Thermodynamic properties of species (Sinnott, 2000).

Species	MW kg/kmol	ΔH_f^0 kj/kmol	$C_{p,Ref}$ j/molK
CH_4	16.043	-74860	35.55
O_2	31.999	0	29.37
CO_2	44.010	-393770	37.16
H_2O	18.015	-242000	33.66
CO	28.010	-110620	29.18
H_2	2.016	0	28.88
N_2	28.013	0	29.18

3.8.1. Heat Capacity

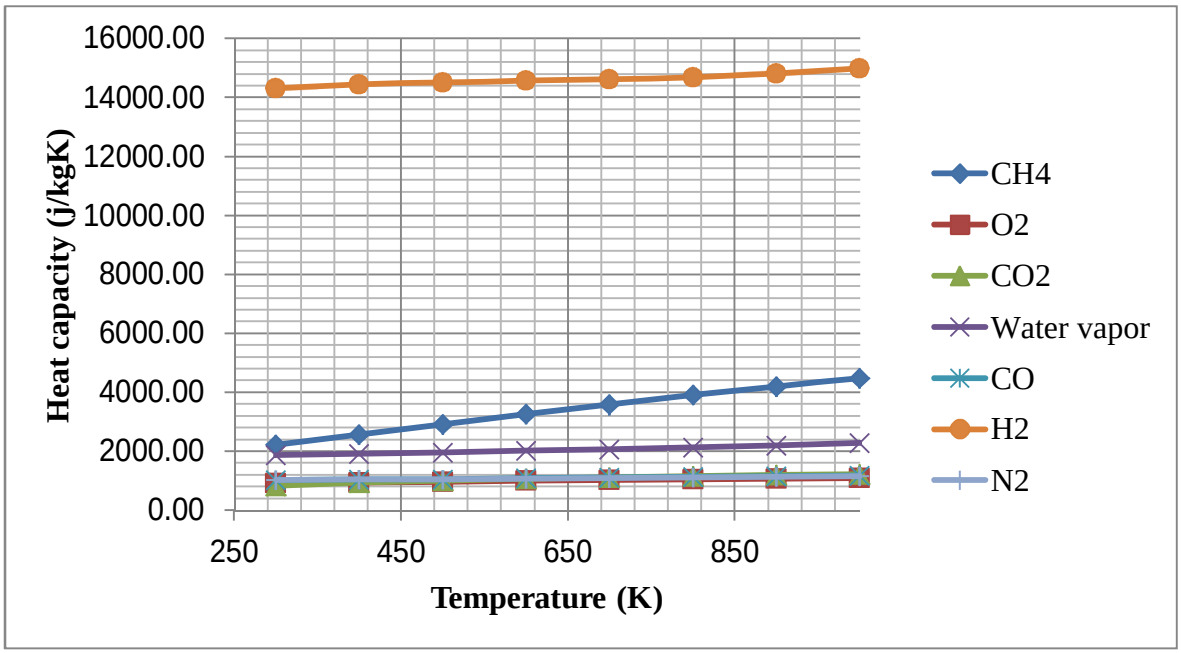

Figure 3.7. Heat capacities of species per kg versus temperature (Sinnott, 2000).

Heat capacity is assumed as a linear function of temperature for each species.

$$C_P = \sum_i x_i C_{P,i} \tag{3.36}$$

Heat capacity of species mixture is calculated according to ideal gas.

3.8.2. Viscosity

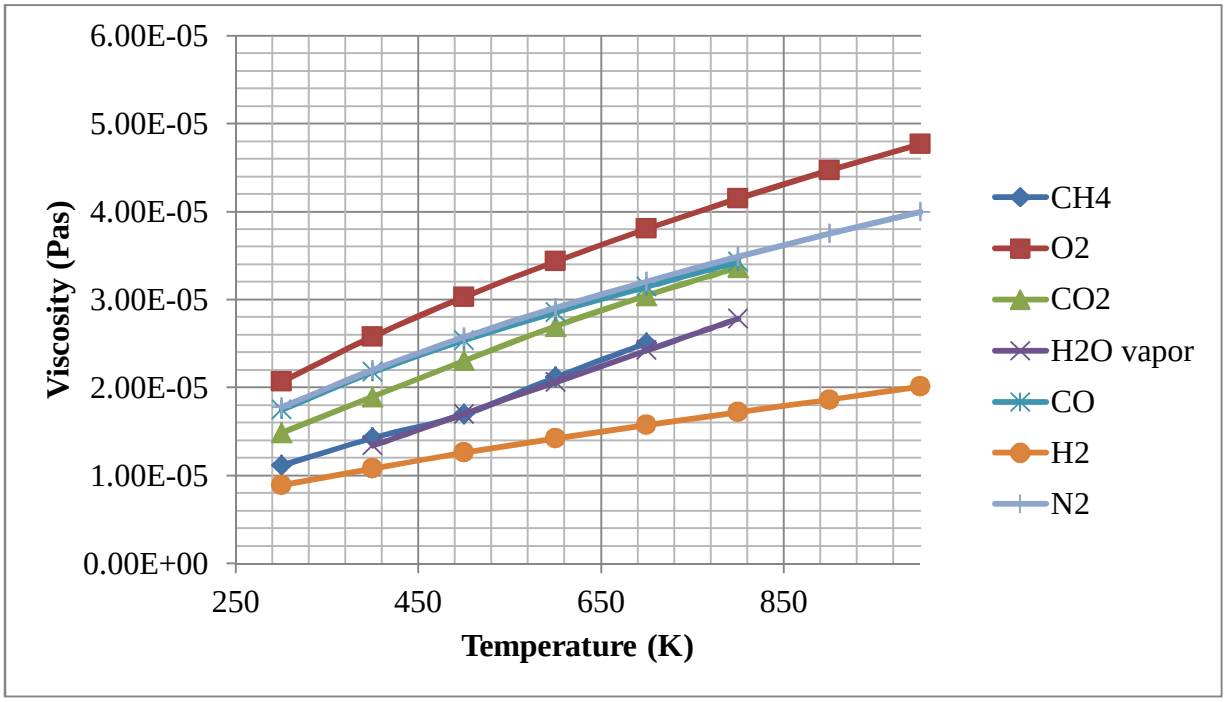

Figure 3.8. Viscosity of species versus temperature (Poling, Prausnitz, & O'Connell, 2001).

Viscosity is assumed as a linear function of temperature for each species. Ideal gas mixing law is applied to compute mixture viscosity.

$$\mu = \sum_i \frac{x_i \mu_i}{\sum_j x_j \phi_{ij}}; \quad \phi_{ij} = \frac{\left[1 + \left(\mu_i / \mu_j\right)^{1/2} \left(M_{w,j} / M_{w,i}\right)^{1/4}\right]^2}{\left[8\left(1 + M_{w,j} / M_{w,i}\right)\right]^{1/2}} \tag{3.37}$$

3.8.3. Thermal Conductivity

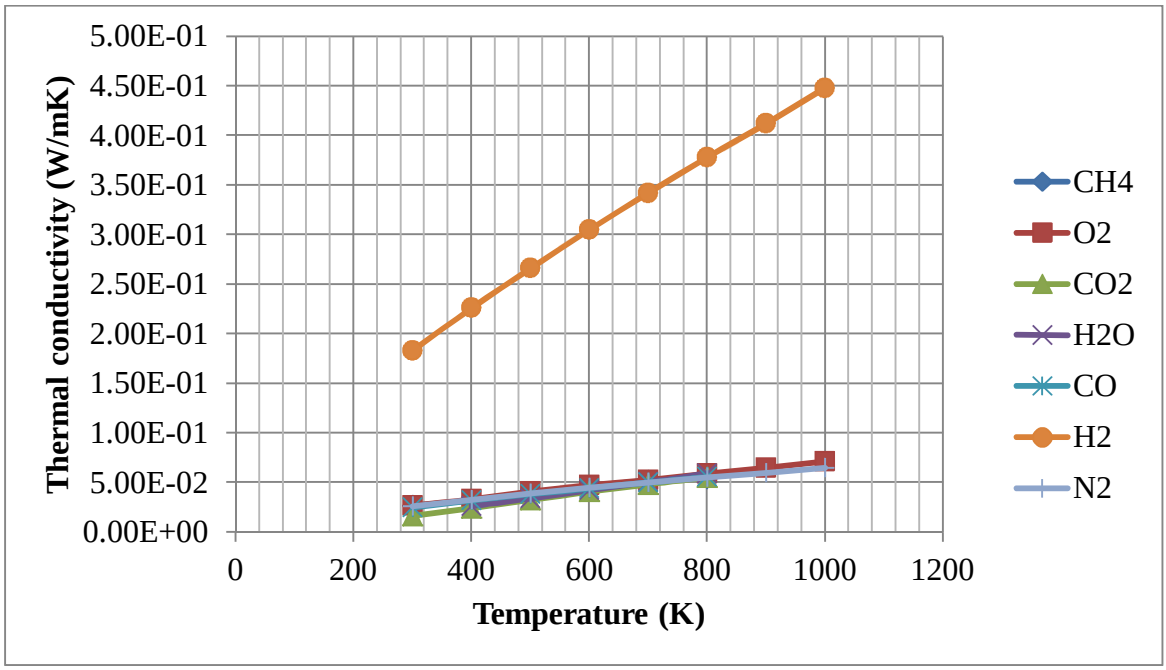

Figure 3.9. Thermal conductivity of species versus temperature (Poling, Prausnitz, & O'Connell, 2001).

Thermal conductivity is assumed a linear function of temperature for each species. Ideal gas mixing law is applied to compute thermal conductivity of mixture.

$$k = \sum_i \frac{x_i k_i}{\sum_j x_j \phi_{ij}}; \quad \phi_{ij} = \frac{\left[1 + \left(\mu_i/\mu_j\right)^{1/2} \left(M_{w,j}/M_{w,i}\right)^{1/4}\right]^2}{\left[8\left(1 + M_{w,j}/M_{w,i}\right)\right]^{1/2}} \tag{3.38}$$

Thermal conductivity of delta alumina wall is taken as 20 W/m K.

3.8.4. Enthalpy of Reaction

Enthalpy of reaction is calculated for different temperatures with the method presented in Equation 3.39.

$$\Delta H_{rxn}(T) = \sum_{reactants} \int_{T}^{T_{ref}} C_p \, dT + \Delta H^0_{rxn} + \sum_{products} \int_{T_{ref}}^{T} C_p \, dT \tag{3.39}$$

Table 3.4. Enthalpy of simulated reactions for different temperatures.

Temp.(*K*)	298	500	600	700	800	900	1000
$\Delta H_{rxn,TOX}\left(\frac{kj}{mol}\right)$	-802.9	-801.8	-802.0	-802.9	-804.8	-807.7	-811.8
$\Delta H_{rxn,SR}\left(\frac{kj}{mol}\right)$	206.2	214.2	217.0	219.0	220.2	220.3	219.4
$\Delta H_{rxn,sSR}\left(\frac{kj}{mol}\right)$	165.1	179.8	185.5	191.3	197.2	203.2	209.4
$\Delta H_{rxn,WGS}\left(\frac{kj}{mol}\right)$	-41.2	-40.4	-40.2	-40.3	-41.0	-42.5	-45.0

4. RESULTS AND DISCUSSION

Methane oxidative steam reforming is simulated three dimensionally in nine wall-coated channels representing a micro reactor. The walls of the reactor channels are made of Al_2O_3 and coated with nickel and platinum, which are randomly dispersed with pre-determined Pt:Ni ratios on each channel. Inlet gases are homogenously mixed and, in order to achieve fully developed flow, first 12 mm at the entrance of the reactor and last 5 mm at the exit of the reactor are used as mixing zones; for mixing zones, the walls of the channels are catalyst free.

Under the light of previous experimental findings, steam to carbon and oxygen to carbon ratio in the feed stream, platinum and nickel ratio on the reactor wall and the inlet temperature of the feed stream are considered as parameters in simulations (Gökaliler, Göçmen, & Aksoylu, 2008). Steam to carbon ratio is kept higher than a certain level in order to guarantee the conditions preventing coke deposition on the reactor walls. Operating conditions for oxidative steam reforming reactor are given in Table 4.1. Considering the depletion of oxygen in the feed in a 200 mm long reactor even for 723 K and for Ni:Pt=30, length of the channels is taken as 200 mm.

Table 4.1. Operating conditions of reactor.

Operating pressure	1 bar	
Reactor length	200 mm	
Channel width / height	4 mm	4 mm
Wall thickness	2 mm	
Channel volume	3200 mm^3	
Reactor volume with walls / without walls	64800 mm^3	28800 mm^3
Void ratio	0.447	
Reactor surface area (Total / per channel)	288 cm^2	32 cm^2
Catalyst coated surface area (Total / per channel)	263.5 cm^2	29.3 cm^2
Flow rate (Total / per channel)	27cm^3/s	3cm^3/s
Inlet velocity normal to boundary	0.1875 m/s	
Catalyst weight per surface area Pt / Ni	0.35 m^2/g	9.30 m^2/g

There are two different Pt:Ni ratios and four different inlet temperature levels used in the simulations and nine different set of conditions, i.e. “Cases”, are used for each “inlet temperature level-Pt:Ni ratio” combinations making total of 72 simulations (Table 4.2). In Table 4.2, carbon to oxygen (C/O_2) and steam to carbon (S/C) ratios used in the feed stream are tabulated along with the mass fractions of CH_4, O_2, H_2O and N_2 in the corresponding feed streams. It should be noted that as the composition of inlet feed changes for each case, molecular weight of mixture is not constant.

Table 4.2. The conditions that are used in simulations.

	C/O_2	H_2O/C	CH_4	O_2	H_2O	N_2	Molecular Weight
case1	1.50	2.35	0.10679	0.14239	0.28234	0.46847	22.967
case2	2.00	2.35	0.12604	0.12604	0.33323	0.41468	22.154
case3	2.70	2.35	0.14659	0.10859	0.38756	0.35726	21.347
case4	1.50	3.00	0.09906	0.13208	0.33432	0.43454	22.517
case5	2.00	3.00	0.11541	0.11541	0.38950	0.37969	21.730
case6	2.70	3.00	0.13240	0.09808	0.44686	0.32267	20.964
case7	1.50	4.00	0.08913	0.11884	0.40107	0.39097	21.964
case8	2.00	4.00	0.10215	0.10215	0.45965	0.33606	21.225
case9	2.70	4.00	0.11524	0.08536	0.51857	0.28084	20.530

Simulations were conducted by utilizing FLUENT™ version 6.3.26 and hydrogen yield, methane conversion and carbon monoxide to hydrogen ratio (CO/H_2) in the product stream are tabulated for each simulation case at Tables 4.3 and 4.4 on page 65. It should be noted that, reactor temperature and concentration of species in the channel indicate temperature and concentration of species at or along the center line of the channel. It is explicitly specified when temperature and/or concentration of species at the channel wall is reported. Hydrogen yield is defined as the ratio of moles of hydrogen produced per moles of methane consumed.

4.1. Temperature Profile Along the Reactor

4.1.1. Effect of Inlet Temperature on Temperature Profile

Reactor temperature and wall temperature of channels are important parameters in studying the hot spot formation along the reactor as well as course of reaction. In studying the effect of inlet temperature on the reactor and channel wall temperature profiles, results obtained from the simulation performed for case 5, which has moderate S/C and C/O_2 ratios in the feed, for a reactor having Ni:Pt = 20 metal loading ratio, running at 923 K feed temperature are used first in the reporting the trends, then are used as a reference base in analyzing the changes of temperature profiles between the cases. The results obtained from case 5 with Ni:Pt = 20 metal loading ratio reveal that, temperature of the reactor and channel walls near inlet are warmer than rest of the reactor (Figure 4.1). Rapid consumption of oxygen led by fast total oxidation near inlet area is the main reason for sudden increase in temperature.

Reactor temperature changes between from 917 to 940 K. High thermal conductivity of Al_2O_3 monolith reactor wall results in large heat flow from the total oxidation dominated parts of the reactor close to inlet to the steam reforming dominated parts. Additionally, presence of Ni sites catalyzing SR near the inlet is another factor limiting the temperature rise at total oxidation dominated part of the channel. On the other hand, heat coming from the TOX dominated part of the reactor is fastly conducted steam reforming (SR) dominated part with the help of high conductivity of walls, and thus, the temperature decrease is very gradual for SR dominated part of the reactor.

The temperature and concentration profiles obtained from the simulations for other cases for 923 K feed temperature follow similar trends with that obtained from case 5. On the other hand, upper and lower limits of reactor temperature are 923 and 958 K for case 1 having the highest temperatures, and 931 and 905 K for case 9, having the lowest temperatures respectively.

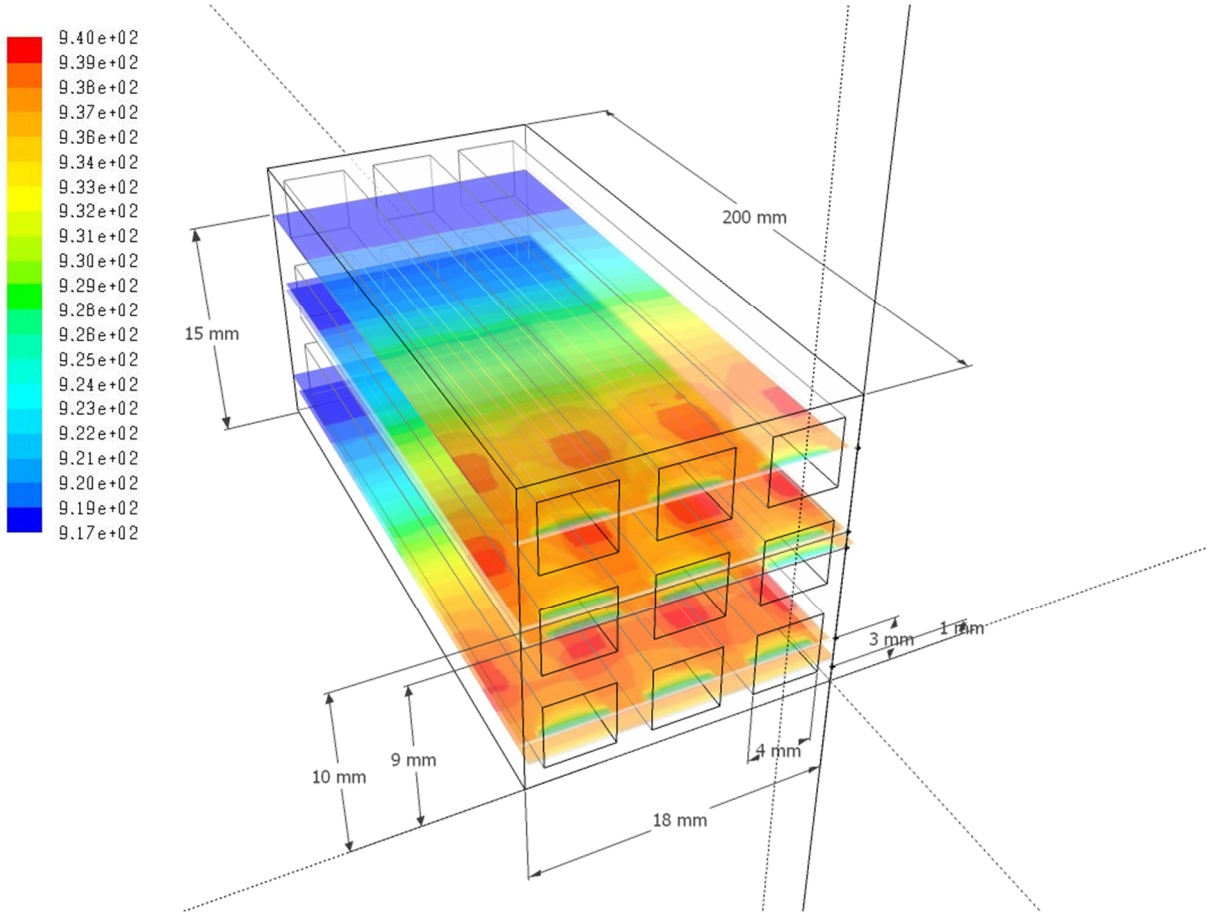

Figure 4.1. Temperature profile along the reactor for different layers, for case 5 with inlet temperature of 923 K, C/O_2 ratio of 2, S/C ratio of 3 and Ni:Pt ratio of 20.

Temperature profile of central line and catalyst walls are plotted in Figure 4.2 for case 5; as can be seen in Figure 4.2 and 4.3, the wall temperature is slightly higher at the inlet due to fast oxidation kinetics and gets colder along the channel as going away from the inlet with the domination of endothermic steam reforming reaction due to scarcity of oxygen. Walls near inlet are warmer than average temperature of the channel and part of the walls far from inlet.

The reason of sudden temperature increase near the inlet region is the presence of nonreaction region at the entrance followed by a catalytic zone for which total oxidation dominates. It should be noted that the conduction from total oxidation dominated zone to non reaction region through the wall led to higher wall temperatures at the entrance compared to the temperature of the central line. On Figure 4.2, there are two peaks which points out the existence of micro steam reforming dominated region at the entrance of reac-

tor caused by random catalyst dispersion. Wall temperature is more uniform for feed with 1023 K inlet temperature (Figure 4.3).

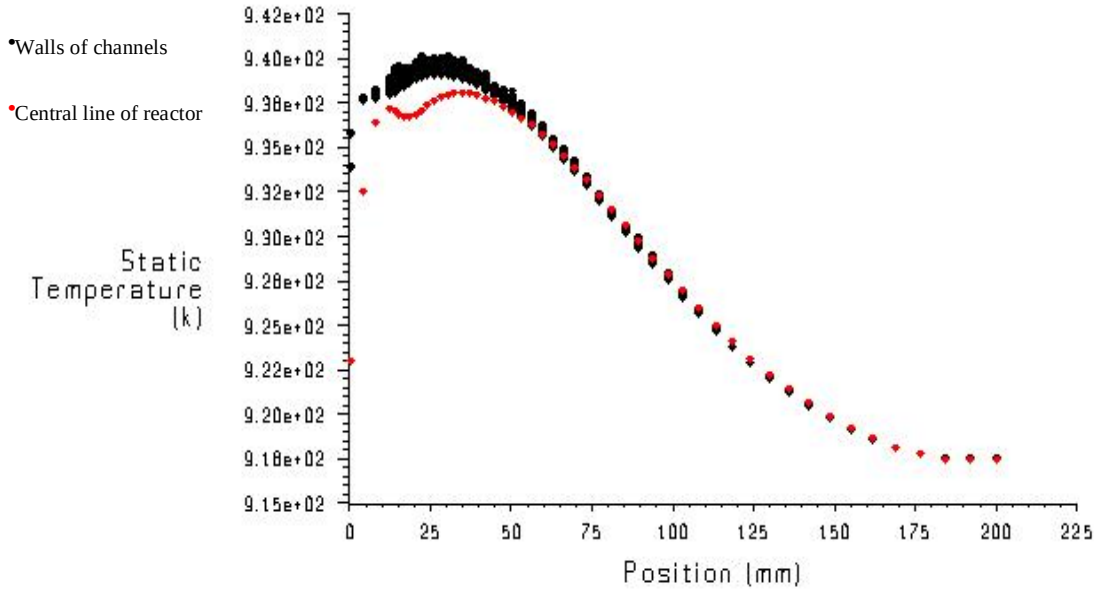

Figure 4.2.Tempearature of walls (black) and central line of central channel (red) for case 5 with 923 K inlet temperature, C/O_2 ratio of 2, and H_2O/C ratio of 3.

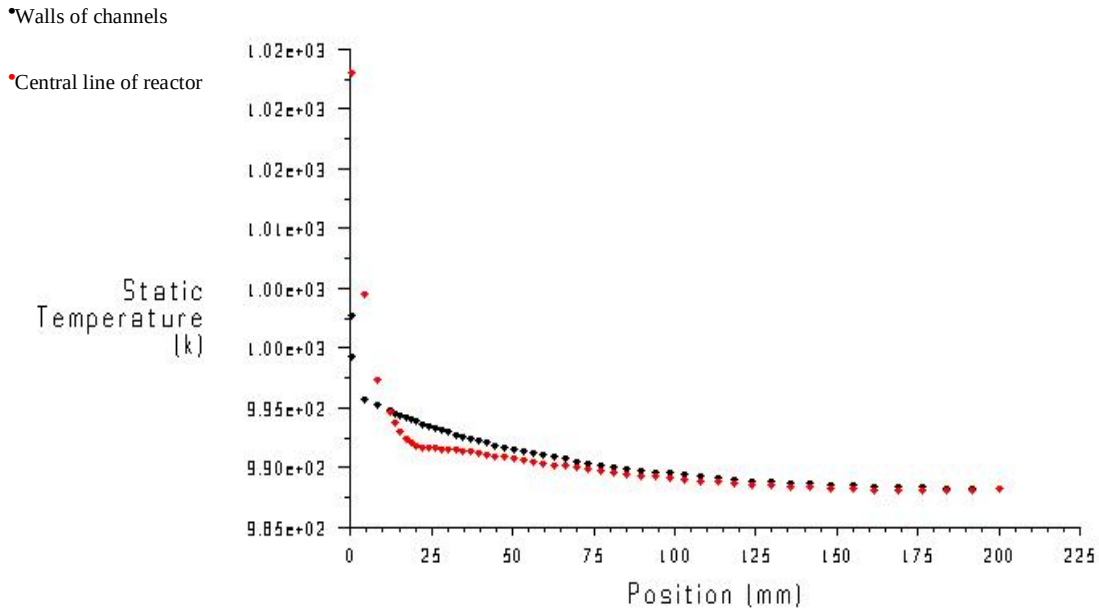

Figure 4.3. Temperature of walls (black) and central line of central channel (red) for case 5 with 1023 K inlet temperature, C/O_2 ratio of 2, and H_2O/C ratio of 3.

Distinct temperature profiles are obtained for different inlet temperatures. Except the case with inlet temperature of 1023 Kelvin, temperature profiles have similar shapes; temperature sharply rises following the mixing zone, its increase then becomes gradual, and finally after 50 mm channel length it shows a gradual decrease in the SR dominated region. For the runs having inlet temperatures between 723-923 K, the temperature rise gets more pronounced with the decrease in inlet temperature. There is a temperature decrease at the initial section of the reactor only for the case with 1023 K inlet temperature led by insufficient heat transfer rate from total oxidation dominated zone to non-reacting zone at the inlet for keeping the temperature at or above 1023 K. Temperature change is very small on reacting zone for that case, which stays around 980 K. On the other hand, for other inlet temperatures reactor temperature gradually decreases and stabilized around 910 K near the outlet of the reactor.

The temperature profile of the reactor for different inlet temperatures follows similar trends for different cases as the trends obtained for case 5; the profiles obtained in case 1, which has the lowest C/O_2 and S/C ratios and case 9, which has the highest C/O_2 and S/C ratios are given in Figures 4.5 and 4.6 respectively.

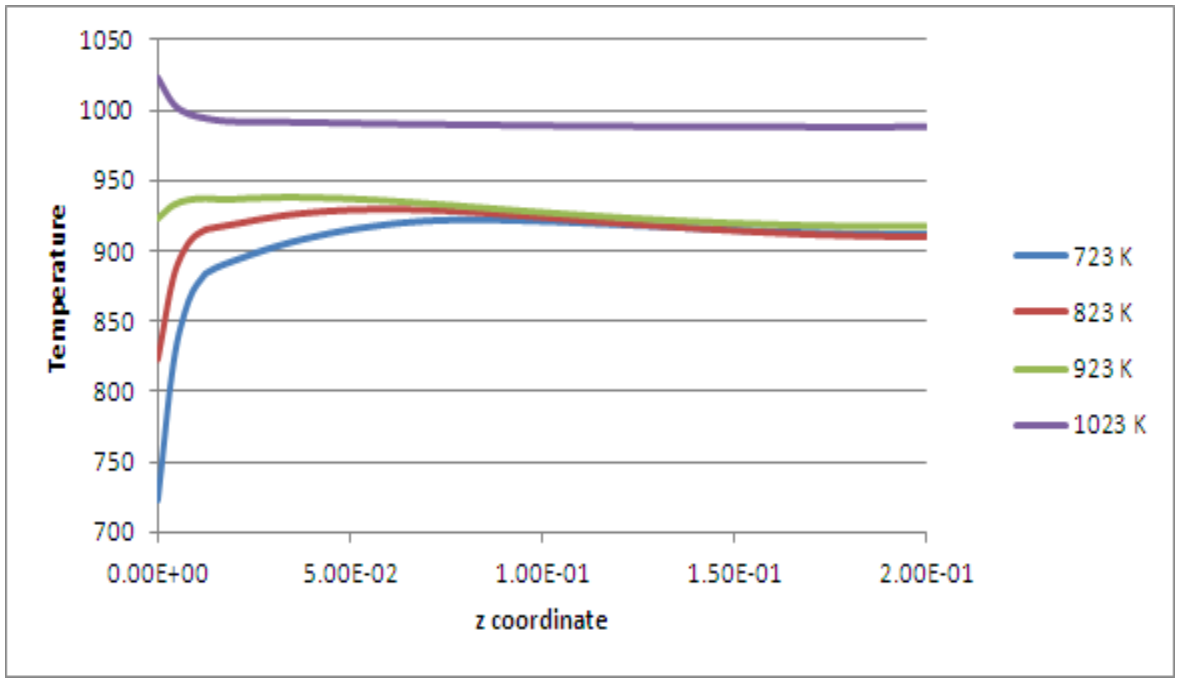

Figure 4.4. Temperature profile along the reactor for different inlet temperatures for case 5 with C/O_2 ratio of 2, S/C ratio of 3.

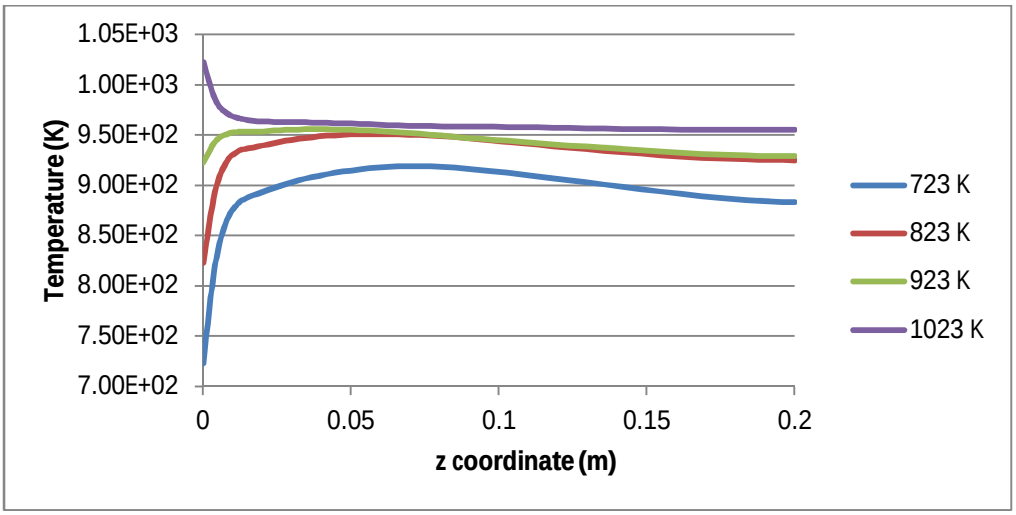

Figure 4.5. Temperature profile along the reactor for different inlet temperatures for case 1 with C/O_2 ratio of 2, S/C ratio of 3.

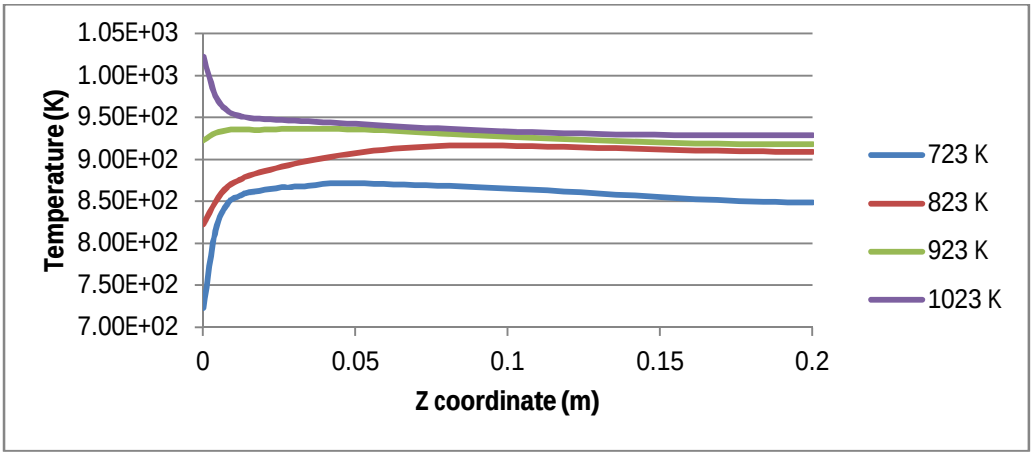

Figure 4.6. Temperature profile along the reactor for different inlet temperatures for case 9 with C/O_2 ratio of 2, S/C ratio of 3.

4.1.2. Effect of Carbon to Oxygen Feed Ratio (C/O_2) on Temperature Profile

In studying the effect of C/O_2 feed ratio on the temperature profile along the reactor length, set of results obtained from simulations performed for cases 4, 5 and 6 in a reactor having Ni:Pt = 20 metal loading running at 923 K inlet temperature are used as reference bases. Different pseudo isothermal conditions are achieved in response to changing inlet oxygen composition. The temperature at the inlet part of the reactor rises to a higher level

for the lowest C/O_2 feed ratio enhancing oxidation activity. An increase in C/O_2 ratio to 2.0 limits the temperature rise and further increase to 2.7 leads to fast temperature decrease in the inlet zone led by low O_2 concentration limiting exothermic TOX. Similar trends in temperature profiles are obtained from the simulations for the same cases at other temperature levels and with Pt:Ni =30.

It should be noted that the similar trends in temperature profiles are obtained for the cases with S/C = 2.35 (Cases 1, 2, 3) and for S/C = 4.0 (Cases 7, 8, 9) except the sharp decrease for C/O_2 = 2.7 for S/C = 3.0 has slightly flatten out S/C = 2.35 and S/C = 4.0.

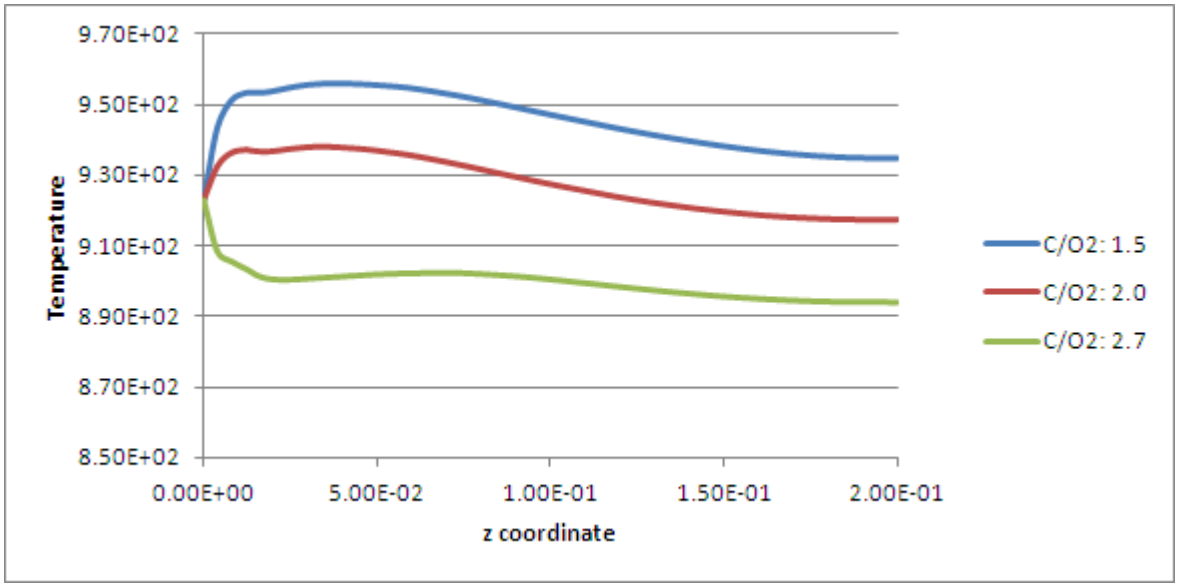

Figure 4.7. Temperature profiles for central line of case 4, 5 and 6 for inlet temperature of 923 K. each has S/C ratio of 3.

4.1.3. Effect of Steam to Carbon (S/C) Feed Ratio on Temperature Profile

Effect of S/C feed ratio on the temperature profile of the reactor is studied through comparative analysis of the data obtained from the simulations performed with the parameters in cases 2, 5 and 8 having S/C as 2, 3 and 4, respectively, for a reactor operating at 923 K and having Pt:Ni loading ratio of 20. As can be followed from Figure 4.8, S/C ratio has relatively limited effect on temperature profile compared to that of C/O_2 ratio. The reason of lower temperatures obtained in the SR dominated part of the reactor for higher steam amounts is the increase in steam concentration favoring endothermic steam reforming reaction along the reactor.

On the other hand, higher temperatures can be achieved with higher steam amount near inlet region. There, higher gaseous thermal conductivity of steam causes an increase in heat conductivity of reacting fluid, which results in slightly higher temperature of central line. Similar trends in temperature profiles are obtained from the simulations at other inlet temperature levels and with Pt:Ni = 30.

A comparative analysis of temperature profiles obtained at the same temperature level but for different C/O_2 feed ratios, ie. temperature profiles obtained in Figures 4.8, 4.9 and 4.10 for C/O_2 = 2, 1.5, 2.7, respectively, shows that the temperature profiles gets close to each other with the increase in C/O_2 ratios indicating that increase in C/O_2 ratio lessens the effect of S/C change on temperature profile of the reactor

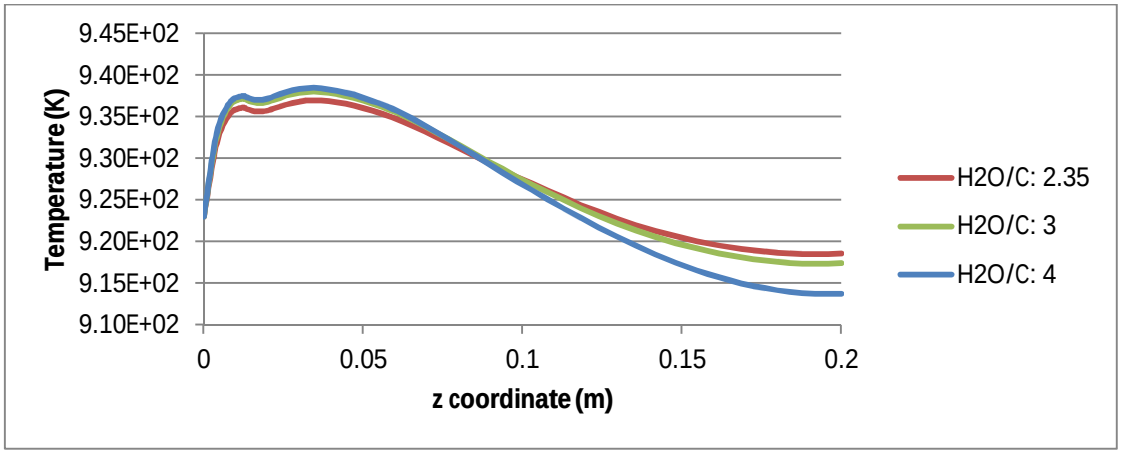

Figure 4.8. Temperature profiles for central line of case 2, 5 and 8 for inlet temperature of 923 K. Each has C/O_2 ratio of 2.

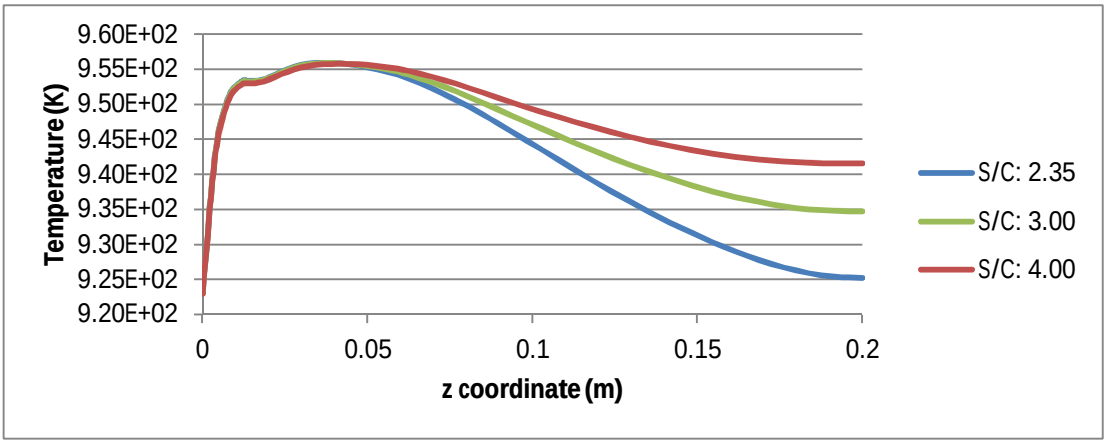

Figure 4.9. Temperature profiles for central line of case 1, 4 and 7 for inlet temperature of 923 K. Each has C/O_2 ratio of 1.5.

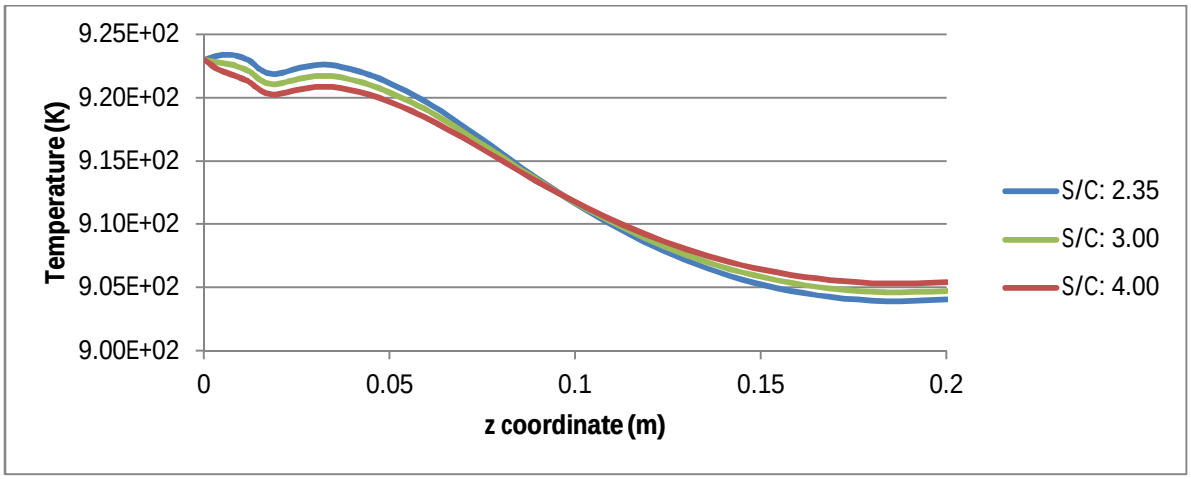

Figure 4.10. Temperature profiles for central line of case 3, 6 and 9 for inlet temperature of 923 K. Each has C/O_2 ratio of 2.7.

4.1.4. Effect of Ni:Pt ratio on Temperature Profile

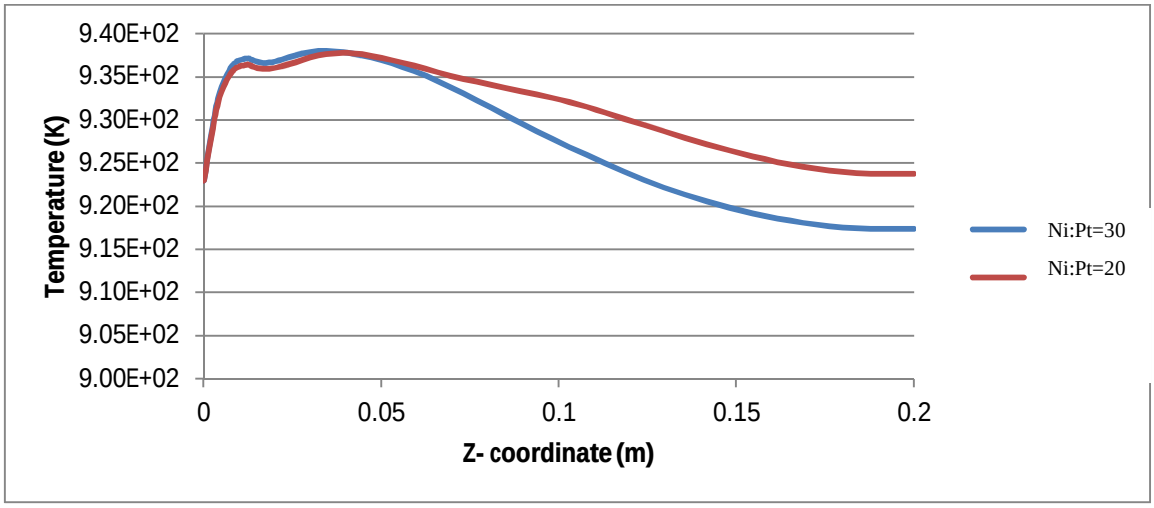

Figure 4.11. Effect of Ni:Pt ratio on temperature profile for case 5 with inlet temperature of 923 K, C/O_2 ratio of 2, S/C ratio of 3.

Effect of Ni:Pt loading ratio on the temperature profile of the reactor is studied through comparative analysis of the data obtained from the simulations performed with parameter in case 5 for a reactor operating at 923 K having Ni:Pt loading ratios of 20 and 30. At the inlet zone of the reactor, where TOX dominates, very close temperature levels are observed. On the other hand, the decrease in reactor temperature on the SR dominated part is more significantly for the reactor with Ni:Pt = 30. This can be explained by the fact that for the reactor zone between 50-200 mm, where the SR dominates TOX activity is suppressed further by low Pt content for Ni:Pt=30 case due to decreased oxygen concentra-

tion, decreasing heat production through TOX while endothermic SR activity is enhanced by higher Ni content, leading a fast temperature decrease.

4.2. Concentration Profiles of Species Along the Reactor

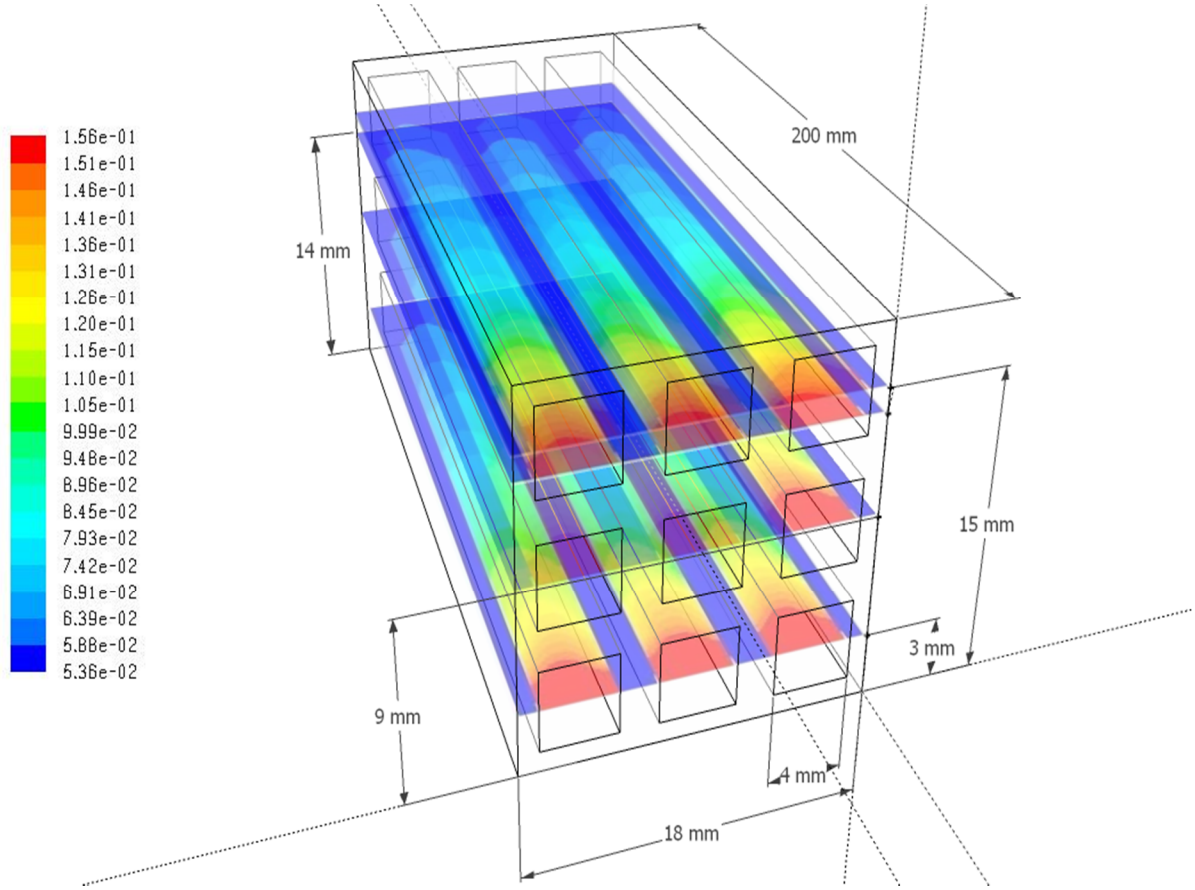

Figure 4.12. CH_4 molar fraction along the reactor for different layers, for case 5 with inlet temperature of 923 K, C/O_2 ratio of 2, and S/C ratio of 3.

The concentration profiles of all species along the reactor, both on the channel walls and at the channel centers, are calculated through simulations performed for case 5 at 923 K for a reactor having Ni:Pt=20 metal loading ratio as a reference case. Small differences of the concentration profiles between channels are caused by non-symmetric catalyst dispersion. First 12 mm of each channel has no catalyst and is used as a mixing zone. Though there is no reaction at the mixing zone, methane starts to decrease as it is diffusing from the reactor inlet to the reacting zone where methane concentration is lower. Methane concentration along the central parts of each channel is higher comparing to that on the wall, meaning that methane is diffusing along z coordinate faster near reacting channels

walls compared to the central line, which leads to a decreased methane concentration near the walls. Note that methane also diffuses from center to near channel walls along x and y coordinate, which decreases methane concentration further on the central line along z coordinate. Concentration profiles of species for case 5 obtained along the imaginary center lines of the channels are presented in Figure 4.13.

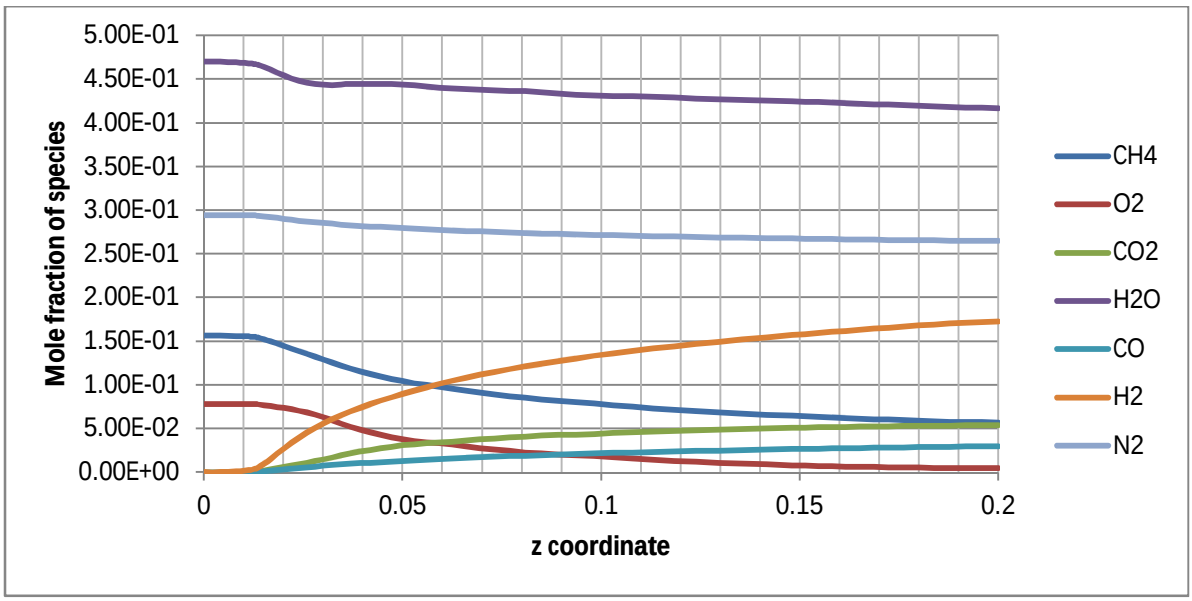

Figure 4.13. Mole fractions of species along the centerline for case 5 with inlet temperature of 923 K, C/O_2 ratio of 2, S/C ratio of 3.

Methane conversion is calculated as the ratio of methane flow rate anywhere inside the channel over the inlet methane flow rate. For all cases methane conversion is rapid in the inlet region led by SR and fast TOX, and gradually slows down, due to diminishing methane and oxygen concentrations in the reacting fluid especially for the SR dominated zone, which starts at ca. 45 mm distance from the reactor entrance. Hydrogen yield is defined as moles of hydrogen produced per methane molar inlet flow, and as hydrogen is the desired product, high levels of yield is targeted. Hydrogen to carbon monoxide ratio is mole fraction of hydrogen over mole fraction of carbon monoxide. As carbon monoxide is poisonous to Pt anode of the fuel cell, H_2/CO molar ratio, which is used as the measure of selectivity, should be as high as possible.

Rapid methane consumption between the end of the mixing zone and ca. 40 mm from the inlet is caused by fast kinetics of TOX reaction. After ca. 40 mm methane con-

sumption slows down due to relatively lower temperatures and depletion of oxygen concentration in the reacting fluid limiting TOX.

Fastest consumption of steam is observed between ca. 12^{th} - 25^{th} millimeters of reactor though additional steam is produced by fast TOX in this region. Thus, it can be safely said that steam reforming is faster on this part of the reactor. From 25^{th} to 55^{th} millimeter of reactor, steam flow ratio is nearly invariant but methane concentration decreases. As water is the product of TOX and a reactant of both SR and WGS reaction, unchanging steam concentration indicates that in that region total oxidation is significanly faster.

Nitrogen is chemically inert, and a decrease of nitrogen mole fraction is caused by overall increase in total molar flow. Since combined molar production of total oxidation and steam reforming reactions, and water gas shift as the side reaction is greater than their total molar consumptions, decrease in nitrogen mole fraction is an indication of increase in total overall rate.

Methane conversion, hydrogen yield and H_2/CO selectivity are given in Figure 4.14. Note that as in Langmuir-Hinshelwood type kinetics equation for steam reforming and CO_2-producing steam reforming have hydrogen concentration on denominator, hydrogen concentration at inlet feed is assumed as 10^{-5} mol/L while inlet feed is assumed carbon monoxide free; this results in infinite value for H_2/CO in the inlet part.

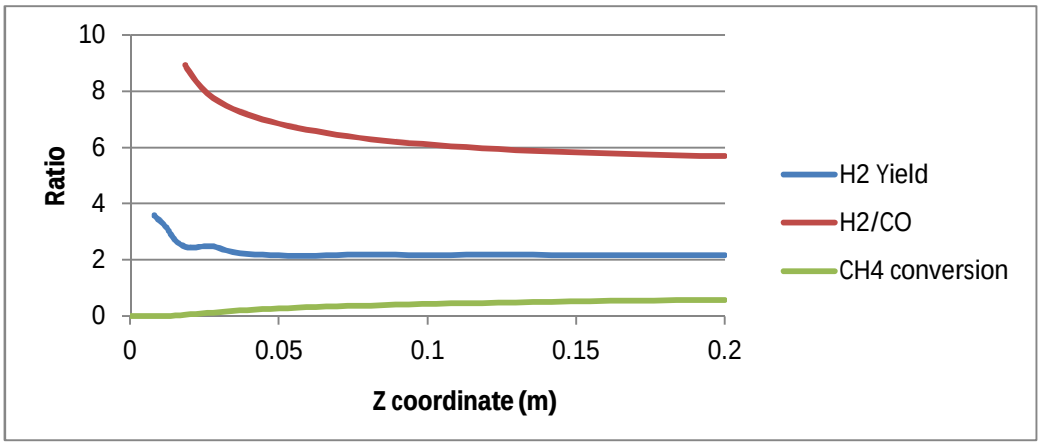

Figure 4.14. Methane conversion, hydrogen yield and H_2/CO ratio along the central line of reactor for case 5 with inlet temperature of 923 K, and C/O_2 ratio of 2, S/C ratio of 3.

Hydrogen yield decreases with a decreasing slope as a function of reactor length; especially after the reacting fluid reaches steam reforming dominated zones, H_2/CO ratio decreases along the reactor.

4.2.1. Effect of Inlet Temperature on Concentration Profiles of the Species

In order to understand the effect of inlet temperature on the concentration profiles of the species along the reactor, data obtained from simulations for case 5, (C/O_2:2, H_2O/C:3) with inlet temperatures of 723, 823, 923 and 1023 K over catalyst with Ni:Pt=20 are comparatively studied first to form a reference base. Species concentrations are given in Figure 4.15 to 4.17. Figures from 4.18 to 4.20 show methane conversion, hydrogen yield and hydrogen to carbon monoxide ratio over reactor length for different inlet temperatures.

The results clearly show that higher inlet temperature of the feed increases the methane conversion indicated by lower methane concentrations. Since methane is not fully converted even at the exit of the reactor, hydrogen yield can be increased through rising the inlet temperature. As methane is consumed by both TOX and SR, and oxygen is consumed very fast by TOX at the first ca. 50 mm of the reactor; most of the methane consumption after ca. 50 mm of reactor is by steam reforming, which is indicated by fast rise in methane conversion and hydrogen yield. Both CO and CO_2 producing SR reactions produce H_2 and reverse water gas shift produces CO and consumes hydrogen at high reactor temperature. The decrease in hydrogen to carbon monoxide selectivity ratio is decreased with increasing temperature reveals that increase in reverse WGS activity is relatively larger than the increase in steam reforming at high inlet temperatures.

Comparative analysis of O_2 and CH_4 concentration profiles obtained for different inlet temperatures indicates that effect of temperature is less significant on TOX reaction than on both steam reforming reactions. Oxygen concentration drops with similar rates, and depletes before the end of the reactor for all of the inlet temperatures.

Comparative analysis of the concentration profiles show that carbon dioxide concentration profile is nearly same for all feed inlet temperatures. Carbon dioxide is product of combustion and steam reforming reaction while it is a reactant of reverse water gas shift reaction. As oxygen concentration indicates, total oxidation is nearly same for all inlet

temperatures, steam reforming reactions and reverse water gas shift reaction produce and use nearly same amount of carbon dioxide at different inlet temperatures. Despite hydrogen concentration also increases with increased inlet temperature of the feed due to faster SR kinetics at higher temperature, as it can be seen in Figure 4.16, overall hydrogen over carbon monoxide ratio reduces more for higher inlet temperatures.

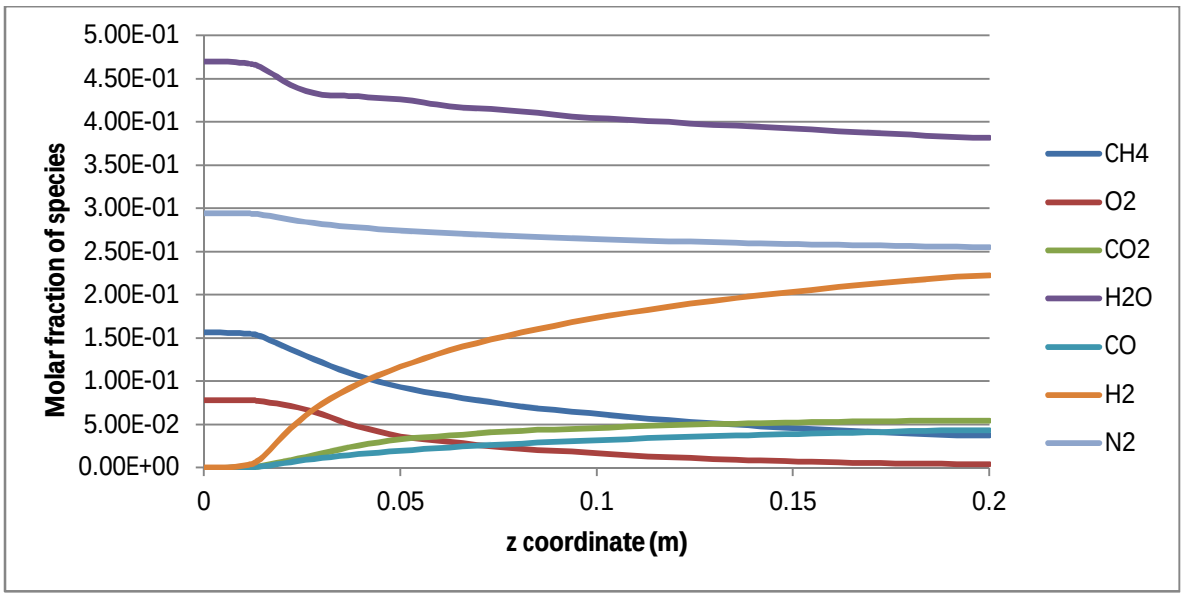

Figure 4.15. Mole fractions of species along the centerline for case 5 with inlet temperature of 1023 K, with C/O_2 ratio of 2, S/C ratio of 3.

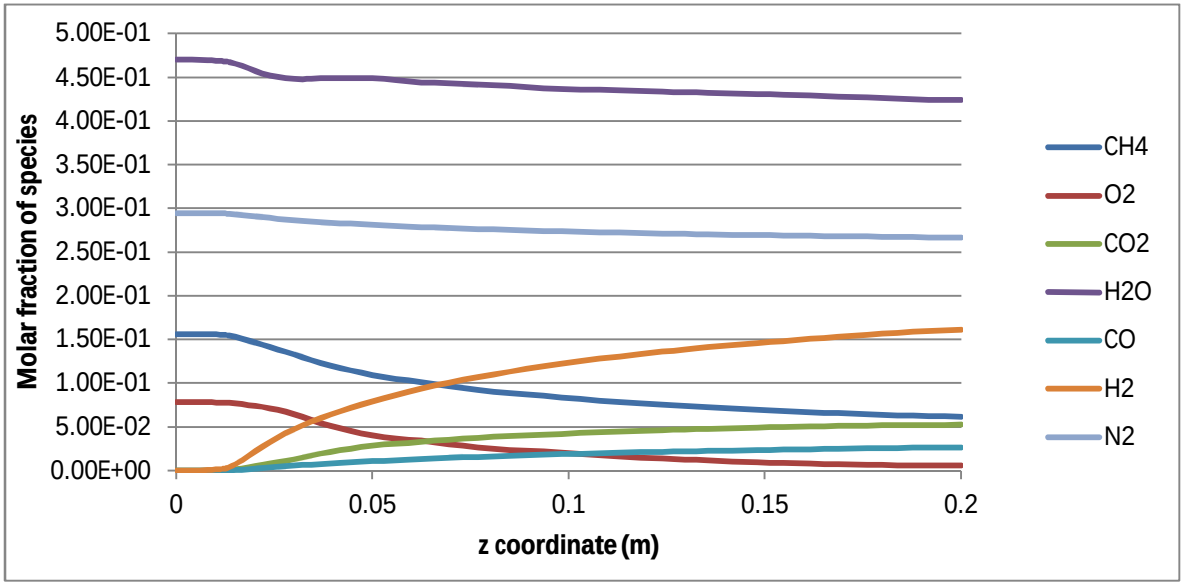

Figure 4.16. Mole fractions of species along the centerline for case 5 with inlet temperature of 823 K, with C/O_2 ratio of 2, S/C ratio of 3.

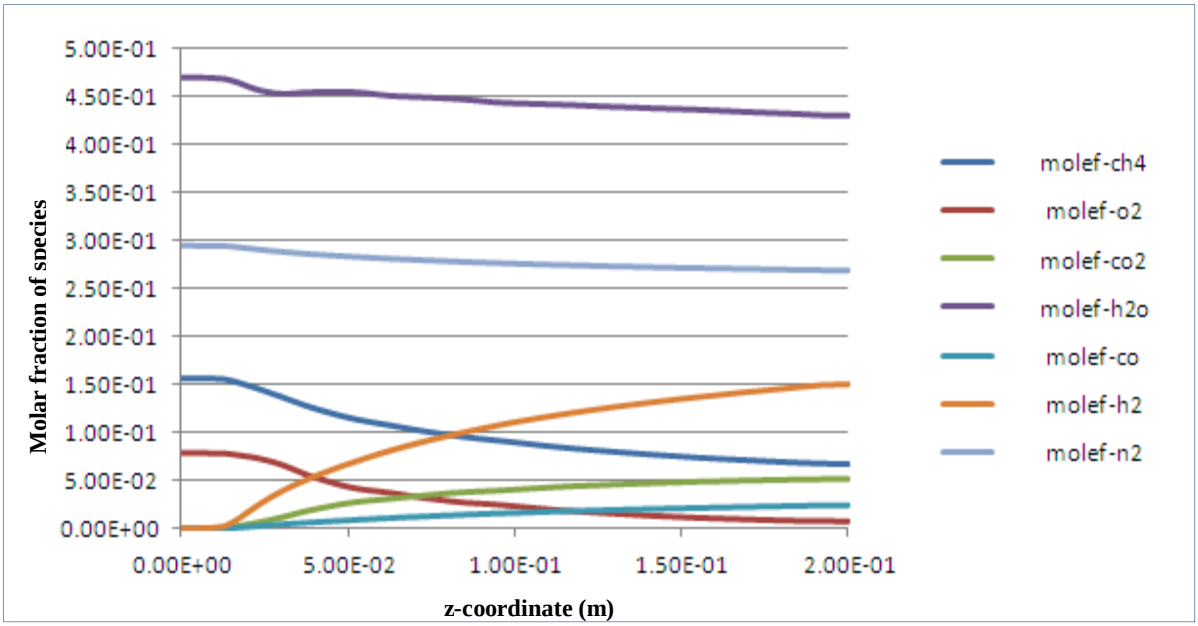

Figure 4.17. Mole fractions of species along the centerline for case 5 with inlet temperature of 723 K, with C/O_2 ratio of 2, S/C ratio of 3.

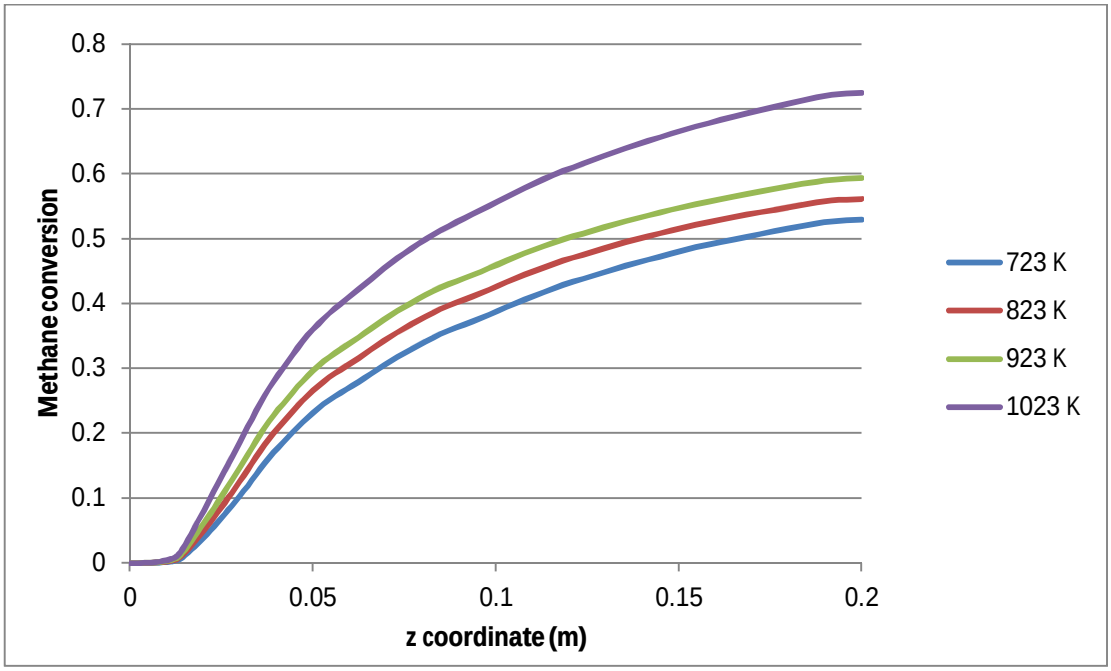

Figure 4.18. Methane conversion for different inlet temperatures along the centerline for case 5, with C/O_2 ratio of 2, S/C ratio of 3.

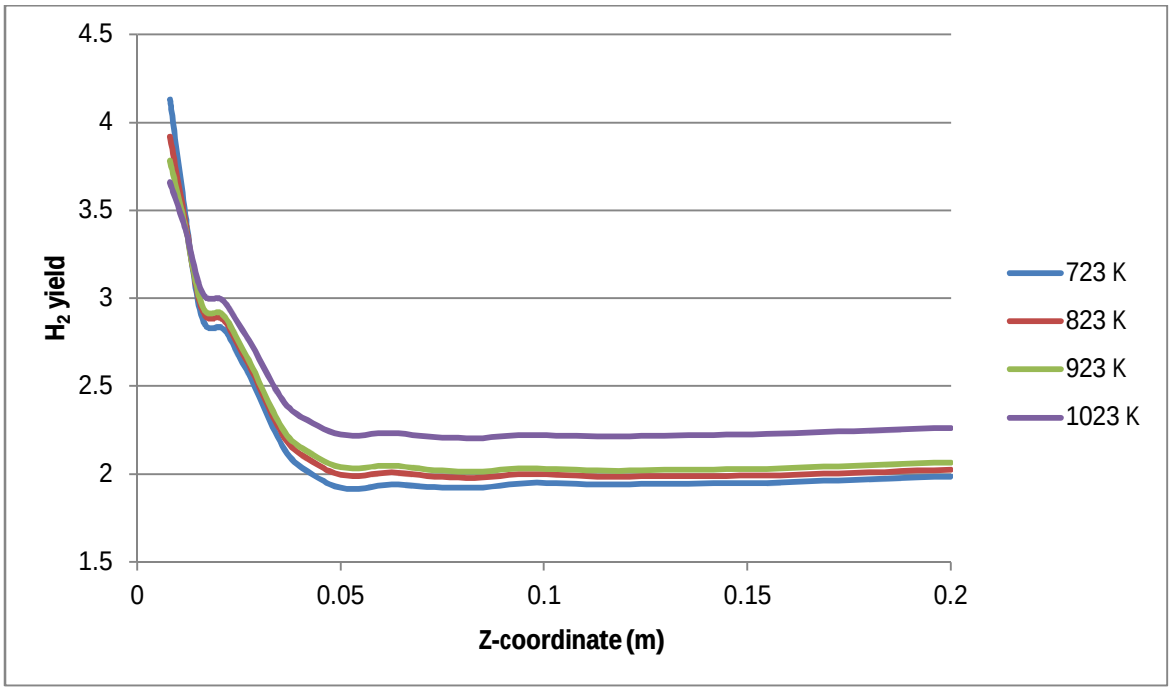

Figure 4.19. Hydrogen yield for different inlet temperatures along the centerline for case 5, with C/O_2 ratio of 2, S/C ratio of 3.

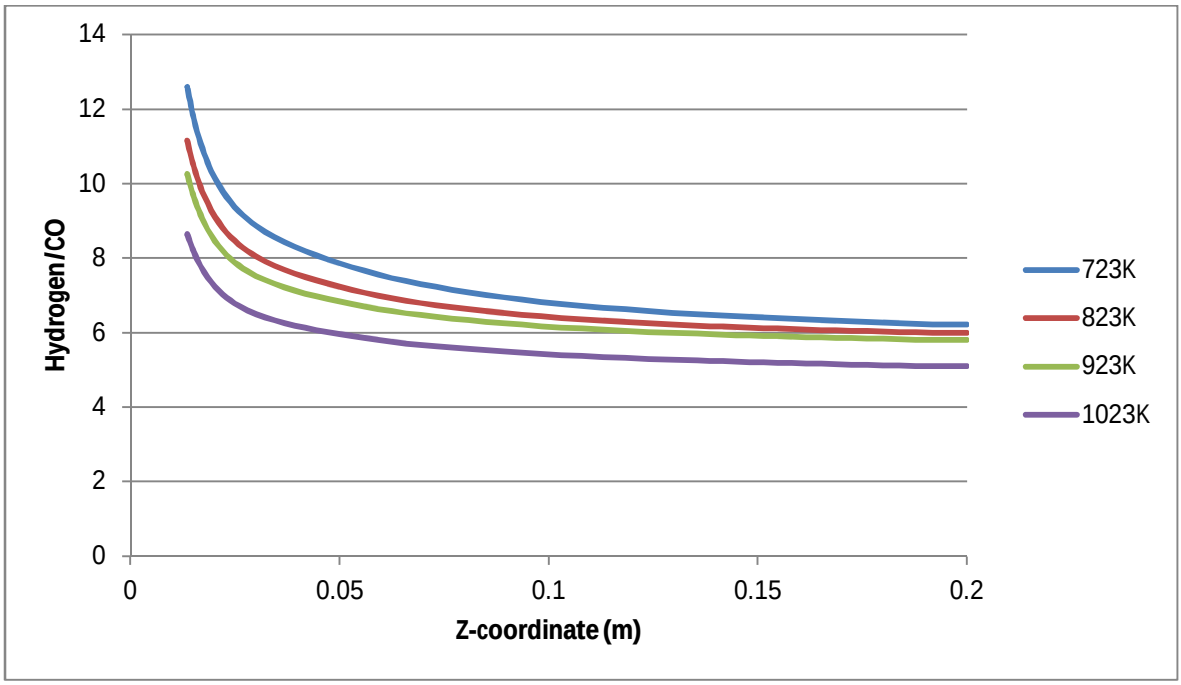

Figure 4.20. H_2/CO ratio for different inlet temperatures along the centerline for case 5, with C/O_2 ratio of 2, S/C ratio of 3.

4.2.2. Effect of S/C Ratio on Concentration Profiles of the Species

Aiming to see the effect of S/C on the concentration profiles of the species, and activity and selectivity, OSR simulation results obtained for Cases 2, 5 and 8 at 923 K over the reactor with Ni:Pt = 20 are comparatively analyzed.

It can be seen from Figures 4.21 to 25 that the effect of S/C ratio on methane conversion is not significant. But hydrogen yield and hydrogen to carbon ratio increase with the increase in steam to carbon ratio. This can be explained by the enhancement of both water gas shift and steam reforming reactions. As the effect of S/C increase is more pronounced on H_2/CO selectivity (Figure 4.25) compared to that of hydrogen yield (Figure 4.24). One can conclude that the enhancement at WGS is more significant. Increased hydrogen yield (Figure 4.24) and nearly invariant methane conversion (Figure 4.21) indicates that TOX is slightly suppressed with the increase in S/C.

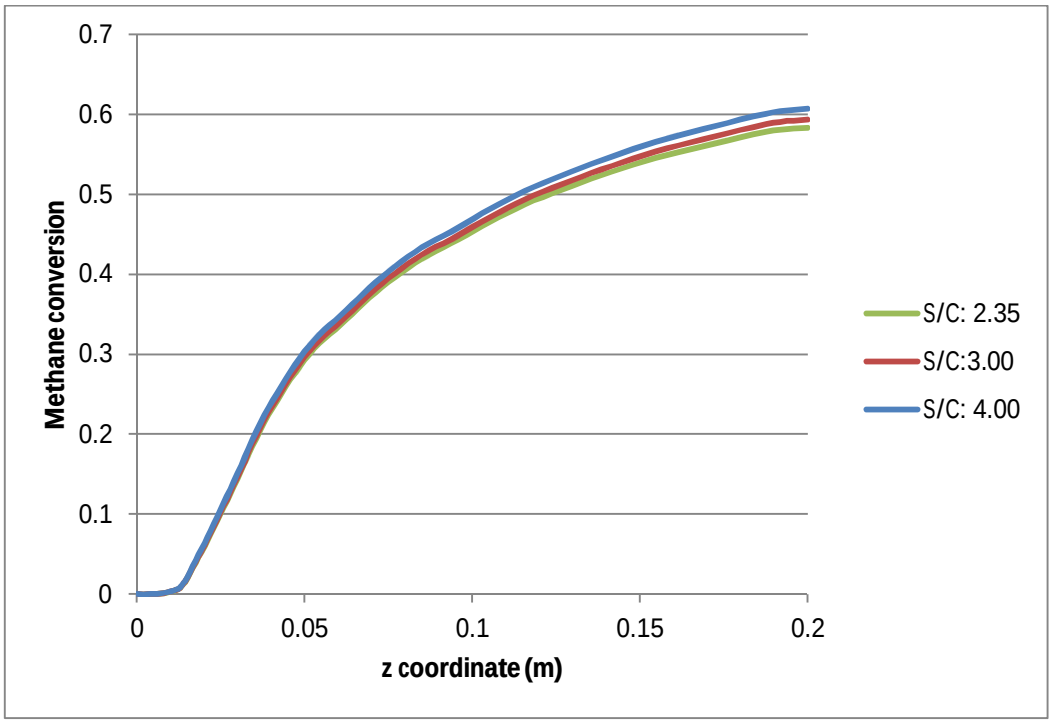

Figure 4.21. Effect of steam to carbon ratio on methane conversion, for inlet temperature of 923 K and each has C/O_2 ratio of 2.

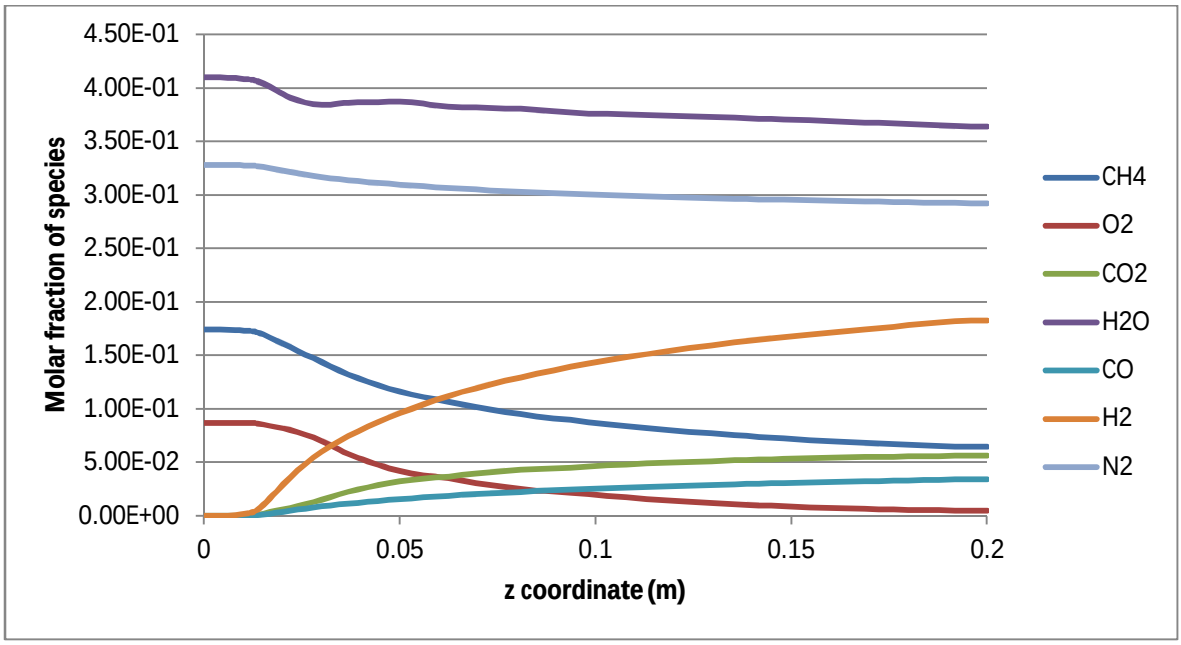

Figure 4.22. Mole fractions of species along the centerline for case 2 with 923 K inlet temperature, C/O_2:2, S/C: 2.35.

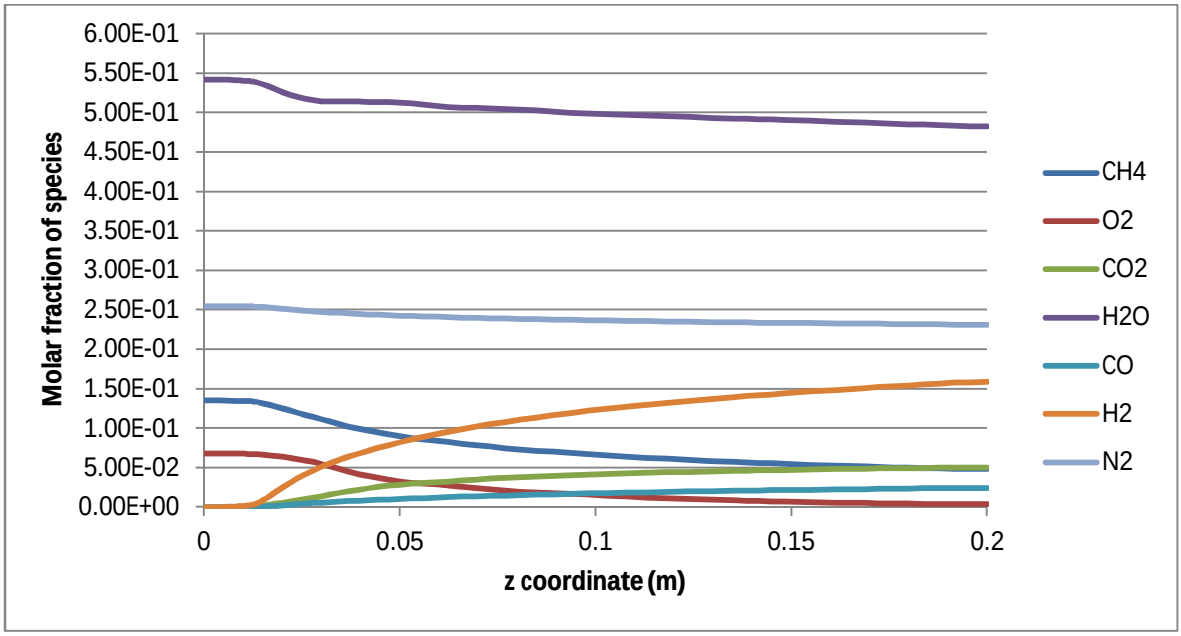

Figure 4.23. Mole fractions of species along the centerline for case 8 with 923 K inlet temperature, C/O_2:2, S/C: 4.

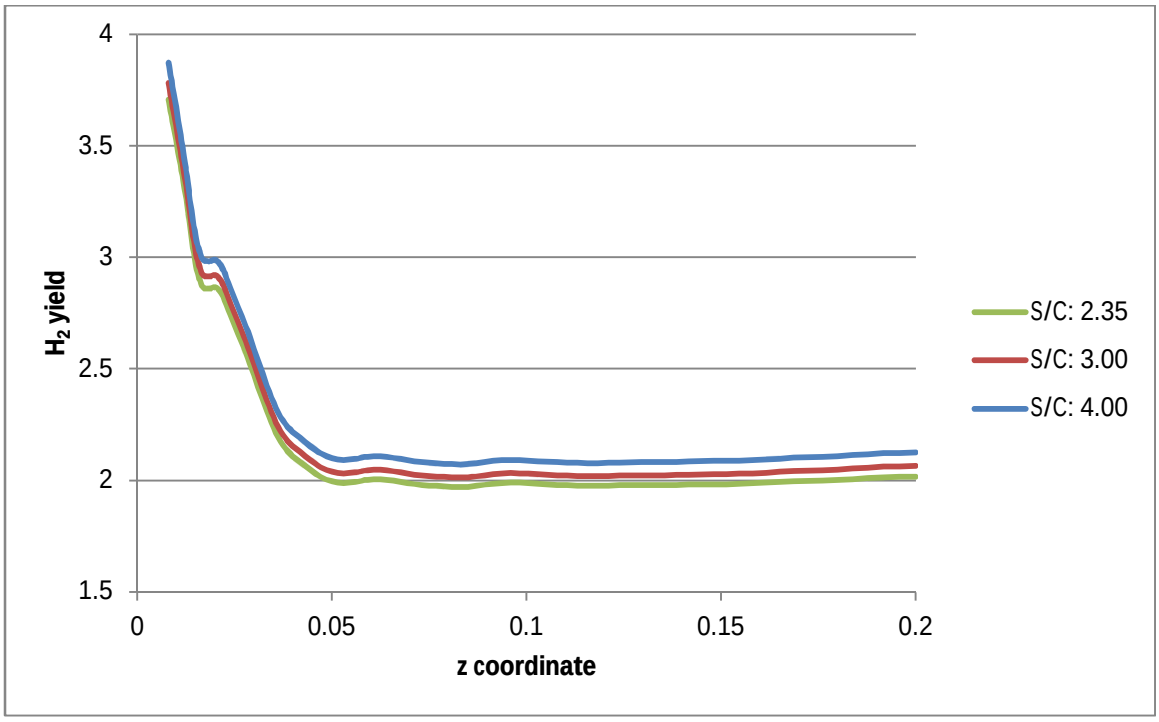

Figure 4.24. Effect of steam to carbon ratio on hydrogen yield, for inlet temperature of 923 K and each has C/O_2 ratio of 2.

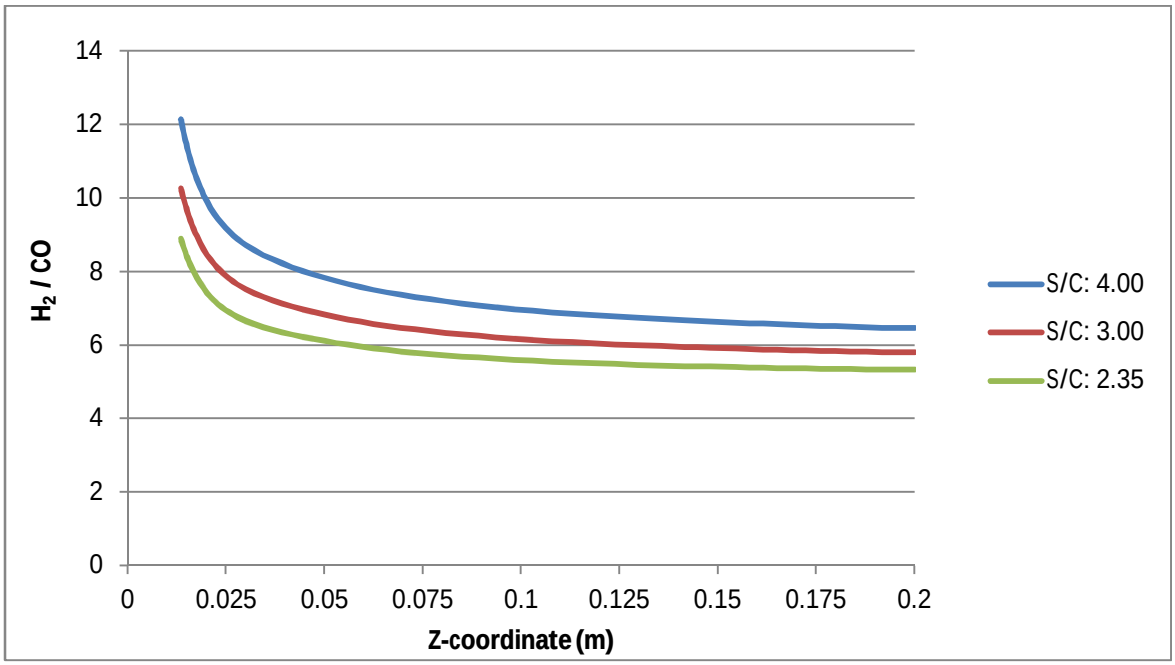

Figure 4.25. Effect of steam to carbon ratio on H_2/CO, for inlet temperature of 923 K and each has C/O_2 ratio of 2.

4.2.3. Effect of C/O_2 Ratio on the Concentration Profiles of the Species

The results obtained from the OSR simulations for Cases 4, 5 and 6 conducted at 923 K in a reactor having Ni:Pt=20 are comparatively analyzed aiming to see the effect of carbon to oxygen ratio (C/O_2) in the feed on concentration profiles of the species along the reactor, conversion of methane, hydrogen yield and H_2/CO selectivity. Case 4 has the most abundant oxygen with the C/O_2=1.5, while case 6 has the least amount of oxygen with the C/O_2=2.7.

It can be seen from Figures 4.26 to 4.30 that methane conversion increases with a decrease in C/O_2 ratio. Since TOX reaction have tendency to deplete oxygen fast, increasing the oxygen naturally consumes more methane in the process (Figure 4.26). The results, which show that methane conversion increases (Figure 4.26) while hydrogen yield decreases (Figure 4.29) in response to a decrease in C/O_2 feed ratio, indicate that when higher amount of oxygen in the feed is available, a higher fraction of methane is used in TOX leading to a limited hydrogen yield. Rather limited decrease in H_2O for low C/O_2 feed ratio (Figure 4.27) compared to that for high C/O_2 feed ratio (Figure 4.28) confirms enhanced TOX activity for low C/O_2 ratios as H_2O is the product of TOX, and the reactant of both SR and WGS. It should be noted that as the increase in the hydrogen yield with an increase in C/O_2 is more pronounced than that of the increase in H_2/CO ratio, there should be a pronounced WGS activity at lower C/O_2 feed ratio for the given condition.

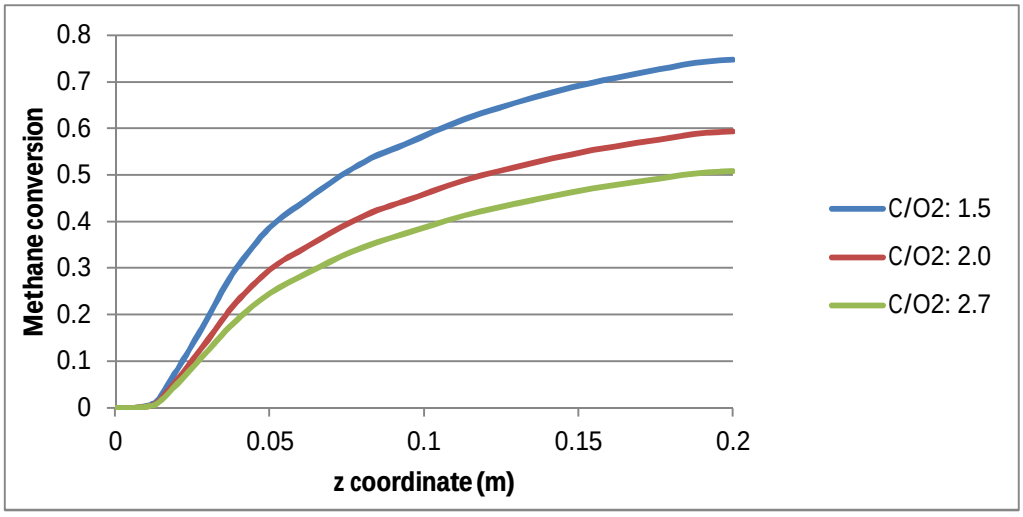

Figure 4.26. Effect of C/O_2 ratio on CH_4 conversion, for inlet temperature of 923 K and each has S/C ratio of 3.

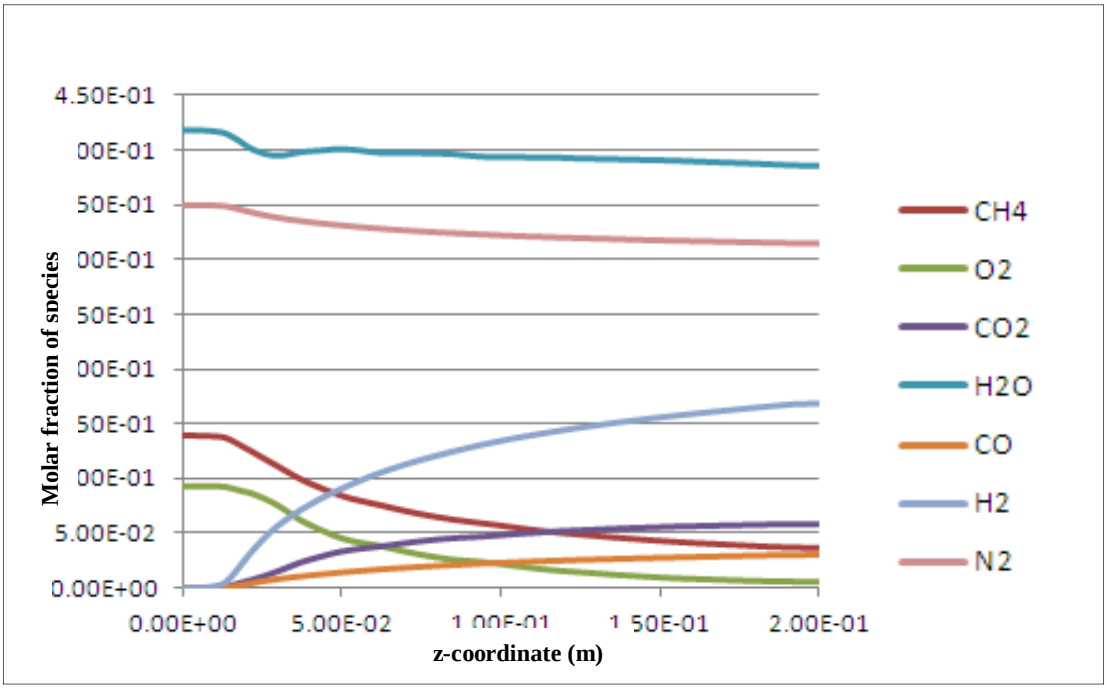

Figure 4.27. Mole fractions of species along the centerline for case 4 with inlet temperature of 923 K, C/O_2 ratio of 1.5 and S/C ratio of 3.

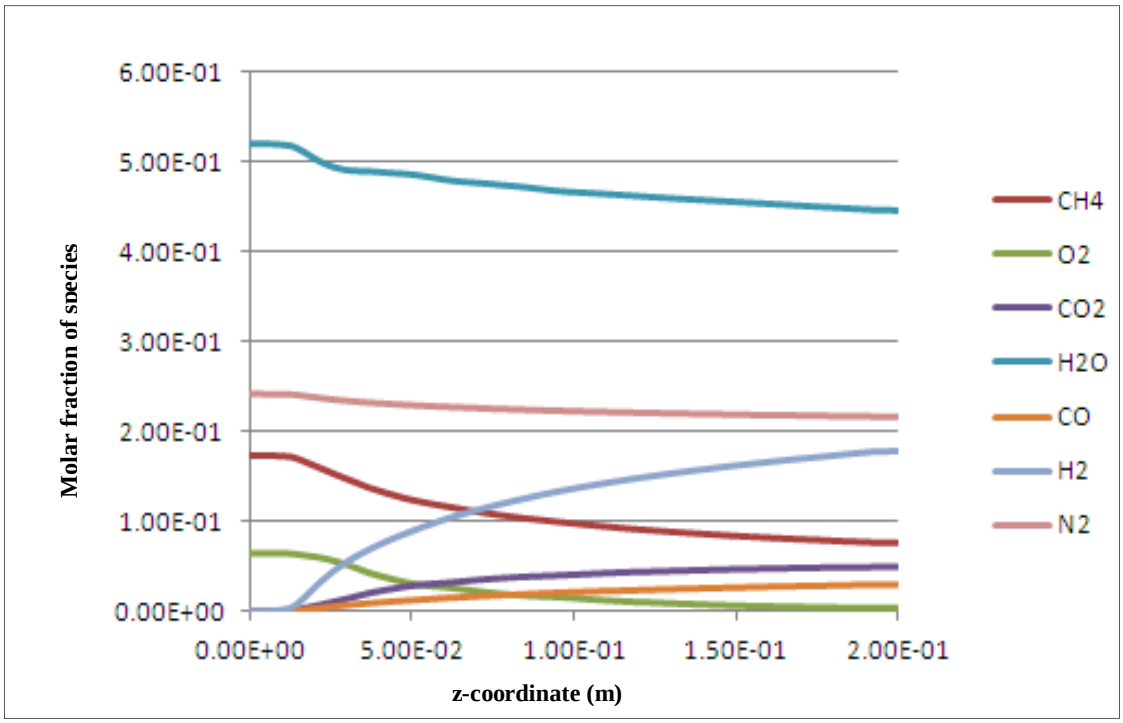

Figure 4.28. Mole fractions of species along the centerline for case 6 with inlet temperature of 923 K, C/O_2 ratio of 2.7, S/C ratio of 3.

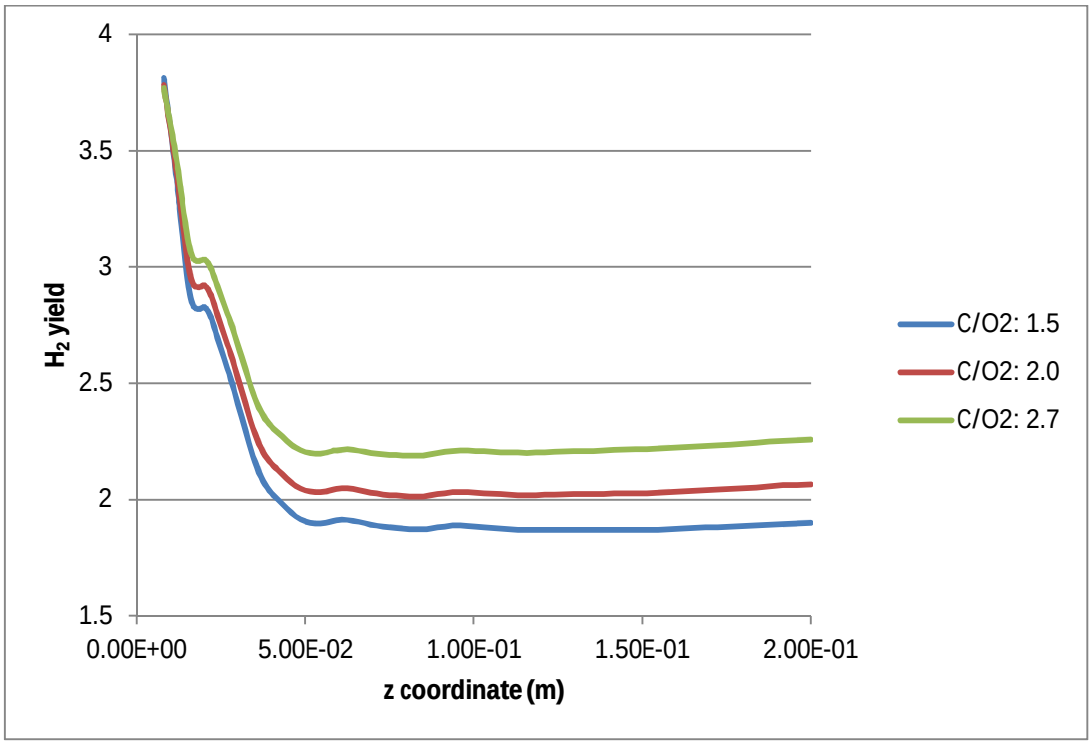

Figure 4.29. Effect of carbon to oxygen ratio on hydrogen yield, inlet temperature of 923 K, and each has C/O_2 ratio of 2.

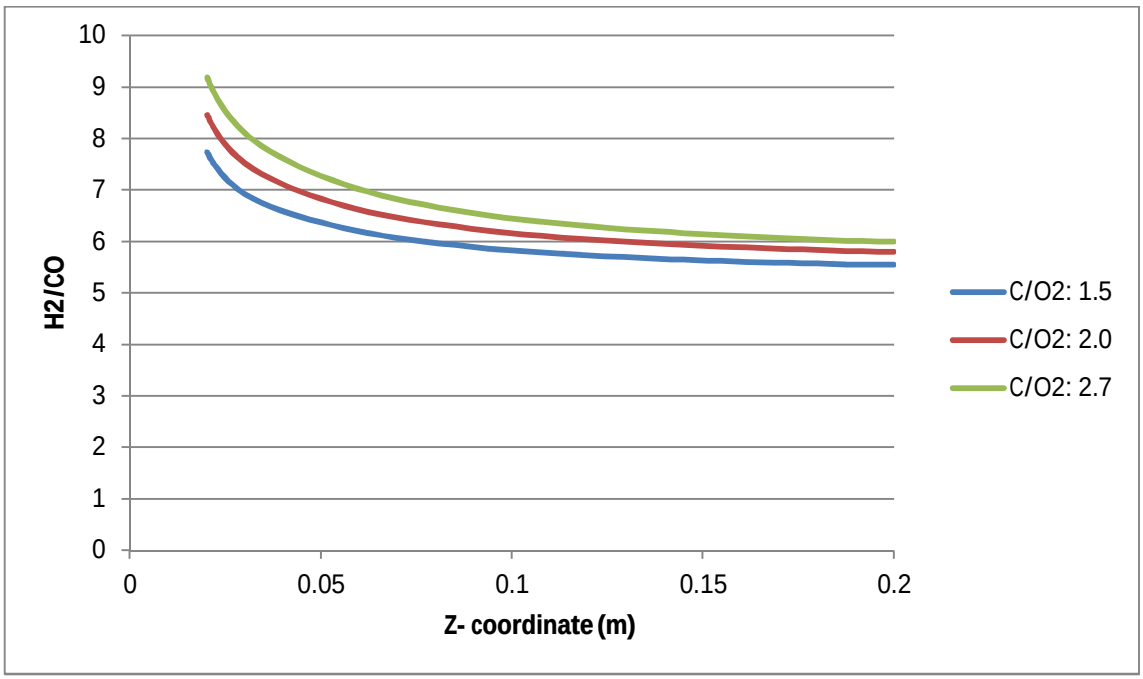

Figure 4.30. Effect of carbon to oxygen ratio on H_2/CO, inlet temperature of 923 K, each has C/O_2 ratio of 2.

4.2.4. Effect of Pt:Ni Ratio on the Concentration Profiles of the Species

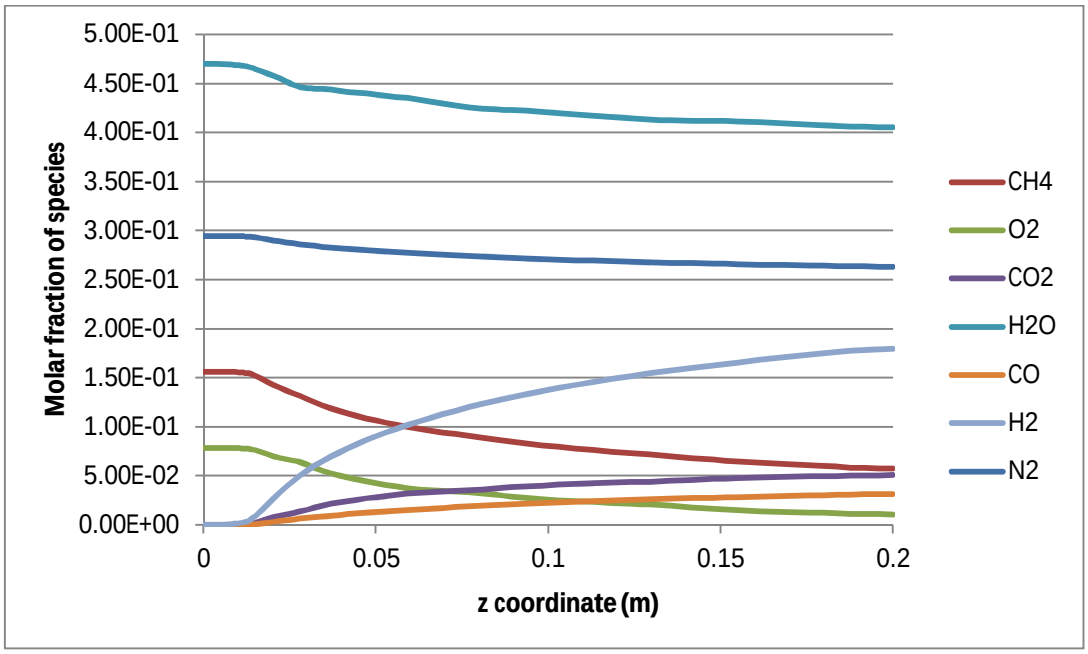

Figure 4.31. Mole fractions of species along the centerline for case 5 with inlet temperature of 923 K, C/O_2 ratio of 2, S/C ratio of 3 and Pt:Ni ratio of 30.

Aiming to study the effect of Ni:Pt ratio on concentration profiles of the species, activity and H_2/CO selectivity is OSR reaction, the simulation results obtained from case 5 at 923 K with Ni:Pt =30 and 20 are comparatively analyzed. The concentration profiles presented in Figure 4.31 is similar to those in Figure 4.15 in terms of their trends. On the other hand with the increase in Ni:Pt, slightly more oxygen left the reactor unused due to suppressed TOX led by low Pt amount. For Ni:Pt =30 case, combined in SR and TOX methane conversion follows almost equivalent profile as in Ni:Pt=20 case. (Figure 4.32)

The distinct difference in H_2/CO selectivity profiles is worth to be mentioned; there, hydrogen yield is higher Ni:Pt=20 case for the first 40 mm due to enhanced SR activity triggered by high temperature results from high TOX activity, whereas after ca. 40 mm of reactor length hydrogen yield is stabilized at higher level for Ni:Pt =30 case caused by higher SR activity of Ni:Pt = 30 case. On the other hand hydrogen to carbon monoxide selectivity ratio is nearly the same for two different Ni:Pt ratios (Figure 4.34).

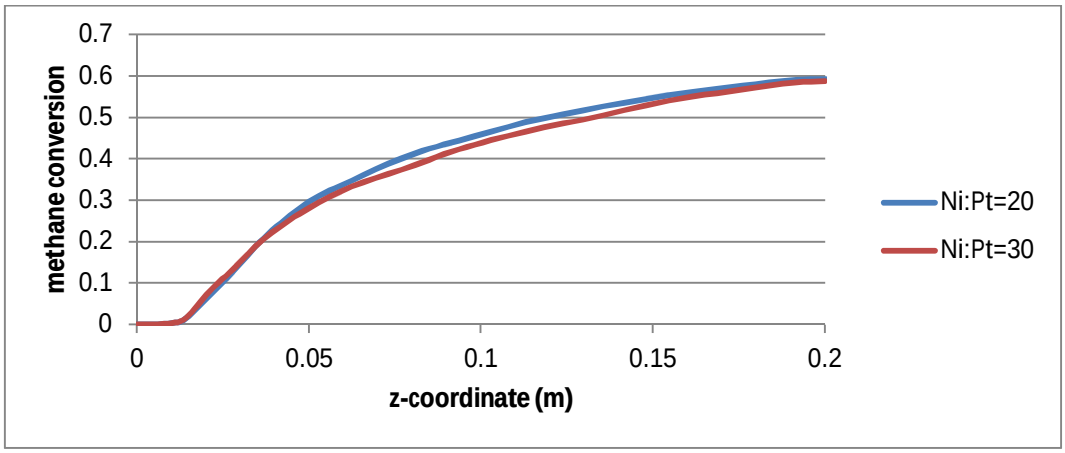

Figure 4.32. Effect of Pt:Ni ratio on methane conversion, inlet temperature of 923 K, S/C ratio of 3, and C/O_2 ratio of 2.

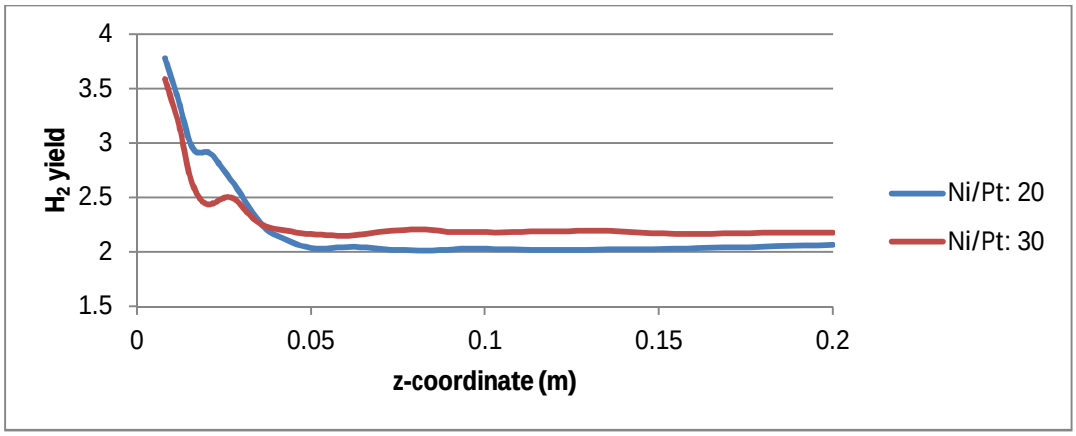

Figure 4.33. Effect of Pt:Ni ratio on hydrogen yield, inlet temperature of 923 K, S/C ratio of 3, and C/O_2 ratio of 2.

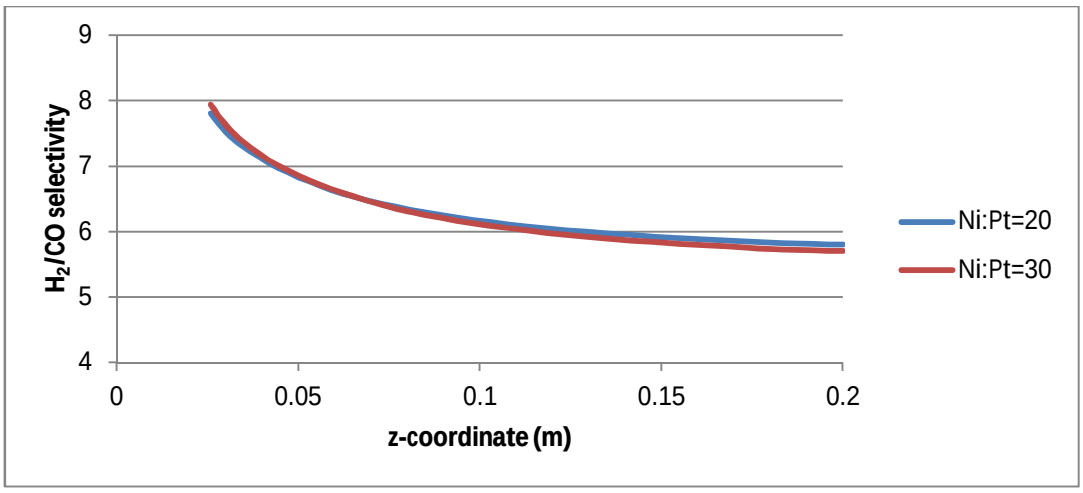

Figure 4.34. Effect of Pt:Ni ratio on H_2/CO , inlet temperature of 923 K, S/C ratio of 3, and C/O_2 ratio of 2.

4.3. Velocity Distribution along the Reactor

In the simulations velocity of the reacting fluid is 0.1875 m/s at inlet. Channel walls have no slip condition; therefore velocity increases from channel walls to the center. Velocity is dependent on temperature and total molar flow rate. Since reaction activity may increase both of them, average velocity is expected to increase with time. For case 5 with 923 K inlet, outlet flow rate is 30 cm^3/s, and average of mean velocities for all channels is increased by 11%. In Figure 4.35, a vertical layer from the middle of channel and another layer that has one millimeter close to channel wall are given. Velocity distribution is also given for the end of channel's outlet.

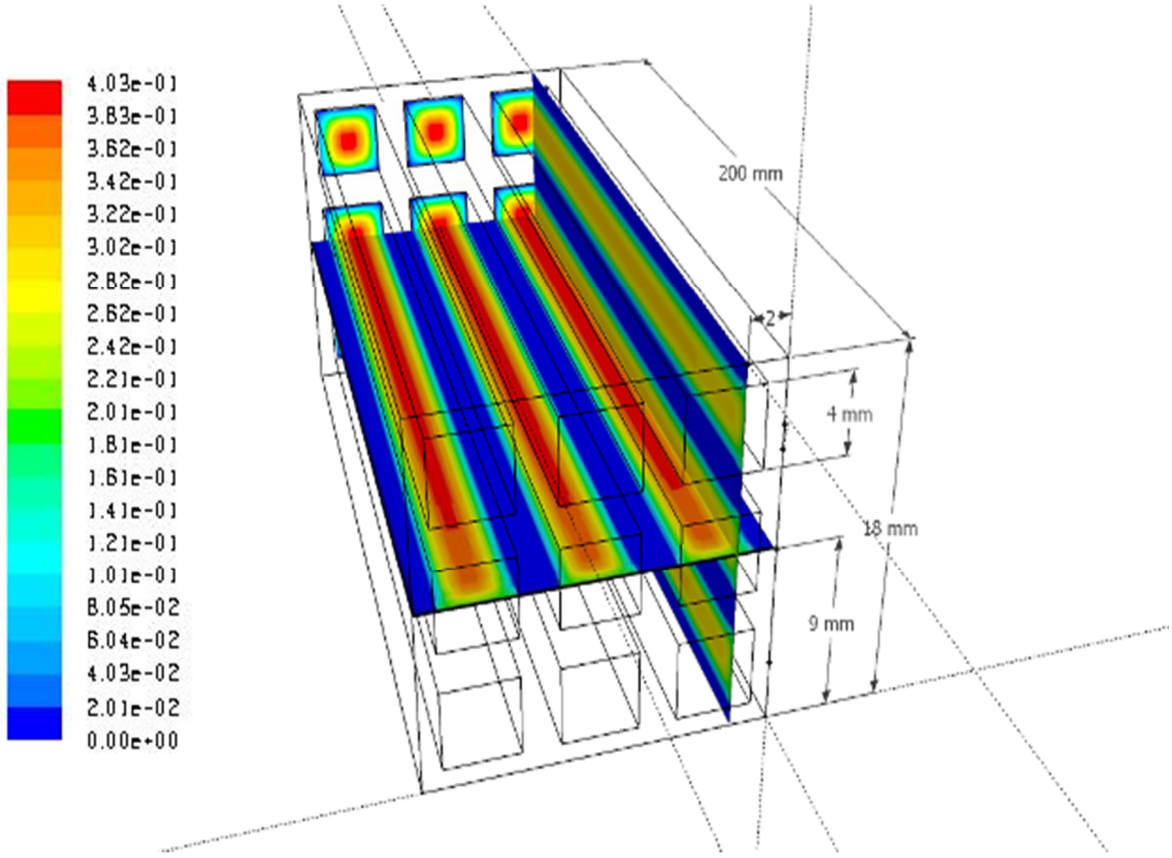

Figure 4.35. Velocity profile (m/s) for middle cross sectional and fully developed outlet along the reactor for case 5 with inlet temperature of 923 K, C/O_2 ratio of 2, S/C ratio of 3.

4.4. Pressure Distribution along the Reactor

Flow along the reactor is a result of pressure gradient. Pressure drop for reactor is linear and is calculated as 1.80 Pa for 200 mm reactor, which is negligible. Operating pressure is 101300.00 Pa.

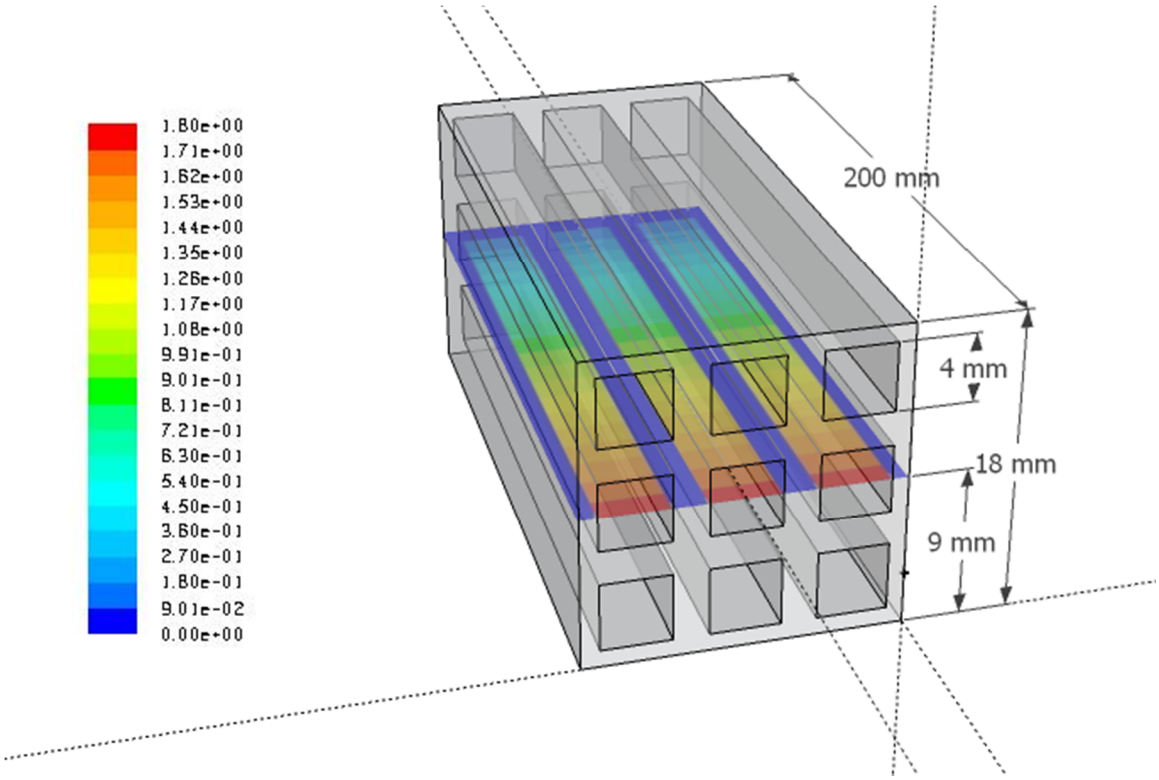

Figure 4.36. Pressure profile (Pa) for middle cross sectional and fully developed outlet along the reactor for case 5 with inlet temperature of 923 K, C/O_2 ratio of 2, and S/C ratio of 3.

4.5. Summary of the Results for All Cases

Methane and hydrogen molar flow rates are calculated for all cases by taking surface integral of contours at the exit of channels. Figures 4.33 and 4.34 are the examples of outlet mass fraction contours for case 5 with 923 K inlet temperature and Ni:Pt =30. Methane conversion, hydrogen yield, and hydrogen to carbon monoxide ratio are calculated from the outlet methane, hydrogen and carbon monoxide mass flow rates. Slight differences between channels are caused by the asymmetrical nature of random grid dispersion. All results are tabulated at Table 4.3 and 4.4.

Figure 4.37. Outlet mole fraction contours of methane for case 5 with 923 K inlet temperature, C/O_2:2, H_2O/C: 3.

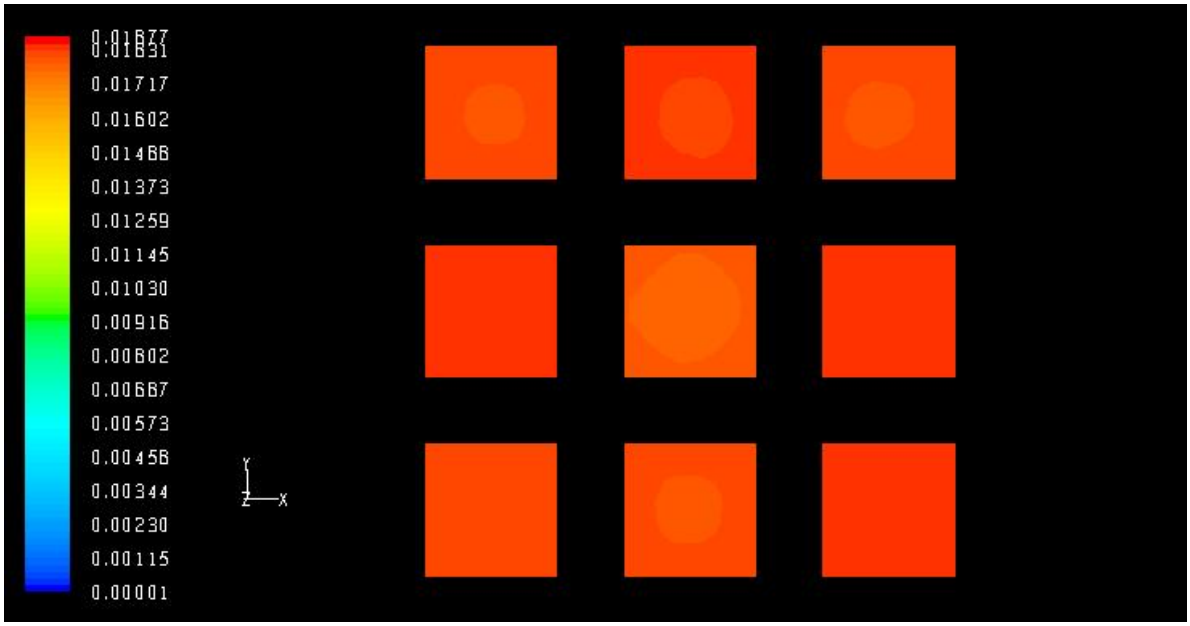

Figure 4.38. Outlet mole fraction contours of hydrogen for case 5 with 923 K inlet temperature, C/O_2:2, H_2O/C: 3.

Table 4.3. Results of cases at reactor length 200 mm for Pt:Ni surface ratio 1:20.

			CH_4 Conversion				H_2 yield				H_2/CO			
	C/O_2	S/C	723	823	923	1023	723	823	923	1023	723	823	923	1023
case1	1.50	2.35	0.58	0.67	0.70	0.76	1.73	1.91	1.92	2.01	4.93	5.11	5.04	4.80
case2	2.00	2.35	0.43	0.55	0.58	0.64	1.74	2.04	2.07	2.16	6.53	5.42	5.27	5.01
case3	2.70	2.35	0.34	0.45	0.49	0.54	1.83	2.17	2.23	2.31	7.26	5.79	5.52	5.25
case4	1.50	3.00	0.60	0.66	0.71	0.75	1.82	1.95	1.96	2.05	6.09	6.53	5.46	6.05
case5	2.00	3.00	0.52	0.56	0.59	0.73	2.06	2.09	2.12	2.31	6.13	5.91	5.73	5.04
case6	2.70	3.00	0.43	0.46	0.51	0.53	2.19	2.24	2.29	2.32	6.60	6.28	5.94	5.85
case7	1.50	4.00	0.62	0.67	0.72	0.77	2.12	1.97	2.02	2.08	6.38	6.35	6.07	5.84
case8	2.00	4.00	0.53	0.51	0.61	0.64	2.10	2.20	2.18	2.22	6.95	6.87	6.39	6.19
case9	2.70	4.00	0.43	0.47	0.51	0.52	2.24	2.30	2.35	2.38	7.54	7.06	6.69	6.44

Table 4.4. Results of cases at reactor length 200 mm for Pt:Ni surface ratio 1:30.

			CH_4 Conversion				H_2 yield				H_2/CO			
	C/O_2	S/C	723	823	923	1023	723	823	923	1023	723	823	923	1023
case1	1.50	2.35	0.57	0.66	0.69	0.73	1.95	2.07	2.07	2.09	5.44	4.99	4.91	4.81
case2	2.00	2.35	0.45	0.54	0.58	0.61	2.02	2.19	2.20	2.23	5.95	5.30	5.18	5.04
case3	2.70	2.35	0.39	0.44	0.48	0.51	2.24	2.30	2.34	2.37	6.06	5.67	5.44	5.31
case4	1.50	3.00	0.61	0.64	0.69	0.74	2.07	2.05	2.09	2.13	5.72	5.59	5.37	5.20
case5	2.00	3.00	0.35	0.55	0.58	0.62	1.59	2.24	2.24	2.27	8.92	5.77	5.63	5.47
case6	2.70	3.00	0.37	0.44	0.49	0.52	2.22	2.35	2.38	2.42	7.05	6.27	5.97	5.75
case7	1.50	4.00	0.60	0.62	0.70	0.74	2.06	2.03	2.14	2.17	6.62	6.55	6.01	5.81
case8	2.00	4.00	0.48	0.51	0.60	0.64	2.15	2.07	2.30	2.33	7.30	7.50	6.28	6.06
case9	2.70	4.00	0.37	0.42	0.52	0.53	2.22	2.31	2.49	2.52	8.29	7.53	6.48	6.21

General trend of methane conversion, hydrogen yield and H_2/CO that has been observed can be seen in Table 4.3 and 4.4. As kinetics of steam reforming reaction is faster for higher temperatures; conversion of methane increases with increasing temperature on

all cases (Figure 4.39). Increasing the inlet temperature of reactor has also positive effect on hydrogen yield for all cases (Figure 4.40). As it can be seen from the results of simulations, inlet feed temperature of 723 K is relatively low for the OSR system, as there is a wide gap between conversion and yield data obtained for 723 K and those obtained for higher inlet temperatures. For the increase in inlet temperature from 823 to 923K and from 923 to 1023 K, hydrogen yield rises steadily with increasing temperature. H_2/CO selectivity is inversely proportional to temperature (Figure 4.41), except case 1 and 4 for Ni:Pt ratio of 20 and case 8 for Ni:Pt ratio of 30.

Increasing oxygen content increases methane conversion due to faster TOX kinetics. The extra heat released by TOX at high inlet temperatures causes better hydrogen yield at the expense of higher carbon monoxide content. Increasing steam to carbon ratio fastens steam reforming and slightly suppresses TOX. Effect of steam to carbon ratio is not so strong on methane conversion, but more pronounced effect is observed on hydrogen to carbon monoxide ratio. Higher steam to carbon ratio in the inlet stream results in less carbon monoxide per hydrogen produced. As inlet temperature increases effect of steam to carbon ratio at the inlet is more pronounced on hydrogen yield. Changing platinum to nickel ratio have relatively low effect on methane conversion. Increased platinum amount causes oxygen depletion, while for lower platinum load small amount of unconsumed oxygen leaves the reactor. Increased platinum amount results in better hydrogen yield for higher inlet temperatures, while for lower temperatures higher nickel loading is beneficial. Temperatures are slightly lower for the catalyst surface that contains less platinum.

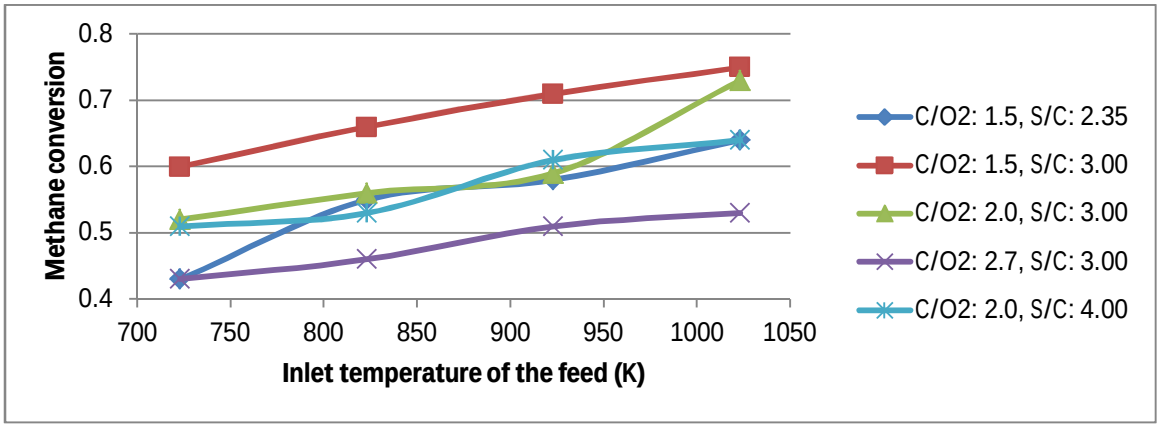

Figure 4.39. Methane conversion vs. inlet temperature of the feed on a reactor with Ni:Pt metal loading ratio of 20 for cases 2,4,5,6 and 8 respectively.

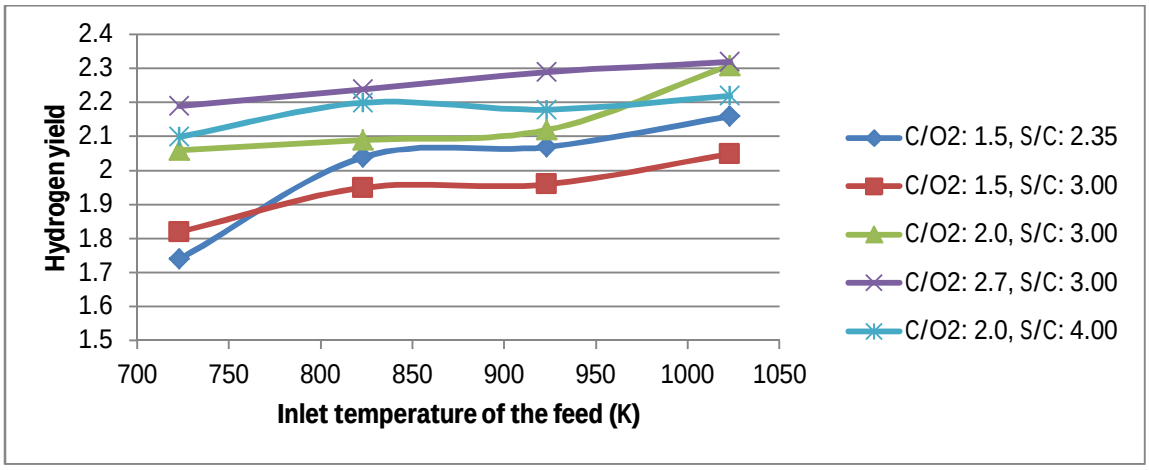

Figure 4.40. Hydrogen yield vs. inlet temperature of the feed on a reactor with Ni:Pt metal loading ratio of 20 for cases 2,4,5,6 and 8 respectively.

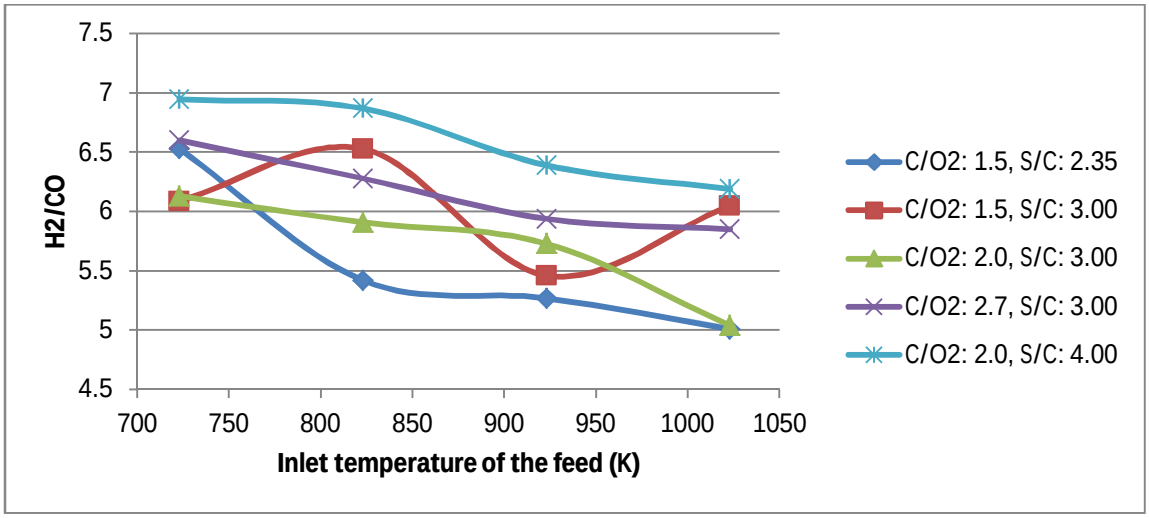

Figure 4.41. H_2/CO selectivity vs. inlet temperature of the feed on a reactor with Ni:Pt metal loading ratio of 20 for cases 2,4,5,6 and 8 respectively.

4.6. Reactor sizing

90 L H_2/min at STP has to be supplied to produce 5 kWe in PEM FC (Karakaya, 2006), which equals to 3.6326 mol H_2/min. It has 35% efficiency. This is lowest limit of the range given by Department of Energy. If it is converted to mass units, 1.2206×10^{-4} kg/s of hydrogen is needed to produce 5 kWe from PEM FC. Number of channels needed for each case is tabulated in Table 4.5.

Table 4.5. Outlet mass flow rates for all cases & inlet temperatures on Pt:Ni ratio of 1:20.

		C/O_2	S/C	CH_4 (kg/s)	H_2 (kg/s)	CO (kg/s)	Channels
723 K	case1	1.5	2.35	4.74E-07	1.40E-07	3.94E-07	7861
	case2	2	2.35	7.21E-07	1.21E-07	2.57E-07	9101
	case3	2.7	2.35	9.46E-07	1.10E-07	2.11E-07	9950
	case4	1.5	3	4.06E-07	1.39E-07	3.18E-07	7886
	case5	2	3	5.43E-07	1.55E-07	3.51E-07	7096
	case6	2.7	3	7.26E-07	1.48E-07	3.11E-07	7427
	case7	1.5	4	3.38E-07	1.48E-07	3.21E-07	7443
	case8	2	4	4.63E-07	1.38E-07	2.77E-07	7934
	case9	2.7	4	6.12E-07	1.31E-07	2.41E-07	8404
823 K	case1	1.5	2.35	3.23E-07	1.58E-07	4.29E-07	6964
	case2	2	2.35	5.03E-07	1.57E-07	4.03E-07	6984
	case3	2.7	2.35	6.94E-07	1.52E-07	3.65E-07	7217
	case4	1.5	3	2.87E-07	1.37E-07	2.91E-07	8035
	case5	2	3	4.43E-07	1.47E-07	3.45E-07	7483
	case6	2.7	3	5.98E-07	1.44E-07	3.19E-07	7629
	case7	1.5	4	2.58E-07	1.30E-07	2.85E-07	8441
	case8	2	4	4.14E-07	1.25E-07	2.54E-07	8759
	case9	2.7	4	4.98E-07	1.29E-07	2.55E-07	8484
923 K	case1	1.5	2.35	2.65E-07	1.47E-07	4.05E-07	7479
	case2	2	2.35	4.16E-07	1.51E-07	3.98E-07	7274
	case3	2.7	2.35	5.73E-07	1.52E-07	3.84E-07	7207
	case4	1.5	3	2.33E-07	1.39E-07	3.53E-07	7918
	case5	2	3	3.65E-07	1.41E-07	3.42E-07	7784
	case6	2.7	3	4.86E-07	1.45E-07	3.39E-07	7569
	case7	1.5	4	1.96E-07	1.27E-07	2.92E-07	8618
	case8	2	4	3.05E-07	1.28E-07	2.79E-07	8556
	case9	2.7	4	4.10E-07	1.29E-07	2.67E-07	8548
1023 K	case1	1.5	2.35	1.86E-07	1.52E-07	4.40E-07	7212
	case2	2	2.35	3.20E-07	1.57E-07	4.35E-07	6997
	case3	2.7	2.35	4.66E-07	1.57E-07	4.15E-07	7005
	case4	1.5	3	1.71E-07	1.31E-07	3.01E-07	8392
	case5	2	3	2.19E-07	1.71E-07	4.71E-07	6436
	case6	2.7	3	4.24E-07	1.37E-07	3.24E-07	8037
	case7	1.5	4	1.47E-07	1.26E-07	3.00E-07	8705
	case8	2	4	2.51E-07	1.25E-07	2.80E-07	8817
	case9	2.7	4	3.68E-07	1.24E-07	2.58E-07	8860

Table 4.6. Outlet mass flow rates for all cases & inlet temperatures on Pt:Ni ratio of 1:30.

		C/O_2	S/C	CH_4 (kg/s)	H_2 (kg/s)	CO (kg/s)	Channels
723 K	case1	1.5	2.35	4.76E-07	1.57E-07	4.00E-07	7011
	case2	2	2.35	6.96E-07	1.47E-07	3.42E-07	7491
	case3	2.7	2.35	8.65E-07	1.57E-07	3.61E-07	6976
	case4	1.5	3	3.98E-07	1.60E-07	3.90E-07	6845
	case5	2	3	7.44E-07	7.97E-08	1.24E-07	13779
	case6	2.7	3	7.91E-07	1.32E-07	2.60E-07	8335
	case7	1.5	4	3.58E-07	1.38E-07	2.89E-07	7967
	case8	2	4	5.16E-07	1.28E-07	2.43E-07	8615
	case9	2.7	4	6.77E-07	1.12E-07	1.87E-07	9830
823 K	case1	1.5	2.35	3.32E-07	1.69E-07	4.69E-07	6514
	case2	2	2.35	5.11E-07	1.67E-07	4.37E-07	6596
	case3	2.7	2.35	6.99E-07	1.60E-07	3.93E-07	6858
	case4	1.5	3	3.19E-07	1.48E-07	3.68E-07	7420
	case5	2	3	4.51E-07	1.56E-07	3.75E-07	7062
	case6	2.7	3	6.19E-07	1.45E-07	3.22E-07	7568
	case7	1.5	4	2.99E-07	1.24E-07	2.62E-07	8884
	case8	2	4	4.55E-07	1.07E-07	1.99E-07	10242
	case9	2.7	4	5.48E-07	1.16E-07	2.14E-07	9463
923 K	case1	1.5	2.35	2.68E-07	1.58E-07	4.48E-07	6944
	case2	2	2.35	4.23E-07	1.58E-07	4.25E-07	6935
	case3	2.7	2.35	5.79E-07	1.58E-07	4.04E-07	6944
	case4	1.5	3	2.45E-07	1.45E-07	3.74E-07	7588
	case5	2	3	3.73E-07	1.47E-07	3.63E-07	7463
	case6	2.7	3	5.10E-07	1.44E-07	3.35E-07	7637
	case7	1.5	4	2.11E-07	1.31E-07	3.02E-07	8397
	case8	2	4	3.13E-07	1.33E-07	2.95E-07	8243
	case9	2.7	4	4.04E-07	1.38E-07	2.96E-07	7942
1023 K	case1	1.5	2.35	2.11E-07	1.52E-07	4.39E-07	7229
	case2	2	2.35	3.48E-07	1.54E-07	4.25E-07	7114
	case3	2.7	2.35	4.93E-07	1.53E-07	4.00E-07	7181
	case4	1.5	3	1.86E-07	1.43E-07	3.81E-07	7703
	case5	2	3	3.04E-07	1.44E-07	3.65E-07	7643
	case6	2.7	3	4.25E-07	1.43E-07	3.45E-07	7705
	case7	1.5	4	1.61E-07	1.28E-07	3.06E-07	8596
	case8	2	4	2.52E-07	1.31E-07	3.00E-07	8407
	case9	2.7	4	3.72E-07	1.24E-07	2.68E-07	8829

Optimum conditions for micro channeled OSR reactor and the corresponding number of channels for a given ratio of Pt:Ni can be calculated according to the targeted hydrogen molar flow, H2/CO selectivity ratio at the exit, hydrogen yield and the cost of the reactor.

5. CONCLUSIONS AND RECCOMENDATION

Three dimensional mathematical model was developed for a methane micro channel autothermal reactor by using FLUENT computational fluid dynamics program. Inside surface area of channels are washcoated with platinum and nickel bimetallic catalyst for a ratio of 1:20 and 1:30. Area covered with platinum is randomly distributed. Randomness of platinum dominating region is generated with EXCEL random function. Reactor channel has a dimension of 4x4x200 mm, grids are meshed with GAMBIT program. Inlet temperatures, steam to carbon, carbon to oxygen and platinum to nickel ratios are selected as parameters, while temperature profiles, conversion of methane, hydrogen yield, carbon monoxide concentration per hydrogen along the reactor is studied.

An increase in C/O_2 ratio to 2.0 limits the temperature rise and further increase to 2.7 leads to fast temperature decrease in the inlet zone led by low O_2 concentration limiting exothermic TOX. S/C ratio has relatively limited effect on temperature profile compared to that of C/O_2 ratio. The reason of lower temperatures obtained in the SR dominated part of the reactor for higher steam amounts is the increase in steam concentration favoring endothermic steam reforming reaction along the reactor.

Since methane is not fully converted even at the exit of the reactor, hydrogen yield can be increased through rising the inlet temperature. The effect of S/C ratio on methane conversion is not significant. But hydrogen yield and H_2/CO ratio increase with the increase in steam to carbon ratio. Methane conversion increases while hydrogen yield and H_2/CO decreases in response to a decrease in C/O_2 feed ratio. The distinct difference in H_2/CO selectivity profiles is worth to be mentioned; there, hydrogen yield is higher Ni:Pt=20 case for the first 40 mm, whereas after ca. 40 mm of reactor length hydrogen yield is stabilized at higher level for Ni:Pt =30 case.

APPENDIX A: GRID DISPERSION

Inner surface of a channel has been exploded according to Figure A.1. A is top surface, B is left side wall, C is bottom surface and D is right side wall. Channel numbers are expressed on the figure.

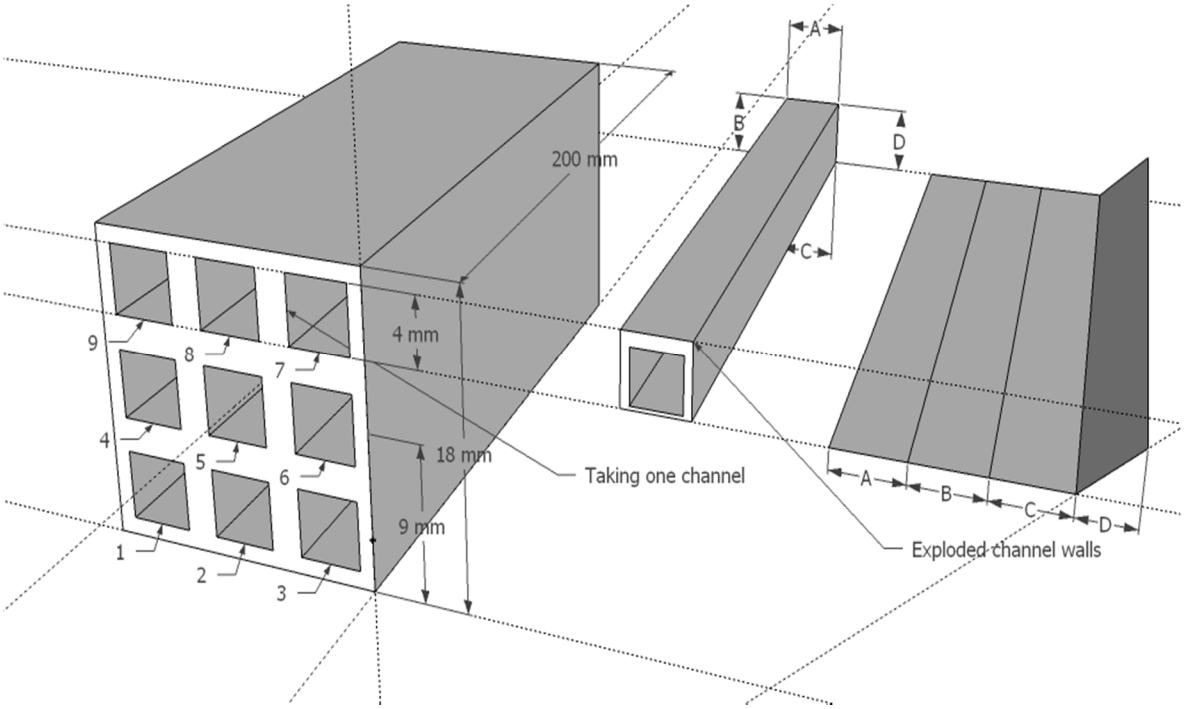

Figure A.0.1. Applied expression of how to coordinate the channel walls.

Platinum is dispersed on nickel with random function of Excel. Zeroes signifies a region with nickel. 1 signifies platinum. In the entrance there is a catalyst free zone for each channel. To determine the catalyst free zone, code overrides the mapping obtained from catalyst dispersion random function.

Z coordinate is divided into 50 parts, and each wall is divided into eight parts. Each catalyst dispersed area is 1 mm^2. Overall 1 channel has 3200 mm^2 surface area. 91.5% of its surface area is washcoated with catalyst.

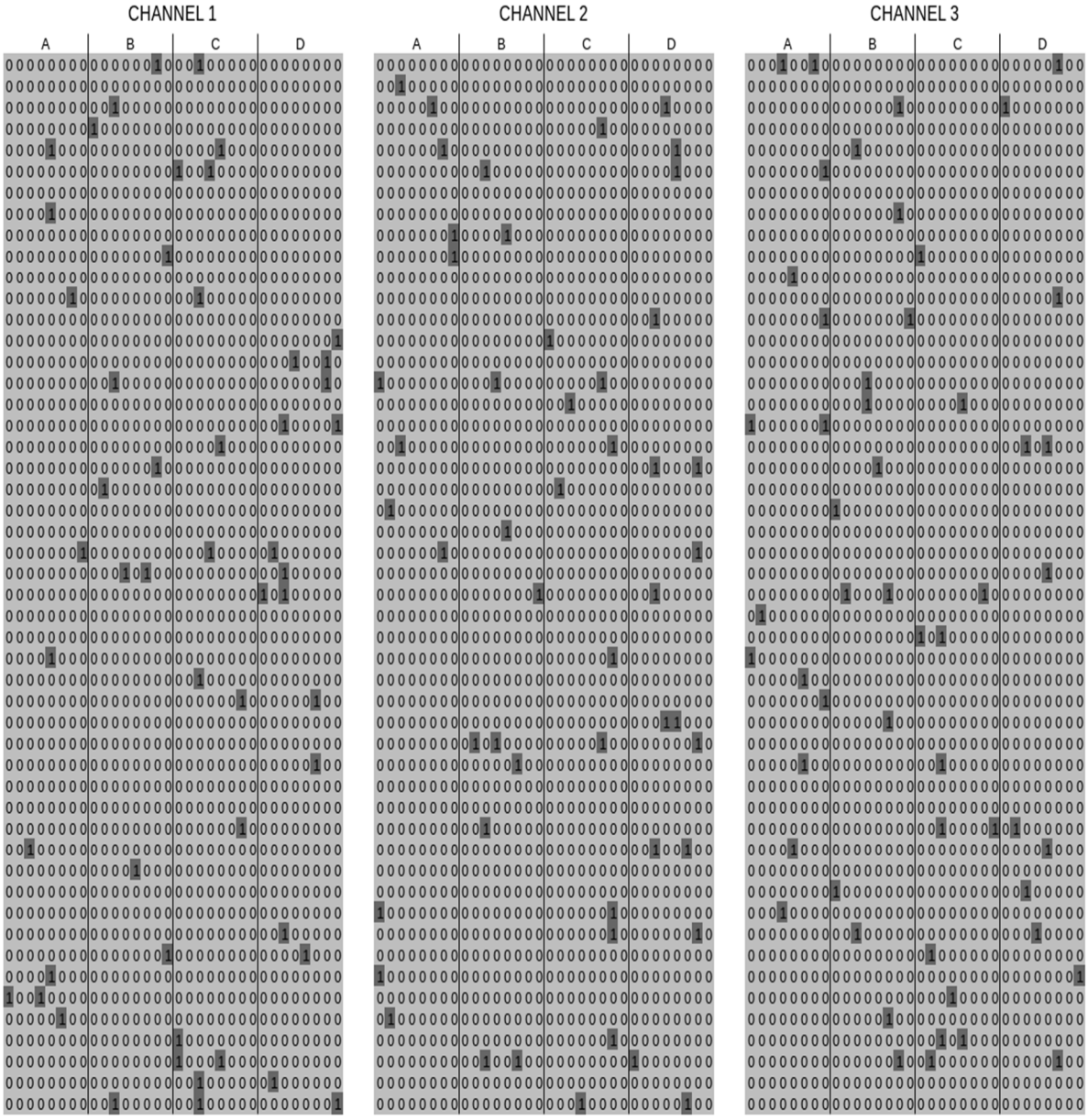

Figure A.0.2. Catalyst dispersion for first three channel, with ratio of 1:30. Darker areas signify platinum dominated area.

REFERENCES

Avci, A. K., Z. I. Önsan and D. L. Trimm, 2001, "On-board Fuel Conversion for Hydrogen Fuel Cells: Comparison of Different Fuels by Computer Simulations", *Applied Catalysis A General*, Vol. 216, pp. 243-256.

Avci, A. K., M. Karakaya and David L. Trimm, 2010, "Microreactor Catalytic Combustion for Chemicals Processing", *Catalysis Today*, Vol. 155, pp. 66-74.

Avci, A. K., D. L. Trimm and Z. İ. Önsan, 2001, "Heterogeneous Reactor Modeling for Simulation of Catalytic Oxidation and Steam Reforming of Methane." *Chemical Engineering Science*. Vol. 56, No. 2, pp. 641-649.

Avci, A. K., D. L. Trimm, A. E. Aksoylu and Z. İ. Önsan, 2004, "Hydrogen Production by Steam Reforming of n-butane over Supported Ni and Pt-Ni Catalysts", *Applied Catalysis A: General*, Vol. 258, pp. 235-240.

Bengaard, H. S., J. K. Nørskov, B. Clausen, L. P. Nielsen, A. M. Molenbroek and J. R. Rostrup-Nielsen , 2002, "Steam Reforming and Graphite Formation on Ni Catalysts", *Journal of Catalysis*, Vol. 209, No. 2, pp. 365-384.

BOTAŞ, 2009, *Supply and Installation of Surface and SubSurface Facilities, Water Supply and Brine Discharge Pipelines and Cavern Leaching of Tuz Gölü Underground Gas Storage Project*, BOTAŞ, Ankara.

British Petroleum, 2012, *2012-2030 Energy Outlook* , British Petroleum, London.

British Petroleum, 2011, *Statistical Review of World Energy*, British Petroleum, London.

Büchi, F. N. and S. Srinivasan, 1999, "Operating Proton Exchange Membrane Fuel Cells Without External Humidification of the Reactant Gases. Fundamental Aspects", *Journal of the Electrochemical Society*, Vol. 144, No. 8, pp. 2767-2772.

Chalk, S. M. and James F. M., 2006, "Key Challenges and Recent Progress in Batteries, Fuel cells and Hydrogen Storage for Clean Energy Systems", *Journal of Power Sources*, pp. 73-80.

Chan, S. H. and H. M. Wang, 2000, "Effect of Natural Gas Composition on Autothermal Fuel Reforming Products", *Fuel Processing Technology*, Vol. 64, pp. 221-239.

Çağlayan, B. S., A. K. Avcı, Z. İ. Önsan and A. E. Aksoylu, 2005, "Production of Hydrogen over Bimetallic Pt–Ni/δ-Al2O3 I. Indirect Partial Oxidation of Propane", *Applied Catalysis A*, pp. 181-188.

Çağlayan, B. S. and A. E. Aksoylu, 2011, "Water–Gas Shift Activity of Ceria Supported Au–Re Catalysts." *Catalysis Communications* Vol. 12, No. 13, pp. 1206-1211.

Dinçer, İ., 2012, "Green Methods for Hydrogen Production", *International Journal of Hydrogen Energy*, Vol. 37, pp. 1954-1971.

EPA, 2004, *Fuel Cell Handbook*, US Department of Energy, West Virginia.

Forsberg, Charles, 2005, "Futures for Hydrogen Produced Using Nuclear Energy", *Progress in Nuclear Energy*, Vol. 47, pp. 484-495.

Gökaliler, F., Bayram A. Göçmen and A. E. Aksoylu, 2008, "The Effect of Ni:Pt Ratio on Oxidative Steam Reforming Performance of Pt–Ni/Al_2O_3 Catalyst", *International Journal of Hydrogen Energy*, Vol. 33, No. 16, pp. 4358-4366.

Gökaliler, F., B. S. Çağlayan, Z. İ. Önsan and A. E. Aksoylu, 2009, "Hydrogen Production by Autothermal Reforming of LPG for PEM Fuel Cell Applications", *International Journal of Hydrogen Energy*, Vol. 33, No. 4, pp. 1383-1391.

Hessel, V., A. Renken, J. C. Schouten and J. Yoshida, 2009, *Micro Process Engineering*, Wiley-VCH, Weinheim.

Hickman, D. A. and L. D. Schmidt, 1993, "Production of syngas by direct catalytic oxidation of methane", *Science*, Vol. 259, pp. 343-346.

Hoogers, G., 2003, *Fuel Cell Technology Handbook*, CRC Press, Florida.

Karakaya, M., 2006, *Dynamic Simulation of an Indirect Partial Oxidation Reactor for Methane Conversion to Hydrogen*, M.S. Thesis, Boğaziçi University.

Karakaya, M. and A. K. Avci, 2011, "Microchannel reactor modeling for combustion driven reforming of iso-octane", *International Journal of Hydrogen Energy*, Vol. 36, No. 11, pp. 6569-6577.

Karakaya, M., S. Keskin and A. K. Avci, 2012, "Parametric Study of Methane Steam Reforming to Syngas in a Catalytic Microchannel Reactor", *Applied Catalysis A: General*, Vol. 411, pp. 144-122.

Kendall, K., 2008, "Hydrogen Fuel Cell for Green House in Black Country." *Fuel Cells Bulletin*, pp. 4-5.

Kolb, G., 2008, *Fuel processing: for Fuel Cells*, Wiley-VCH, Weinheim.

Kurdoğlu, B., 2009, *Modeling of Methane Autothermal Reforming in a Cylindirical Pt-Ni Washcoated Reactor*, M.S. Thesis, Boğaziçi University.

Laosiripojana, N. and S. Assabumrungrat, 2006, "Hydrogen Production from Steam and Autothermal Reforming of LPG over High Surface Area Ceria", *Journal of Power Sources*, Vol. 158, pp. 1348-1357.

Larmine, J. and A. Dicks, 2003, *Fuel Cell Systems Explained*, Wiley, Sussex.

Li, B., S. Kado, Y. Mukainakano, T. Miyazawa, T. Miyao, N. Shuichi, K. Okumura, K. Kunimori and K. Tomishige, 2007, "Surface modification of Ni catalysts with trace Pt for oxidative steam reforming of methane", *Journal of Catalysis*, Vol. 245, No. 1, pp. 144-155.

Ma, L., D. L. Trimm and C. Jiang, 1996, "The design and testing of an autothermal reactor for the conversion of light hydrocarbons to hydrogen I.The kinetics of the catalytic oxidation of light hydrocarbons", *Applied Catalysis A: General*, Vol. 138, pp. 275-283.

Men, Y, G. Kolb, R. Zapf and V. Hessel, 2007, "Selective methanation of carbon oxides in a microchannel reactor primary screening and impact of oxygen additive", *Catalysis Today*, Vol. 125, pp. 81-87.

Mishra, V., F. Yang and R. Pitchumani, 2005, "Analysis and Design of PEM Fuel Cells", *Journal of Power Sources*, Vol. 141, pp. 47-64.

Numaguchi, T. and K. Kikuchi, 1988, "Intrinsic Kinetics and Design Simulation in a Complex Reaction Network: Steam-Methane Reforming", *Chemical Engineering Science*, Vol. 43, pp. 2295-2301.

Poling, Bruce E., John M. Prausnitz and John P. O'Connell, 2001, *Properties of Gases and Liquids*, McGraw-Hill, New York

Qi, A., S. Wang, C. Ni and D. Wu, 2007, "Autothermal reforming of gasoline on Rh-based monolithic catalysts", *International Journal of Hydrogen Energy*, Vol. 32, pp. 981-991.

Ren, X. and S. Gottesfeld, 2001, "Electro-osmotic drag of water in a poly (perfluorosulphonic acid) membrane", *Journal of the Electrochemical Society*, 148, pp. 87-93.

Rostrup-Nielsen, J. R. and J. H. Bak Hansen, 1993, "CO2 reforming of Methane over Transition Metals", *Journal of Catalysis*, Vol. 144, pp. 38-49.

Rostrup-Nielsen, J. R., K. Pedersen and J. Sehested, 2007, "High temperature methanation: Sintering and structure sensitivity", *Applied Catalysis A: General*, Vol. 330, pp. 134-138.

Rostrup-Nielsen, J. R., 1984, "Catalytic Steam Reforming", *Catalysis, Science & Technology*, Vol. 5, pp. 1-117.

Rostrup-Nielsen, J. R., 2000, "New Aspects of Syngas Production and Use", *Catalysis Today*, Vol, 63, No. 2-4, pp. 159-164.

Rostrup-Nielsen, J. R., 2002, "Syngas in Perspective." *Catalysis Today*, Vol. 71, No. 3-4, pp. 243-247.

Rostrup-Nielsen, J. R. and L. Alstrup, 1999, "Innovation and Science in the Process Industry Steam Reforming and Hydrogeolysis". *Catalysis Today*, Vol. 89, pp. 11-13.

Silberova, B., H. Venvik, J. C. Walmsley and A. Holmen, 2005, "Small-scale Hydrogen Production from Propane", *Catalysis Today*, Vol. 100, pp. 457-462.

Sinha, J., 2010, *Cost Analyses of Fuel Cell Stacks/Systems*, Department of Energy, Washington

Sinnott, R. K., 2000, *Coulson & Richardson's Chemical Engineering. Volume 6: Chemical Engineering Design*, Butterworth & Heinemann, Oxford.

Şimşek, E., Ş. Özkara, A. E. Aksoylu and Z. İ. Önsan, 2007, "Preferential CO Oxidation over Activated Carbon Supported Catalysts in H_2-rich Gas Streams Containing CO2 and H_2O", *Applied Catalysis A: General*, Vol. 316, No. 2, pp. 169-174.

Trimm, D. L, 1999, "Catalysts for the Control of Coking During Steam Reforming." *Catalysis Today*, Vol. 49, pp. 3-10.

Turkish Wind Energy Association, 2012, *Turkish Wind Energy Statistics Report*, Ankara.

United Nations, 1998, *Kyoto Protocol to the United Nations Framework Convention on Climate Change*, United Nations, New York.

Versteeg, H. K. ve W. Malalasekera, 1995, *An Introduction to Computational Fluid Dynamics: The Finite Volume Method*, Pearson Prentice Hall, Harlow.

Xu, J. ve G. F. Froment, 1989, "Methane Steam Reforming, Methanation and Water-Gas Shift: I. Intrinsic Kinetics", *AIChe Journal*, Vol. 35, pp. 88-96.

Zhai, X., S. Ding, Y. Cheng, Y. Jin, Y. Cheng, 2010, "CFD Simulation with Detailed Chemistry of Steam Reforming of Methane for Hydrogen Production in an Integrated Micro-reactor", *International Journal of Hydrogen Energy*, Vol. 35, pp. 5383-5392.